DEVELOPMENT AND EVALUATION OF AN AUTOMATIC DEPARTURE PREVENTION SYSTEM AND STALL INHIBITOR FOR FIGHTER AIRCRAFT

Robert T. N. Chen
Fred D. Newell
Arno E. Schelhorn
Calspan Corporation
Buffalo, New York 14221

FOREWORD

This report was prepared by Calspan Corporation (formerly Cornell Aeronautical Laboratory, Inc.) Buffalo, N.Y. for the Air Force Flight Dynamics Laboratory, Wright-Patterson Air Force Base, Ohio. The work was performed under Contract No. F33615-72-C-1162, Projects No. 8225 and 8219, "Stall Inhibitor and Automatic Departure Prevention Device." The Air Force Project Engineer was initially Mr. D.K. Bowser and later Mr. T.J. Cord, both of the AFFDL/FGC. Capt. Ken Bassett was co-project engineer for the effort. Dr. R.T.N. Chen was the principal investigator of Calspan. Mr. F.D. Newell, among other responsibilities, was responsible for the design and conduct of the evaluation program, and Messrs. A.E. Schelhorn and G.E. Martzolf were responsible for the breadboard development.

The authors wish to express their appreciation to many members of Calspan who have contributed to the successful completion of this program. Mr. C.M. Poppenberg of the Flight Research Department performed the computer programming for the 370/165 digital simulation; Messrs. R.F. Gavin and J.R. Knight, both of the Computer Center, performed respectively the digital and analog portions of the programming work on the Calspan ground-based simulator; Mr. A.B. Adler extensively assisted the pre-evaluation work, and Messrs. G.W. Hall and G. Bull served as the formal evaluation pilots.

Acknowledgement is also due to Mrs. J. Martino for her assistance in the preparation of this report and to Messrs. J.M. Schuler, C.R. Chalk, E.G. Rynaski, and W.R. Deazley for their many valuable suggestions and discussion during the course of this work.

This report was submitted by the authors in January 1973, and is being published as Calspan Report No. AK-5112-F-1.

This technical report has been reviewed and is approved.

C.B. WESTBROOK
Chief, Control Criteria Branch
Air Force Flight Dynamics Laboratory

G. PURCELL
Acting Chief, Control Systems
Development Branch
Air Force Flight Dynamics Laboratory

ABSTRACT

This report documents the conceptual design, breadboard development and pilot-in-the-loop evaluation of an automatic departure prevention system and a stall inhibitor for fighter aircraft. Using the A-7D as the study aircraft, a departure boundary characterized by α and β was determined from the available data. This departure boundary was then used to help design an automatic departure preventer and a stall inhibitor. The departure preventer provides automatic control inputs to the pitch and yaw axis. The stall inhibitor increases the longitudinal stick force to provide the pilot with cues of an impending stall; however, the pilot retains override capability. The stall inhibitor, while warning the pilot of the impending stall, tends to produce strong pilot-induced oscillations, and would not be acceptable. An automatic departure prevention device as described in this report works smoothly and will benefit the A-7 aircraft. With just the departure preventer, the pilots could maneuver freely, with great confidence and use the full capability of the airplane, well beyond the present departure boundary.

TABLE OF CONTENTS

LIST OF ILLUSTRATIONS

LIST OF ILLUSTRATIONS (CONTINUED)

LIST OF ILLUSTRATIONS (CONTINUED)

LIST OF TABLES

LIST OF SYMBOLS

c_1, c_2, c_3	coefficients of the switching law
C_D	drag coefficient
C_L	lift coefficient
c_l, c_m, c_n	aerodynamic moment coefficients in body axes
C_x, C_y, C_z	aerodynamic force coefficients in body axes
F_A	total aerodynamic force including engine thrust, lb
F_{as}	lateral stick force, lb
F_{es}	longitudinal stick force, lb
I_x, I_y, I_z	moments of inertia about x, y, z body axes, respectively, slug-ft^2
I_{xz}	product of inertia, body axes, slug-ft^2
K_1, K_2, K_3, K_4 K_5, K_6, K_7, K_8	gains in the departure preventer control law
L, M, N	component of M_A about body system of axes x, y, z
M	Mach number
L_p, L_r	effective roll damping due to roll and yaw respectively, 1/sec
M_A	total aerodynamic moment including moment due to engine thrust, ft-lb
N_p, N_r	effective yaw damping due to roll and yaw respectively, 1/sec
T	total engine thrust, lb
T_x, T_z	component of T along x and z body axes respectively, lb
V	true airspeed, ft/sec
X, Y, Z	components of F_A along body system of axes, x, y, z
b	wing span, ft
$\bar{c}$	mean geometric chord (MGC) of the wing, ft
d	thrust line offset (positive above c.g.), ft
g	gravitational acceleration, 32.17 ft/sec^2

h	altitude, ft
n_y	lateral accelerometer signal along y axis, g units
n_z	normal accelerometer signal along z axis, g units
p, q, r	angular velocity components about body system of axes x, y, z respectively
$\bar{q}$	dynamic pressure = $\frac{1}{2}\rho V^2$, lb/ft^2
s	Laplace transform variable
S	wing area, ft^2
u, v, w	velocity components along x, y, z respectively, ft/sec
x, y, z	body axes (see diagram on next page)
α	angle of attack, degrees or radians
β	angle of sideslip, degrees or radians
α^*	switching function, degrees
$\dot{\alpha}$	time rate of change of the angle of attack, degree/sec or rad/sec
θ, ϕ, ψ	Euler angles for pitch, roll and yaw respectively, degrees or radians
δ_e	unit horizontal tail displacement, degrees
δ_a	aileron displacement (total), degrees
δ_s	spoiler/deflector displacement, degrees
δ_r	rudder displacement, degrees
δ_a'	combined aileron - spoiler/deflector displacement, radians
ρ	density, slug/ft^3

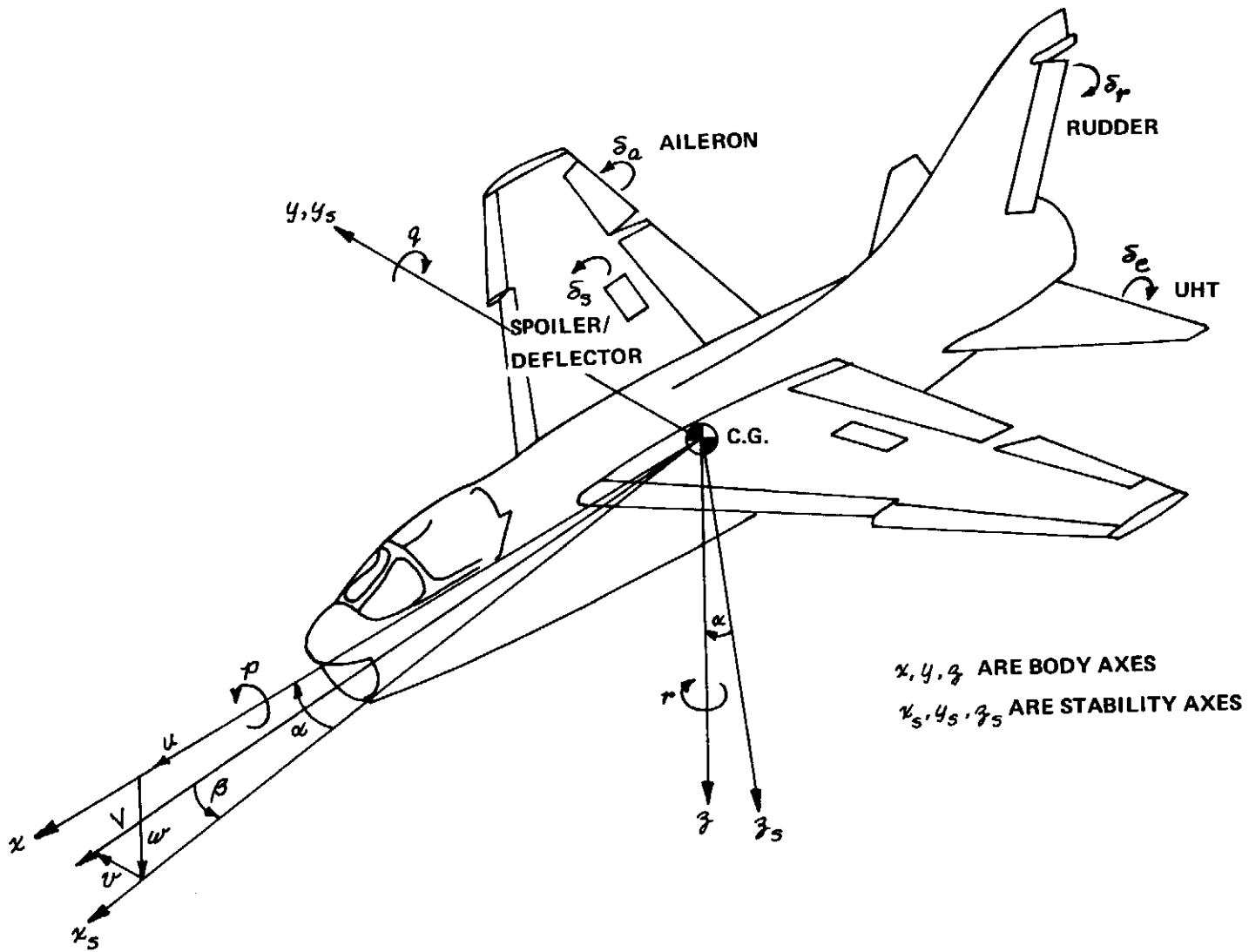

AXIS SYSTEMS

Subscripts

s	stability axes
d	departure preventer

Abbreviations

AFCS	Automatic Flight Control System
c.g.	Center of Gravity
D.P.	Departure Preventer
G.W.	Gross Weight
P.A.	Pitch authority of AFCS
PIO	Pilot Induced Oscillation
S.B.	Switching Boundary
S.I.	Stall Inhibitor
UHT	Unit Horizontal Tail

SECTION I

INTRODUCTION

The loss-of-control accidents due to inadvertent stalls and spins have become a very serious problem in the operational use of some aircraft, especially for fighter aircraft (Reference 1). For fighter aircraft, air combat maneuvers often require operations of this aircraft in the near-stall range of angles of attack. If the aircraft has poor stall characteristics, e.g., the existence of an instability such as directional divergence or "nose slice" as for the A-7 and the F-4 aircraft, it is particularly vulnerable to inadvertent departures from controlled flight, which, if recovery is not effected in time, may develop into various modes of spins. This type of instability at near-stall angles of attack thus becomes a critical problem in both flight safety and operational utility, as it can severely limit the full maneuvering capability of the aircraft. It is desired to eliminate this problem.

Two approaches may be taken to solve the problem: (1) to seek aerodynamic fixes, such as modifications to the wing leading edge geometry, etc. so as to postpone the instability to higher angle of attack (Reference 2), and (2) to modify the flight control system in order to stabilize the aircraft at near-stall angles of attack. The second approach has been studied and developed in this program and is the subject of this report.

The concept of improving the stall and near-stall characteristics by working through the flight control system is not new. Early work (References 3 through 5) has applied this concept to stabilize the large uncontrolled motions of the F9J-3 and other aircraft. Recent work associated with the TWEAD (Tactical Weapon Delivery) Control Augmentation System Development (Reference 6) has also considered using the flight control system to improve the high angle of attack flying characteristics of the F-4C.

Unlike these previous studies in which a "full-time" control system was used, the approach taken in this program was to augment the aircraft only in the dangerous stall departure region through use of a switching law. Once the dangerous region is approached, flight control augmentation is activated to provide the pilot with cues on an impending stall and to prevent the departure of the aircraft from controlled flight, without degrading the full operational flight envelope of the aircraft. The switching law was derived from a departure boundary characterized by the two major parameters α and β . The departure prevention scheme uses nonlinear control laws. The longitudinal control law is a function of the magnitude of the sideslip as well as the longitudinal state variables; and the directional control law is a function of the angle of attack as well as the lateral-directional state variables. Due to pilot preference, an override capability has been maintained.

The study aircraft chosen for this program is the A-7D, a single engine, single place, transonic, light attack aircraft. While the stall and departure characteristics will be unique to the specific aircraft, it is felt that the same basic approach and procedure employed for the study aircraft should be applicable to the development of a similar departure prevention device for other aircraft. The program consisted of five phases: analysis, design, digital simulation, fabrication of breadboard hardware, and piloted ground simulation. These are discussed, in turn, in the following sections.

SECTION II

DEPARTURE BOUNDARY

2.1 INTRODUCTION

The original goal* of the departure preventer was to deter the pilot from departing the aircraft without degrading its full operational flight envelope. To achieve this goal it is desirable that the preventer permit the aircraft to fly along the departure boundary rather than to force the vehicle from it. Clearly, the determination of the departure boundary is the first step toward designing such a departure preventer.

An analytical determination of the departure boundary, however, is by no means trivial. The major difficulties are twofold:

(1) The dynamics of the aircraft in the post-stall, departure flight regime are nonlinear, involving all six degrees of freedom of motion.

(2) The analytical representation of the aerodynamic forces and moments can be accurately described only as complicated nonlinear functions of many variables.

The departure boundary may be considered analytically to be a stability boundary. Two stability criteria may then be used:

(a) A bounded input - bounded output stability criterion.

(b) A stability criterion based on an autonomous system description with initial conditions but without control inputs.

The relatively short duration of the program precluded the practicality of a thorough theoretical study of the nonlinear stability problem associated with the aircraft motion in the near-departure region. Rather, a semi-analytical method relying heavily on a digital computer simulation and physical considerations was employed. The second stability criterion was therefore selected on the basis that it was more amenable to digital computer simulation.

---

*This original goal was subsequently further advanced, because the departure preventer designed was not only capable of automatically preventing the aircraft from departure but also capable of expanding its flight envelope.

Thus, the theoretical basis used in establishing the departure boundary was the stability of the autonomous system at some isolated equilibrium states in the near-departure region. Relying largely on physical considerations and digital computer simulation, a simplified departure boundary described by only two major state variables, α and β, was determined. Subsequent application of this simplified departure boundary in the design of the stall inhibitor and the departure preventer (Section III) has indicated that it was adequate and general enough to meet the program objectives.

In determining the departure boundary, the available flight test data were first scrutinized to see if there existed general trends of the major state variables such as α, β, r, etc., at the departure. The high-angle-of-attack wind tunnel data were then analyzed with the primary emphasis placed on the lateral-directional static derivatives, $C_{n_\beta}(\alpha,\beta)$ and $C_{\ell_\beta}(\alpha,\beta)$. A six-degree-of-freedom digital computer simulation was then performed to verify and refine the simplified boundary. Finally the sensitivity of the boundary to other flight conditions was studied to validate the departure boundary.

2.2 STALL DEPARTURE CHARACTERISTICS OF THE A-7 AIRCRAFT

The stall approach and departure characteristics of the A-7D aircraft have been discussed in Reference 7 based on the flight test results of the A-7A aircraft. For normal 1 g stalls in the cruise configuration, buffet onset occurs at 16 to 18 units of angle of attack (11.5 to 13.5 degrees) and increases its intensity until stall, which occurs at approximately 25 units of angle of attack (21 degrees). Stalls in the landing configuration are generally similar to those in the cruise configuration (see Reference 7) and the stall characteristics of the A-7 aircraft are fairly independent of the external stores arrangement. However, as indicated in Reference 8, the power setting has a strong effect on the stall approach characteristics, as the buffet onset occurs at a considerably lower angle of attack for the high power setting than for idle. The accelerated stalls are similar to the 1 g stalls with the exception that the initial airplane motions such as yaw rate and sideslip, etc. are more violent.

From buffet onset to the stall a relatively wide range of angle of attack exists (as high as 10 degrees). As the angle of attack is increased beyond buffet onset the intensity of the buffet slowly increases for a while then stays constant, providing inadequate stall warning. Because of this the airplane is equipped with an artificial stall warning device in the form of a rudder pedal vibrator on the right pedal which gives the pilot a stall warning at $20.5 \pm .5$ units of angle of attack in both cruise and landing conditions. However, experience has indicated that this form of stall warning has not been effective in the cruise configuration as the pedal shaker is often masked in the airframe buffet.

The A-7 stall is defined as a directional divergence (nose slice) in either direction accompanied by a wing drop in the direction of yaw. Quoting from the A-7E NATOPS manual (pilot's handbook), "Recovery during departure is immediate if the stick is returned to neutral and released while simultaneously applying opposite rudder provided this action is taken before approximately 20 degrees of yaw is reached."

A roll axis Automatic Flight Control System (AFCS) often introduces pro-spin lateral control in response to the roll motion at the stall; therefore, as a passive and limited departure prevention scheme, the roll axis AFCS is automatically disengaged when the angle of attack exceeds 22 units. As an additional precaution, the pilot is trained to manually turn off the roll axis AFCS when the angle of attack exceeds 22 units. The pilot is also discouraged from using the aileron in the near-stall region because the aileron deflection tends to produce inadvertent departure. Thus a pilot has no confidence when operating in the stall-departure region. As a result, he is reluctant to use the full capability of the aircraft.

Figure 1 shows the stall approach characteristics of the A-7D obtained from the stall approach time histories given in Reference 9. The test conditions include various external store loadings, 1 g stalls and accelerated stalls ($2 \sim 3$ g), cruise and power approach configurations, various gross weights, c.g. locations and Mach numbers. From this figure, it is seen that for the Mach range tested, i.e., $0.24 \leq M \leq 0.74$, the stall approach characteristics are relatively insensitive to the Mach number.

2.3 DETERMINATION OF α-β DEPARTURE BOUNDARY

Examination of the stall approach time histories given in References 9 and 10 and the spin evaluation tests of the A-7 A/B and the A-7D (References 8 and 11) revealed a general trend of α vs β in the vicinity of departure. When the sideslip angle was large, the angle of attack at the departure, shown in Figure 2, tended to be smaller. Other variables such as angular velocities and the aileron position were also scrutinized for a recognizable correlation with α (and/or β); however, there was no definable trend for these variables.

Calculations using the high angle of attack wind tunnel data (Reference 12) showed that the lateral and directional static derivatives were strongly affected by the angle of attack as well as the angle of sideslip, i.e.:

$$C_{n_\beta} = C_{n_\beta}(\alpha, \beta)$$

$$C_{\ell_\beta} = C_{\ell_\beta}(\alpha, \beta)$$

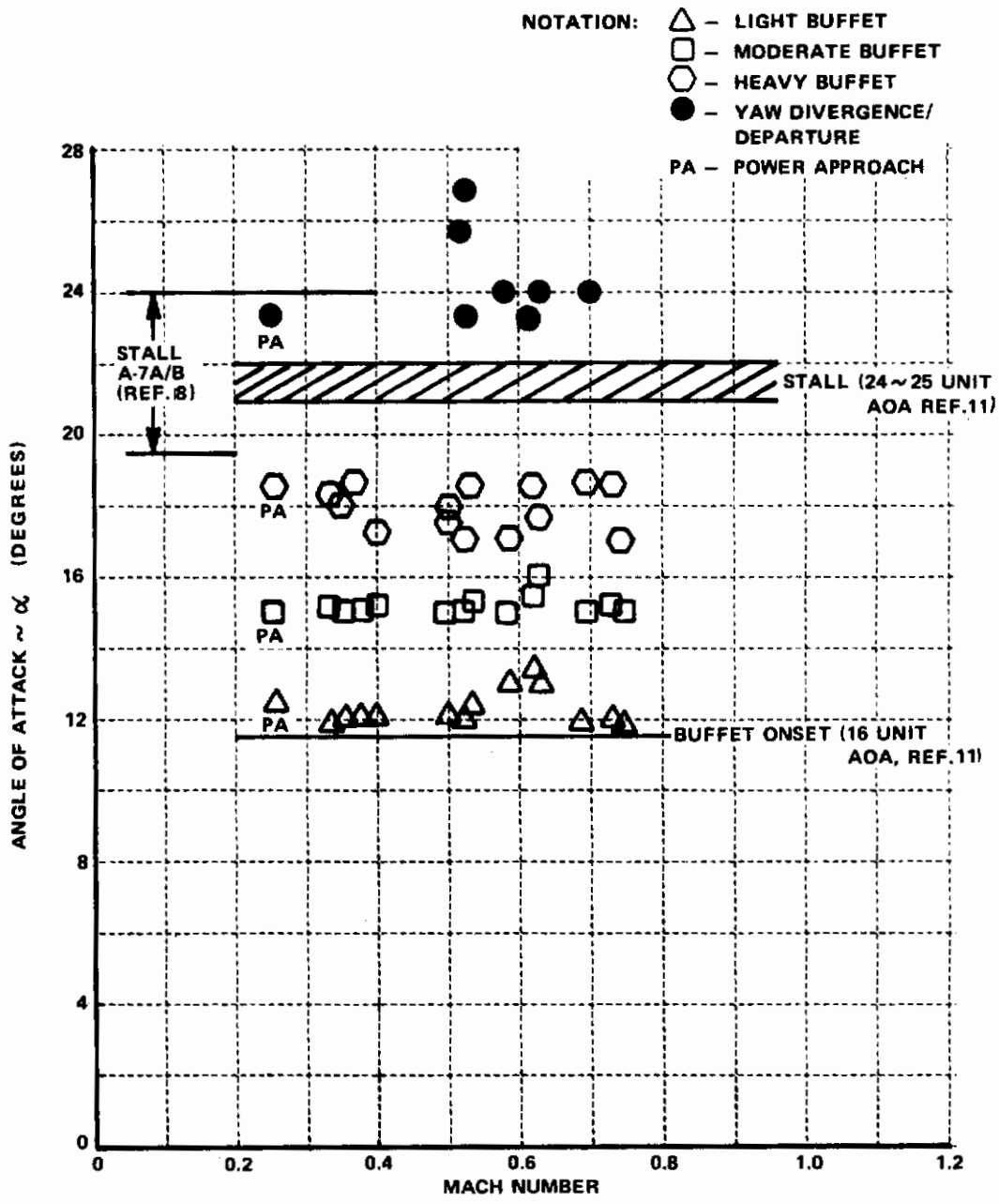

Figure 1 A-7D STALL APPROACH CHARACTERISTICS, CRUISE CONFIGURATION (REF. 9)

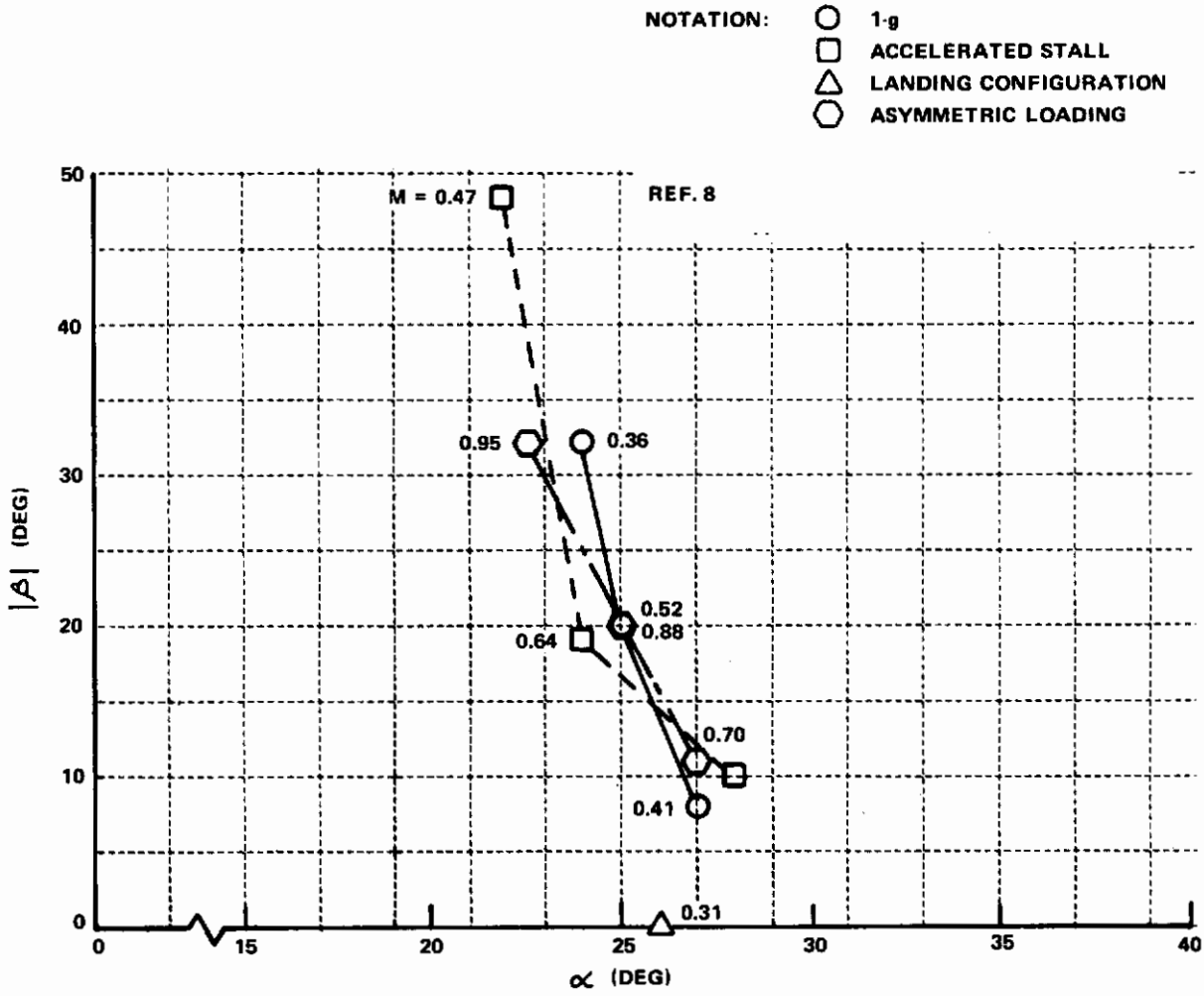

Figure 2 A-7 DEPARTURE CHARACTERISTICS OBTAINED FROM FLIGHT DATA

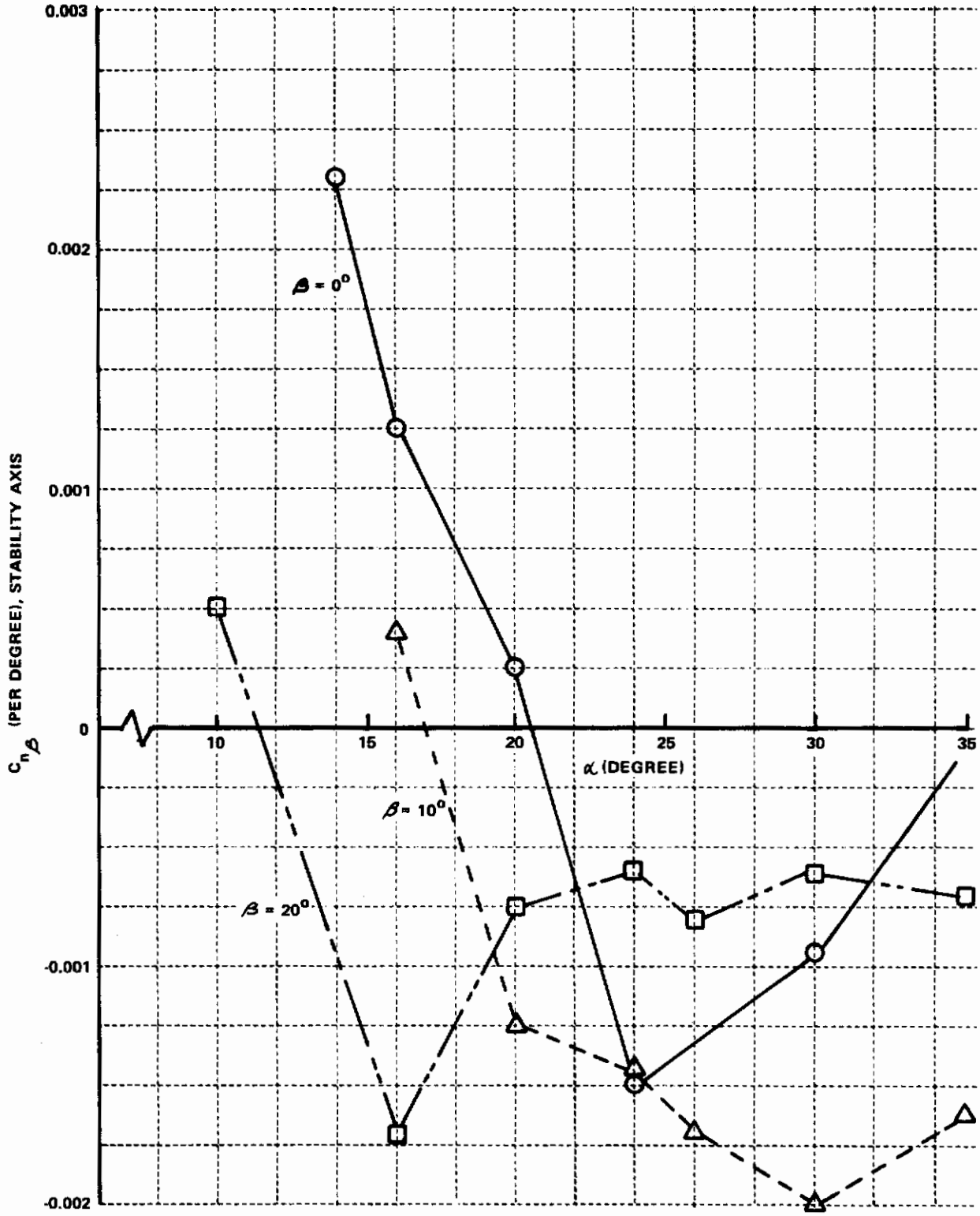

Figure 3 $C_{n_\beta}(\alpha)$ AT $\beta = 0^o$, 10^o, AND 20^o

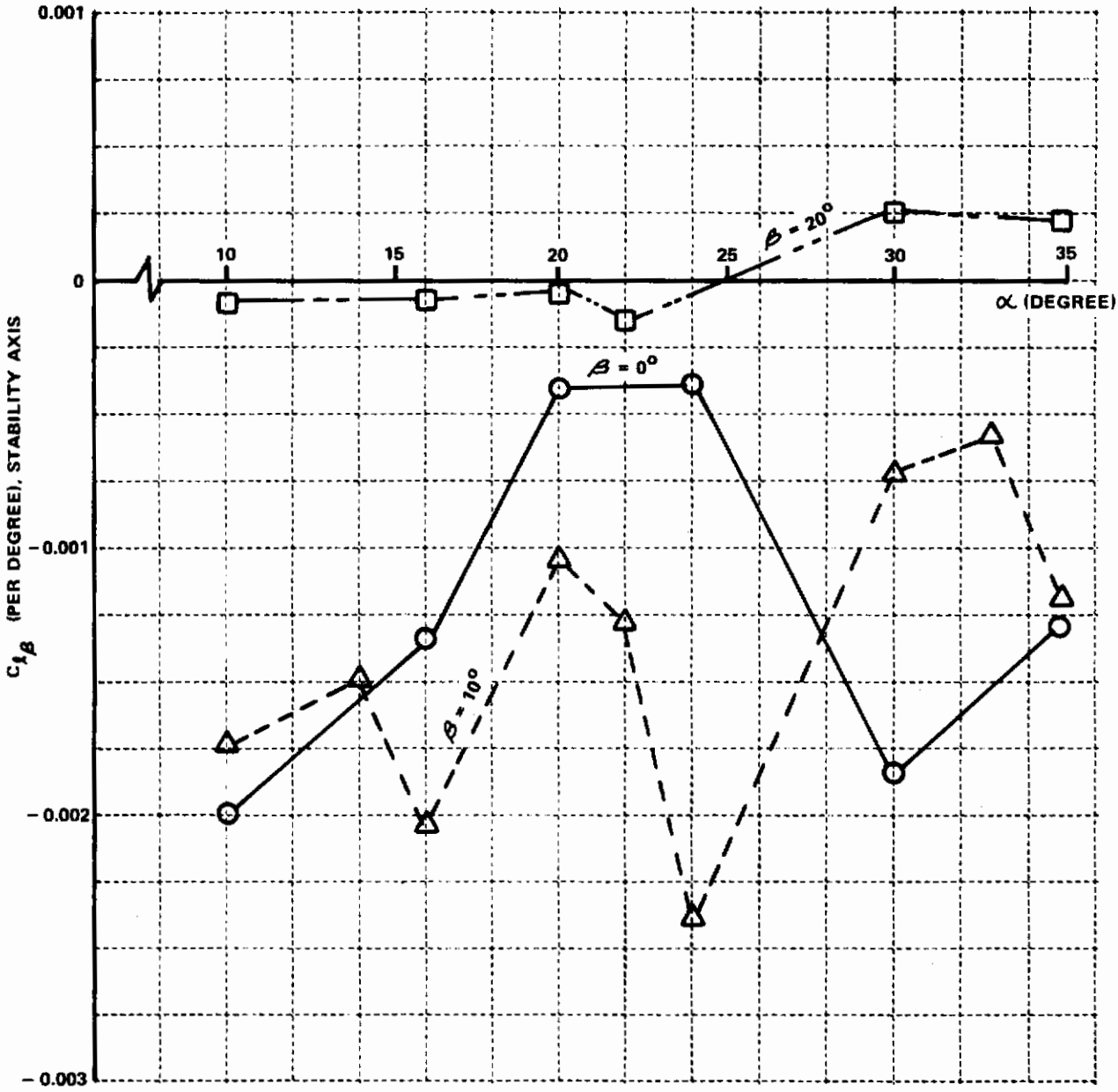

Figure 4 C_{l_β} (α) AT β = 0°, 10°, AND 20°

Indeed, as shown in Figure 3, the directional static derivative C_{n_β}, in stability axes, becomes destabilizing at $\alpha \cong 20°$ for $\beta = 0°$ and becomes destabilizing at 11° angle of attack for $\beta = 20°$. Figure 4 also shows the existence of distinctly different characteristics for the lateral static stability derivative (the dihedral effect), C_{l_β}, in the stability axis, for $\beta = 0°$ and for $\beta = 20°$. At $\beta = 20°$, the lateral static stability becomes practically zero for $\alpha = 10°$ through $\alpha = 25°$. The characteristics of the directional static stability, as shown in Figure 3, tended to verify the observation from flight test as discussed earlier, that the effect of sideslip was to cause the airplane to depart at a reduced angle of attack.

A nonlinear six-degree-of-freedom digital computer program incorporating the A-7 wind tunnel data for high angles of attack was then used to verify and refine the departure characteristics by applying several values of the initial sideslip, β_o, from some isolated equilibrium conditions in the vicinity of stall/departure angles of attack. Figures 5a and 5b show an example of these departure characteristics; at a trim angle of attack of 17°, the airplane did not depart at $\beta_o = 10°$, but it departed (increase in α, β, and yaw rate) at $\beta_o = 30°$. As shown in Figure 6, the six-degree-of-freedom digital simulation verified the general trend of α vs β at the departure.

The α-β departure boundary shown in Figure 6 and defined by the relationship

$$\left.\begin{aligned} \alpha^* &= C_1 - C_2 |\beta| && |\beta| \leq 30° \\ &= C_1 - 30 C_2 && |\beta| > 30° \end{aligned}\right\} \qquad (2\text{-}1)$$

with $C_1 = 20$, $C_2 = 0.2$.

was determined from the digital simulation for straight and level flight at a moderate gross weight and center of gravity location (G.W. = 31,000 lb, c.g. - 30% MGC). The effects of the c.g. location, gross weight, and turn rates (up to 15 deg/sec and 3.5 g level turns) were determined as shown in Figures 7 and 8. It is seen that these effects were relatively insignificant, and modification of the departure boundary established was deemed to be unwarranted.

By comparing the departure boundary defined in Figure 6 with Figure 2, it appears that the boundary determined from the wind tunnel data seems to be somewhat conservative in comparison with that obtained from the flight test. However, it should be noted here that the data presented on Figure 2 must be used with caution. These data were obtained from the stall/spin time histories reported in Reference 8, which were presented in a rather small scale and a precise read-out of the α and β at the departure from these time histories was not feasible. Also, the correction of the position errors in the measurements of the α and β vanes was

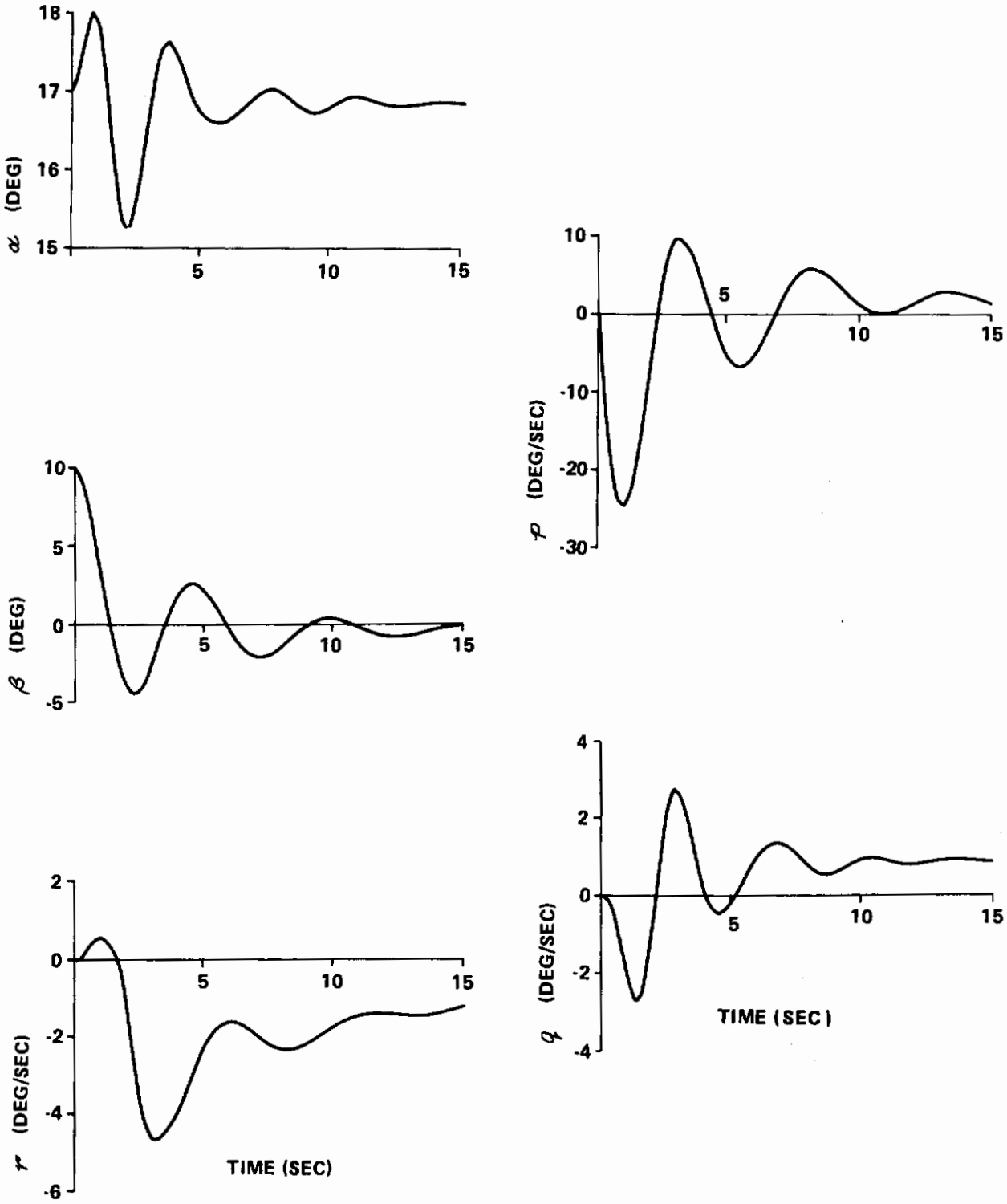

Figure 5 RESPONSES TO INITIAL SIDESLIP
a) 10 DEGREE SIDESLIP

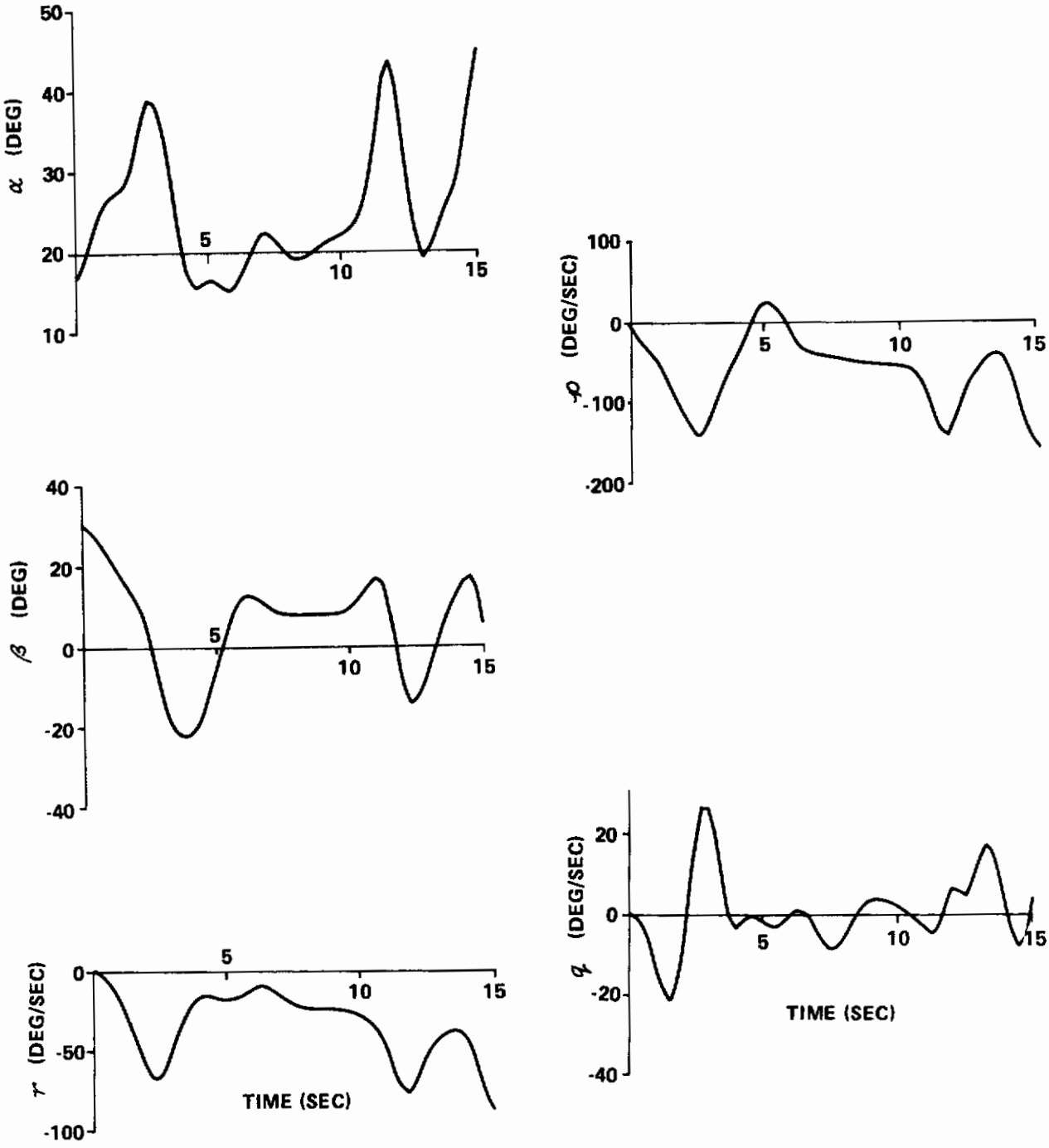

Figure 5 RESPONSES TO INITIAL SIDESLIP
b) 30 DEGREE SIDESLIP

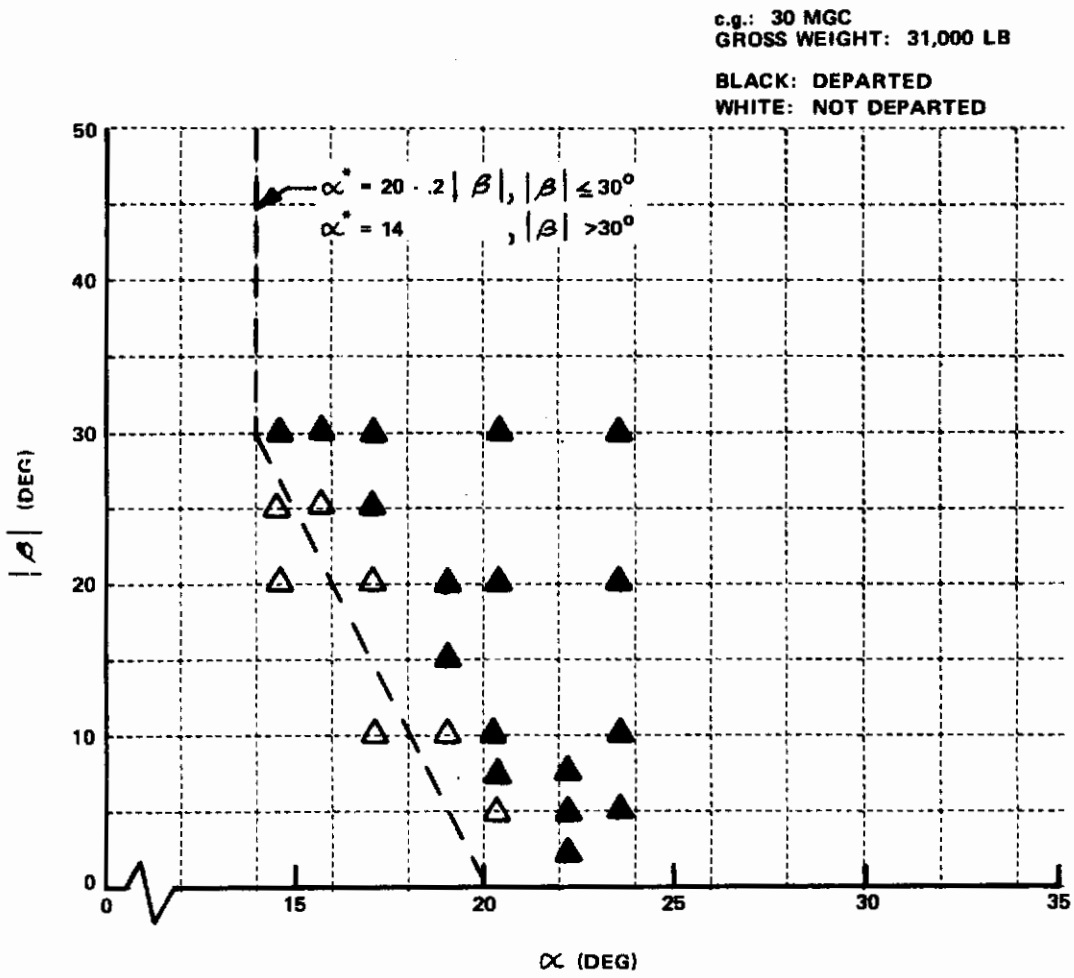

Figure 6 A-7 DEPARTURE CHARACTERISTICS OBTAINED FROM COMPUTER SIMULATION

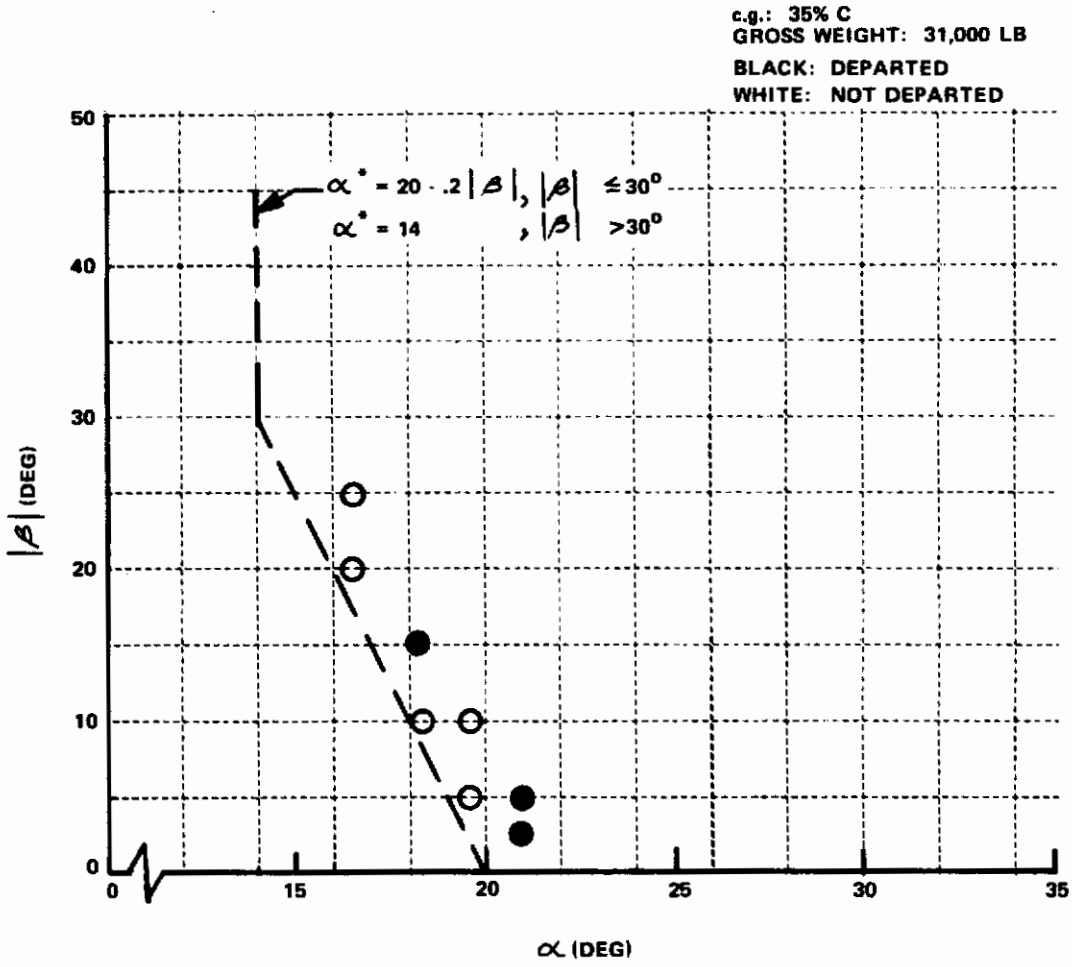

Figure 7 EFFECT OF AFT c.g. ON DEPARTURE

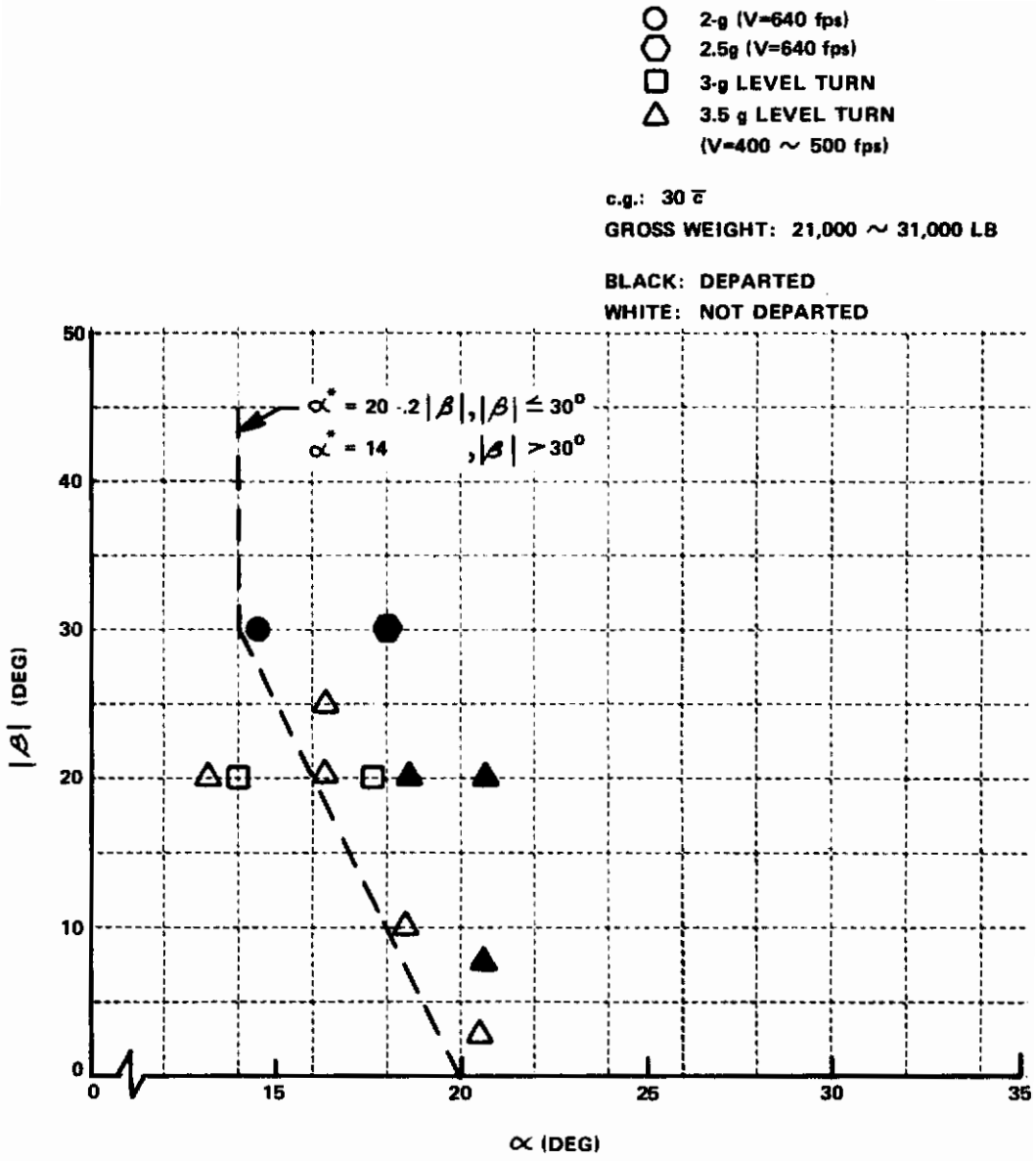

Figure 8 EFFECT OF HIGH g TURNS ON DEPARTURE

done only for the effects of angular velocities of the aircraft motion; other error sources such as possiblity of offset error in α were not assessed.

An attempt was made earlier in the program to correlate the wind tunnel data with the flight data. The computer runs showed that the computer-generated aircraft motion did not have good match with the flight test data. Because of the relatively low quality of the flight test data, no further attempt was made to identify the stability and control parameters of the A-7 aircraft to achieve a better representation of the aerodynamic coeffients for computer simulation. However, to allow for possible discrepancy of the wind tunnel data and the full-scale A-7 aircraft aerodynamic characteristics, the coefficients, C_1 and C_2 , defining the departure boundary were varied in the digital program and their effects were evaluated in the design of the stall inhibitor and the departure preventer. Also, C_1 and C_2 were mechanized as variables in the breadboard of the stall inhibitor and the departure preventer. These evaluations and design considerations are discussed in the following sections.

SECTION III

CONCEPTUAL DESIGN OF THE DEPARTURE PREVENTER

3.1 DESIGN OBJECTIVES AND APPROACH

The design objectives of the departure preventer were twofold:

(1) The preventer must be able to prevent the aircraft from departing into a post stall gyration without degrading the full operational flight envelope of the aircraft.

(2) The preventer must be automatic, simple, and readily adaptable to the existing A-7D flight control system.

To best meet the second objective, it is clear that the preventer must work within the existing Automatic Flight Control System (AFCS) of the A-7D aircraft as shown in the schematic diagrams of Figures 9 through 11. A description of the A-7D flight control system and the simplifications used for the computer simulation are given in Appendix I.

To achieve the first objective, the preventer should perform the following functions:

1. In view of the departure boundary determined in the previous section, it seems appropriate that

   (a) The device should command a longitudinal control action necessary to regulate the aircraft motion at the departure boundary. Specifically, at a given angle of attack in the stall departure region, a nose-down moment must be automatically applied to reduce the angle of attack whenever the angle of sideslip exceeds the boundary, defined by Equation (2.1). In addition, at a given sideslip, a nose down moment must be automatically applied to reduce the angle of attack, whenever α exceeds the boundary.

   (b) The sideslip should be reduced or eliminated in the stall departure region to increase the maximum usable angle of attack to its full capability for the aircraft. To achieve this the directional stiffness of the aircraft should be augmented at the stall boundary, and furthermore the aircraft should be restricted to roll about its flight path.

2. The preventer must not hinder the pilot from using any of the cockpit controls. This avoids degradation of the aircraft's maximum capability while performing the departure prevention function and also provides an override capability to satisfy pilots that the device will not take control of the airplane away from the pilot.

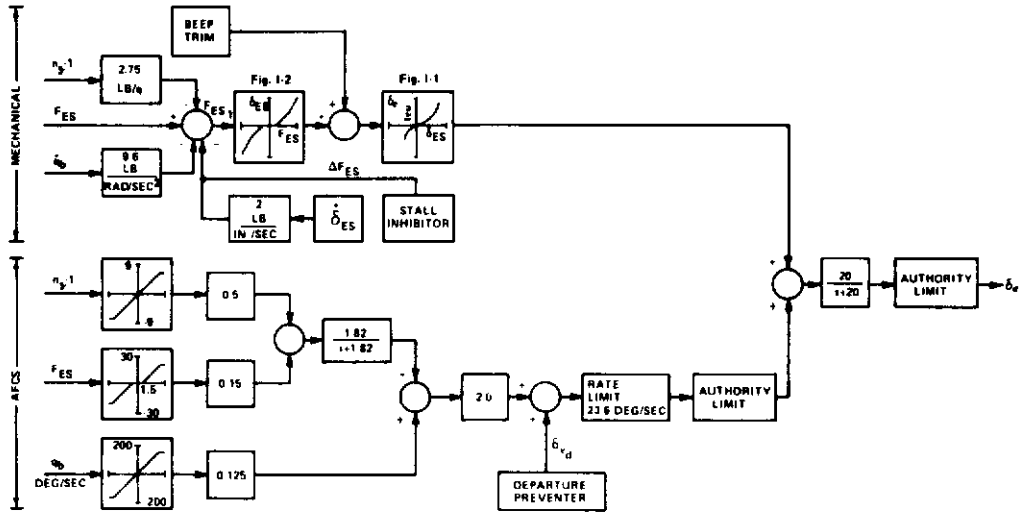

Figure 9 PITCH AXIS SIMULATION -- CRUISE CONFIGURATION

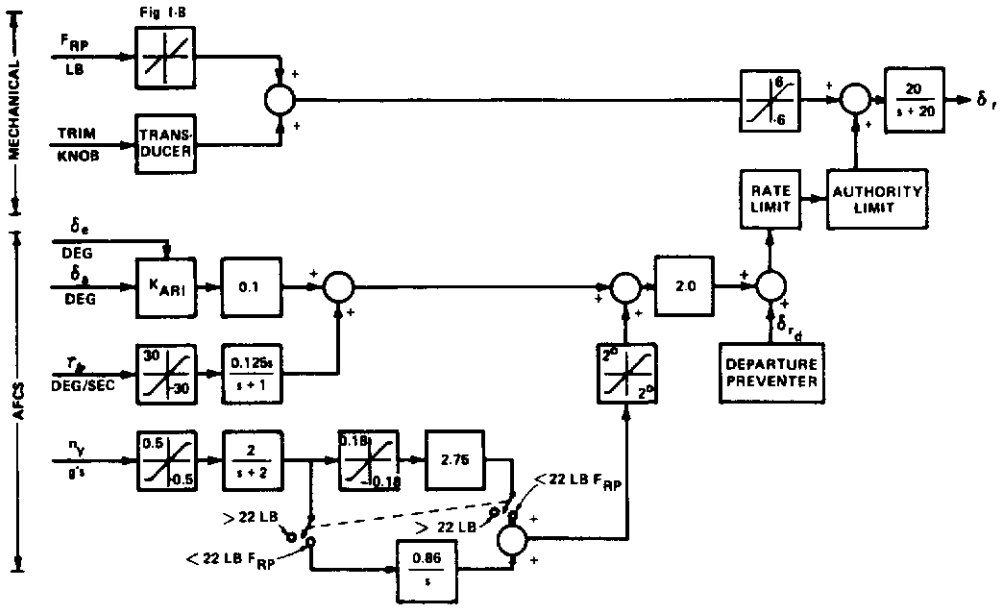

Figure 10 YAW AXIS SIMULATION -- CRUISE CONFIGURATION

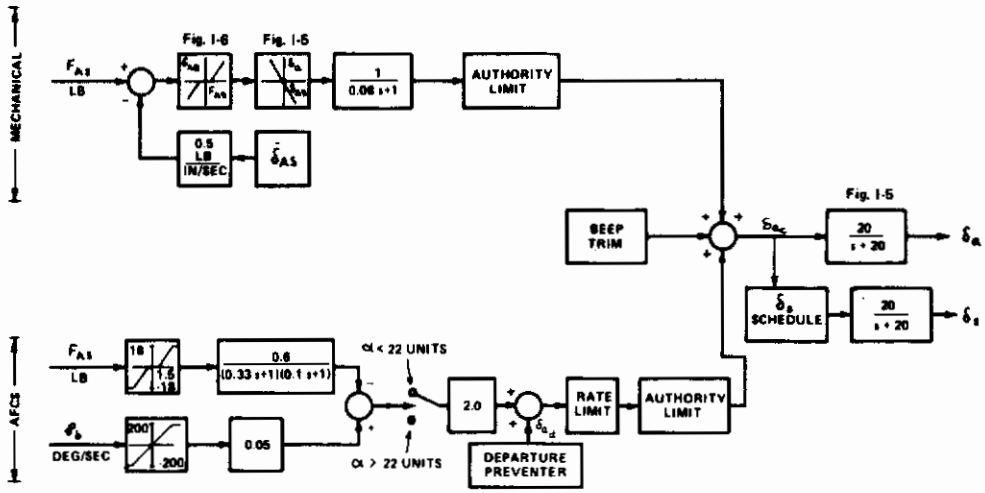

Figure 11 ROLL AXIS SIMULATION -- CRUISE CONFIGURATION

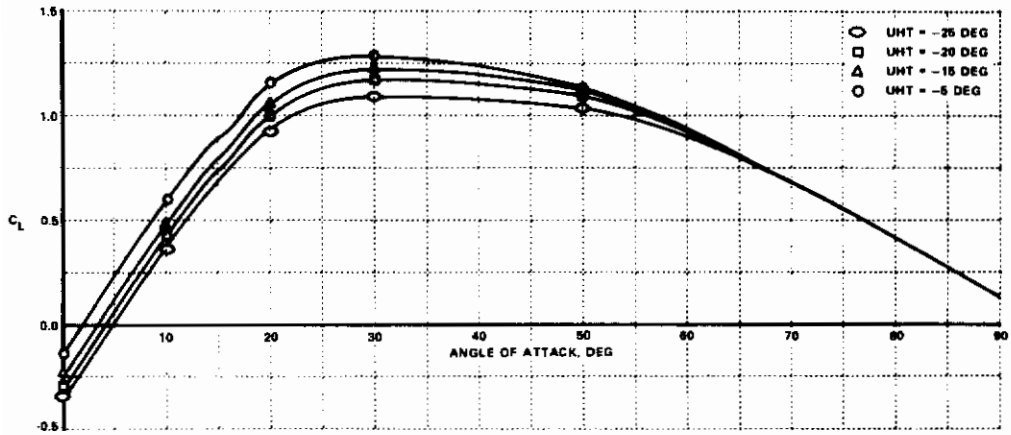

Figure 12 A-7 LIFT COEFFICIENTS FOR A RANGE OF UHT DEFLECTIONS

The control law of the departure preventer evolved from these functional requirements. The development is discussed in the following section.

3.2 DEVELOPMENT OF THE DEPARTURE PREVENTER CONTROL LAW

A. Control Law Formulation

To regulate the angle of attack along the departure boundary, a simple proportional control law for the longitudinal control may be used:

$$\left.\begin{aligned} \delta_{e_d} &= K_1 (\alpha - \alpha^*) \quad \text{if } \alpha - \alpha^* \geq 0 \\ &= 0 \qquad\qquad\quad \text{if } \alpha - \alpha^* < 0 \end{aligned}\right\} \tag{3-1}$$

where α^* is given in Equation (2-1). With a proper selection of the proportional gain K_1, the steady offset resulting from the proportional control will permit the pilot to use the full capability of the aircraft well beyond the previous departure angle of attack toward the conventional aerodynamic stall. This is clear by comparing Figure 6 with Figure 12. (For A-7D the maximum lift coefficient occurs at 28° ~ 30° angle of attack depending on the unit horizontal tail (UHT) position as shown in Figure 12.) In fact, these figures further suggest that a tight or zero steady offset regulation, such as proportional plus integral control, would not be desirable, for it would hinder the pilot from using the full capability of the aircraft.

Substituting (2-1) into (3-1) yields

$$\begin{aligned} \delta_{e_d} &= K_1(\alpha - C_1) + K_1 C_2 |\beta|, && \text{if } \alpha - \alpha^* \geq 0 \text{ and } |\beta| \leq 30^\circ \\ &= K_1(\alpha - C_1) + 30 K_1 C_2, && \text{if } \alpha - \alpha^* \geq 0 \text{ and } |\beta| > 30^\circ \\ &= 0, && \text{if } \alpha - \alpha^* < 0 \end{aligned}$$

Thus, once activated, the departure preventer will command a trailing-edge-down UHT whenever α or $|\beta|$ or both increase, thereby achieving the desirable function. Notice that there will be no transients associated with the activation and de-activation in the longitudinal portion of the departure preventer.

For lateral control, it is desirable to permit the pilot to use the aileron without restriction, i.e.,

$$\delta_{a_d} = 0.$$

Earlier in the design of the departure preventer though, consideration was given to the neutralization of the lateral control upon activation of the departure preventer. A scheme utilizing a proportional plus integral nullification of pilot and AFCS δ_a commands as shown in Figure 26 (Section V) was mechanized on the breadboard of the departure preventer. The motivation was from knowledge that use of the lateral control in the near-stall region often aggravates inadvertent departures as discussed previously in Section II. However, with the longitudinal portion of the departure preventer which tends to limit the excursion of the angle of attack beyond the departure boundary and with the directional portion of the departure preventer which nullifies the sideslip as will be discussed later. The lateral control of the departure preventer becomes unnecessary, thus permitting the pilot to use freely the lateral control for roll maneuver upon activation of the departure preventer.

For the directional control, the main departure prevention function is to keep β small. This is accomplished by use of a proportional plus integral feedback of β to the rudder in addition to the feedback of stability-axis yaw rate, r_s, to the rudder.

$$\left.\begin{aligned} \delta_{r_d} &= K_4\beta + K_5\int\beta + K_6 r_s \qquad \text{if } \alpha-\alpha^* \geq 0 \\ &= 0 \qquad\qquad\qquad\qquad\quad \text{if } \alpha-\alpha^* < 0 \end{aligned}\right\} \tag{3-2}$$

The use of the stability axis yaw rate feedback to the rudder is to restrict the airplane to roll about its flight path. It also tends to minimize the effect of inertia coupling from the longitudinal to lateral-directional motions which is a very desirable feature. To see this, consider the rolling moment and yawing moment equations,

$$L = I_x\dot{p} - I_{xz}\dot{r} + (I_z - I_y)qr - I_{xz}pq$$

$$N = I_z\dot{r} - (I_x - I_y)pq - I_{xz}(\dot{p} - qr)$$

which can be combined to give

$$\left.\begin{aligned} \dot{p} &= \frac{1}{I_xI_z - I_{xz}^2}\left\{q\left[I_{xz}(I_x - I_y + I_z)p + (I_yI_z - I_z^2 - I_{xz}^2)r\right] + I_zL'\right\} \\ \dot{r} &= \frac{1}{I_xI_z - I_{xz}^2}\left\{q\left[(I_x^2 - I_xI_y + I_{xz}^2)p + I_{xz}(I_y - I_z - I_x)r\right] + I_xN'\right\} \end{aligned}\right\} \tag{3-3}$$

where

$$L' \triangleq L + \frac{I_{xz}}{I_z}N \qquad N' \triangleq N + \frac{I_{xz}}{I_x}L \tag{3-4}$$

By expressing L' and N' in the following way

$$\left.\begin{aligned} N' &\cong \bar{q}\, Sb\left[C'_{n_\beta}(\alpha)\beta + C'_{n_{\delta_a'}}(\alpha)\delta_a' + C'_{n_{\delta_r}}(\alpha)\delta_r \right.\\ &\qquad \left. + \frac{b}{2V}\left(C'_{n_p}(\alpha)p + C'_{n_r}(\alpha)r\right)\right] \\ L' &\cong \bar{q}\, Sb\left[C'_{\ell_\beta}(\alpha)\beta + C'_{\ell_{\delta_a'}}(\alpha)\delta_a' + C'_{\ell_{\delta_r}}(\alpha)\delta_r \right.\\ &\qquad \left. + \frac{b}{2V}\left(C'_{\ell_p}(\alpha)p + C'_{\ell_r}(\alpha)r\right)\right] \end{aligned}\right\} \qquad (3\text{-}5)$$

where the static derivatives $C'_{n_\beta}(\alpha)$ and $C'_{\ell_\beta}(\alpha)$ were obtained for $\beta = 0°$. These and other derivatives for the A-7 aircraft in uncompressible flow are plotted as functions of α as shown in Figures 13 and 14. The inertia coupling terms from the pitch rate entering in the lateral-directional motions produce damping effects. Indeed, combining (3-3) and (3-5) yields

$$\left.\begin{aligned} \dot{p} &= L_\beta(\alpha)\beta + L_{\delta_a'}(\alpha)\delta_a' + L_{\delta_r}(\alpha)\delta_r + L_p(\alpha)p + L_r(\alpha)r \\ \dot{r} &= N_\beta(\alpha)\beta + N_{\delta_a'}(\alpha)\delta_a' + N_{\delta_r}(\alpha)\delta_r + N_p(\alpha)p + N_r(\alpha)r \end{aligned}\right\} \qquad (3\text{-}6)$$

where "effective" damping derivatives have been found:

$$\left.\begin{aligned} L_r &= \frac{1}{I_x I_z - I_{xz}^2}\left[\left(I_y I_z - I_z^2 - I_{xz}^2\right)q + I_z \bar{q}\,\frac{Sb^2}{2V}C'_{\ell_r}(\alpha)\right] \\ L_p &= \frac{1}{I_x I_z - I_{xz}^2}\left[I_{xz}\left(I_x - I_y + I_z\right)q + I_z \bar{q}\,\frac{Sb^2}{2V}C'_{\ell_p}(\alpha)\right] \end{aligned}\right\} \qquad (3\text{-}7)$$

$$N_r = \frac{1}{I_x I_z - I_{xz}^2}\left[I_{xz}\left(I_y - I_z - I_x\right)q + I_x \bar{q}\,\frac{Sb^2}{2V}C'_{n_r}(\alpha)\right]$$

$$N_p = \frac{1}{I_x I_z - I_{xz}^2}\left[\left(I_x^2 - I_x I_y + I_{xz}^2\right)q + I_x \bar{q}\,\frac{Sb^2}{2V}C'_{n_p}(\alpha)\right]$$

etc.

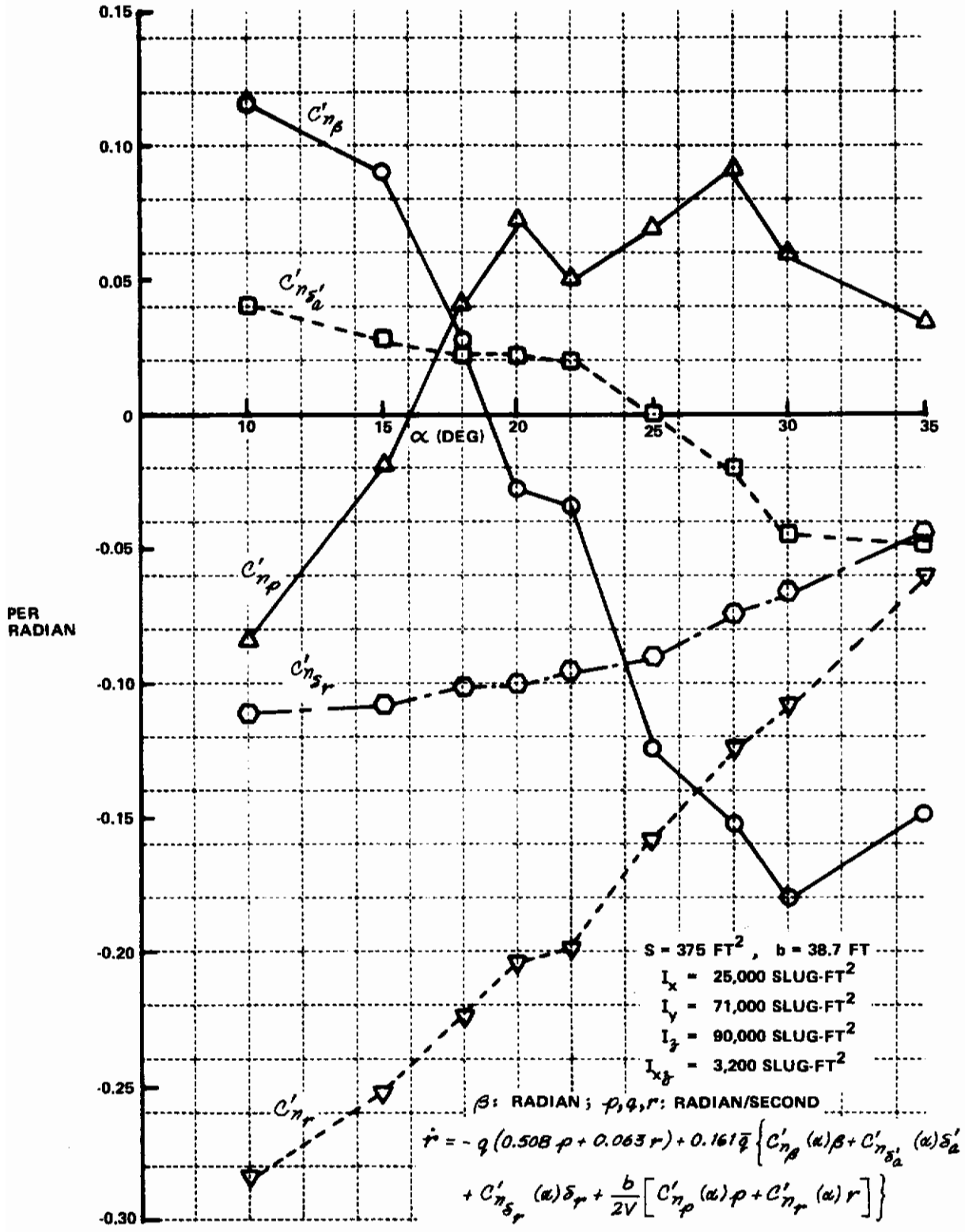

Figure 13 EFFECTIVE AERODYNAMIC YAWING MOMENT CONTRIBUTIONS - BODY AXES

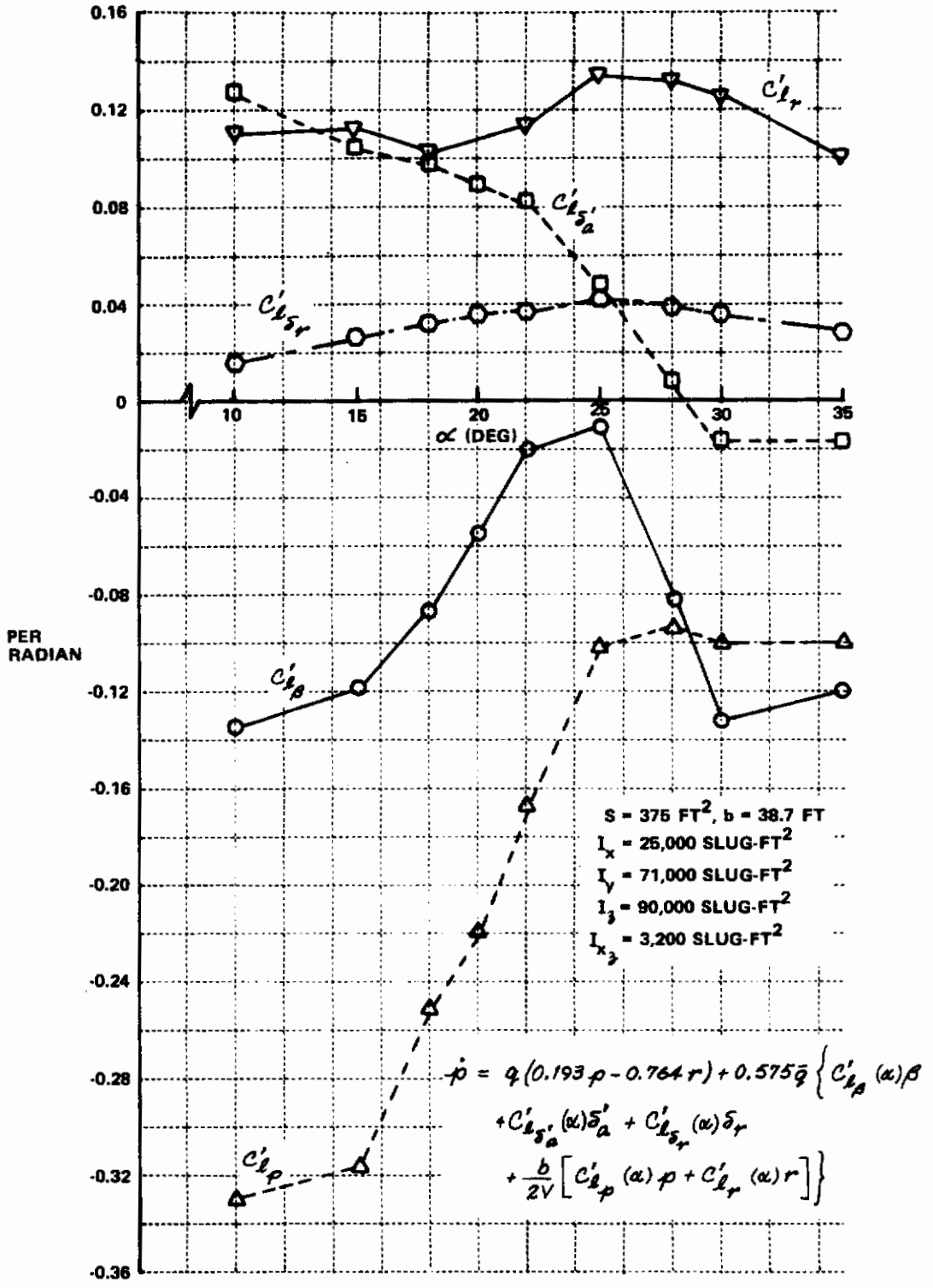

Figure 14 EFFECTIVE AERODYNAMIC ROLLING MOMENT CONTRIBUTIONS - BODY AXES

Figures 15 and 16 show the effective dampings as functions of α for a flight condition of M = 0.4 and h = 25,000 feet. The interesting characteristics of these effective dampings are worth noting: The "direct dampings" $N_r(\alpha)$ and $L_p(\alpha)$ are mainly aerodynamic, while the "cross dampings" $N_p(\alpha)$ and $L_r(\alpha)$ are predominantly due to the inertia coupling, and their signs depend therefore on the sign of q. From Equations (3-6) and (3-7), it will now be shown that the use of the stability-axis yaw rate feedback to rudder can augment the "cross dampings" $N_p(\alpha)$ and $L_r(\alpha)$ such that the effect of the inertia coupling becomes negligible compared to the aerodynamic effects. Let the stability-axis yaw rate, $r_s = r\cos\alpha - p\sin\alpha$, be approximated by

$$r_s \approx r - p\alpha$$

for $\alpha < 25^\circ$ say. Then with the control law of the form

$$\delta_r = K(r - p\alpha)$$

where the gain K is a positive quantity, Equation (3-6) becomes

$$\left.\begin{aligned} \dot{p} &= \left[L_p(\alpha) - K\alpha L_{\delta_r}(\alpha)\right]p + \left[L_r(\alpha) + K L_{\delta_r}(\alpha)\right]r + \dots \\ \dot{r} &= \left[N_p(\alpha) - K\alpha N_{\delta_r}(\alpha)\right]p + \left[N_r(\alpha) + K N_{\delta_r}(\alpha)\right]r + \dots \end{aligned}\right\} \qquad (3\text{-}6a)$$

Notice from Figures 13 and 14 that $L_{\delta_r}(\alpha) > 0$, $N_{\delta_r}(\alpha) < 0$ within the range of angle of attack of interest. It can readily be seen from (3-6a) and (3-7) that the aerodynamic effects of the cross dampings L_r and N_p increase as the feedback gain K increases, thus minimizing the effect of the inertia coupling. Furthermore, as desired, the direct dampings L_p and N_r also increase as K increases. This desirable feature was utilized in the initial selection of the value of the gain K.

The use of the proportional plus integral feedback of β to the rudder was aimed at keeping β near zero in the near-departure region, since there are no known maneuvers that call for intentional sideslip in the post-stall region. As a matter of fact, since rolling is not restricted $\int\beta$ feedback is required when the bank angle is large ($\approx 90^\circ$). With large bank angle, the gravitation force can develop substantial side force and thereby generate a large sideslip. Through the use of integral β feedback, the angle of sideslip can be reduced.

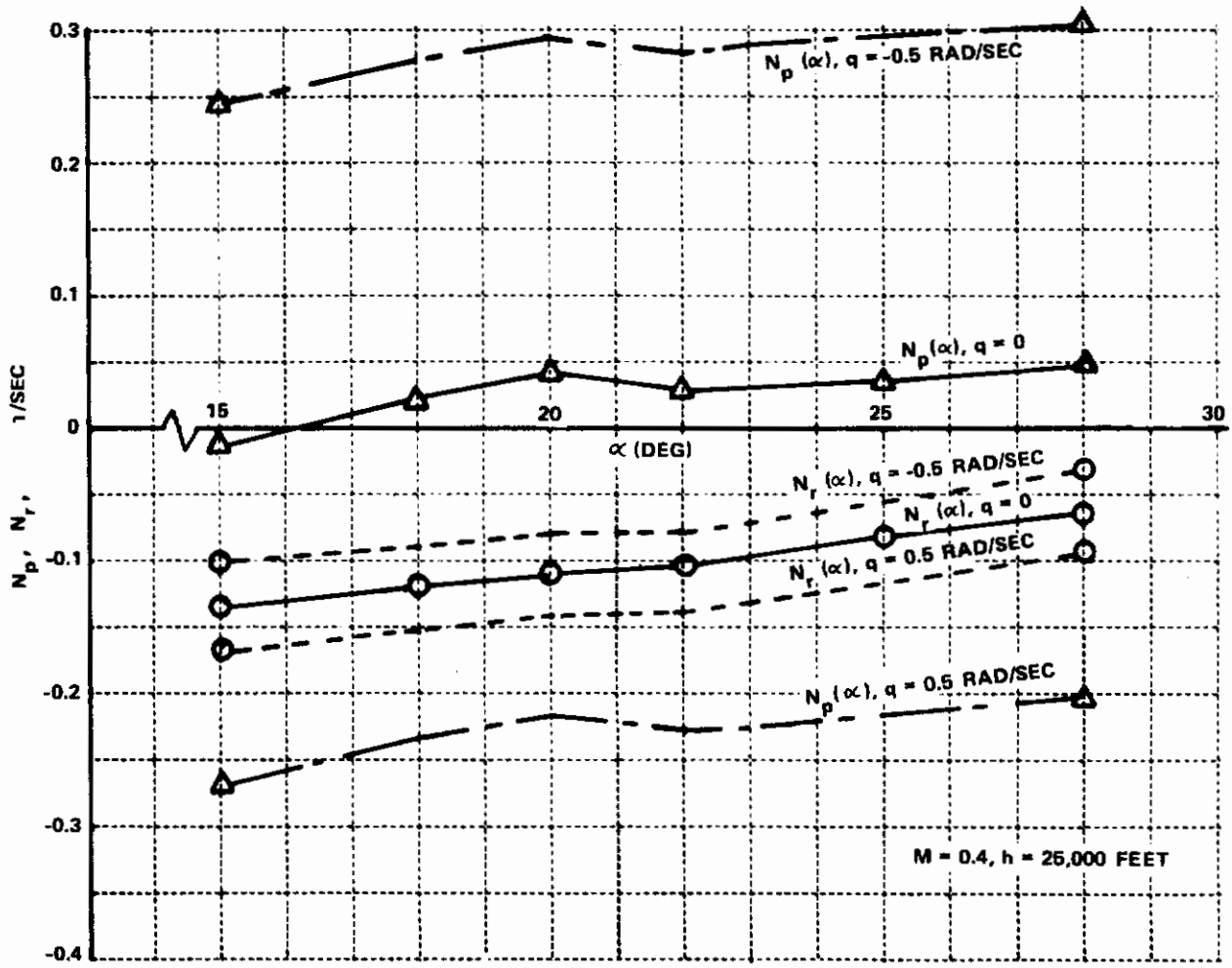

Figure 15 EFFECTIVE DAMPINGS, N_p, N_r

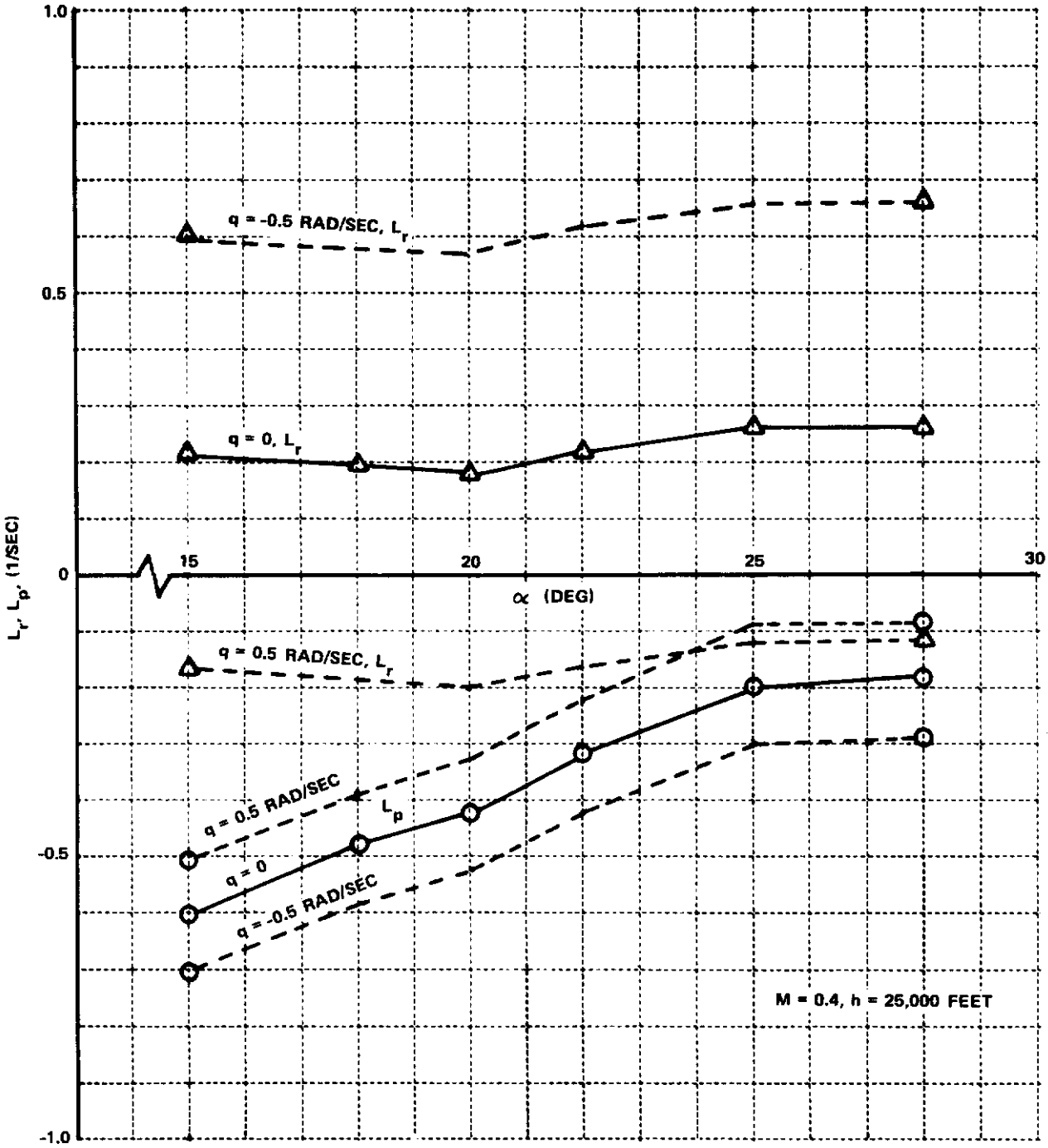

Figure 16 EFFECTIVE DAMPINGS, L_p, L_r

B. Further Considerations and Refinement

Some modifications of the above set of simple control laws were required to achieve better departure prevention. First, the switching boundary that activates the departure preventer was modified to include an anticipation term, $C_3\dot{\alpha}$, to account for rapid changes in angle of attack maneuvering. For the existing authority and rate limit of the pitch AFCS of the A-7D aircraft, it was found desirable to have C_3 in the range of 0.1 to 0.3 deg/deg/sec. The modified switching boundary became

$$\alpha^* = C_1 - C_2|\beta| - C_3\dot{\alpha} \tag{3-8}$$

Thus, when the departure preventer is activated, i.e., $\alpha - \alpha^* \geq 0$, the control law for the pitch axis becomes

$$\delta_{e_d} = K_1(\alpha - C_1) + K_1 C_2|\beta| + K_1 C_3\dot{\alpha} \tag{3-9}$$

It is seen that the modified switching boundary provides a desirable damping term in the longitudinal control law. Since the stiffness of the pitch axis was increased by the proportional feedback $K_1(\alpha - C_1)$, a pitch damping term $K_q q$ was thought to be desirable for independent adjustment of resulting pitch damping. Subsequent digital simulation, however, indicated that the term $K_q q$ introduced an annoying transient during the activating and de-activating of the departure preventer because of the residual pitch rate. Consequently the term $K_q q$ was dropped, and a satisfactory result was achieved by proper adjustment of $C_3\dot{\alpha}$.

In the presence of turbulence, it was felt, the anticipation term $C_3\dot{\alpha}$ could become excessively large, thereby causing "premature" activation and de-activation of the departure preventer. A possible substitution for the anticipation term $C_3\dot{\alpha}$ was therefore sought.

Neglecting the effect of speed changes, which are slow by comparison, the trim rate of change of angle of attack may be approximated by considering the short-period approximate transfer functions in response to elevator deflection

$$\frac{\dot{\alpha}(s)}{\delta_e(s)} = \frac{Z_\delta}{V_o} s \left(s + \frac{V_o M_\delta}{Z_\delta}\right) \Big/ (s^2 + 2\zeta_{sp}\omega_{sp} s + \omega_{sp}^2)$$

$$\frac{q(s)}{\delta_e(s)} = M_\delta (s - Z_w) \Big/ (s^2 + 2\zeta_{sp}\omega_{sp} s + \omega_{sp}^2)$$

The α numerator inverse time constant, $V_o M_\delta / Z_\delta$, is normally large, overpowering s at short period frequencies. Then we have for control-induced motion at frequencies of interest

$$\dot{\alpha}(s) \approx \frac{s}{s - \frac{Z_w}{V_o}} q(s) \tag{3-10}$$

which may be obtained by feeding the pitch rate signal, $q(t)$ (which is generally a smooth signal) through a high pass circuit. Subsequent digital simulation showed that the substitution of the lead term $(s/s+.25)\, q(s)$ for a direct $\dot{\alpha}$ term proved to be adequate and desirable.

The modifications and refinement of the directional control law were pursued in the following two areas: the yaw rate feedback and the proportional gain of the β feedback. To provide better steady-state performance in a coordinated turn, the pure proportional gain for the stability-axis yaw rate feedback loop was replaced by a high-pass circuit with a washout time constant of approximately 1 second. This time constant and the gain were determined from a root locus analysis using the linearized lateral-directional equations of motion. The directional control law for the departure preventer finally took the following form:

$$\delta_{r_d} \begin{cases} = (K_4 + \frac{K_5}{s})\beta + \frac{K_7 s}{s+1}(r - \alpha_p), & \alpha - \alpha^* \geq 0 \\ = 0, & \alpha - \alpha^* < 0 \end{cases} \tag{3-11}$$

It should be noted here that the integrator in the above expression does not start to integrate until $\alpha - \alpha^*$ exceeds zero. If $\alpha - \alpha^*$ becomes less than zero, the integrator resets the zero output, thus assuring that the integrator has a zero initial condition when the departure preventer is activated.

The form of the proportional gain of the β feedback to the rudder K_4 is modified to be a function of $\alpha - \alpha^*$ rather than just a constant such as K_5 and K_7 in Equation (3-11). Two factors were considered in this modification: (1) To prevent the undesirable transients in the lateral-directional motion of aircraft associated with the activation and the de-activation of the departure preventer because of nonzero β and (2) To compensate for C_{n_β}, which is a function of both α and $|\beta|$ (see Figure 3). By choosing K_4 as a linear function of $\alpha - \alpha^*$ such as

$$K_4 = c(\alpha - \alpha^*) \tag{3-11a}$$

where c is a constant (negative), $K_4 = 0$ at the activation and de-activation of the departure preventer. Thus, the first factor is satisfied. Now substituting (3-11a) into(3-8) yields

$$K_4 = c(\alpha - C_1) + cC_2|\beta| + cC_3\dot{\alpha} \tag{3-11b}$$

which shows that K_4 is a function of α, $|\beta|$ and $\dot{\alpha}$, and that $-K_4$ increases as α and $|\beta|$ increase. Thus, a good compensation for C_{n_β} may be achieved by an appropriate choice of c.

The initial determination of the gains in the departure preventer was based largely on physical considerations. For example, K_4 was chosen so that when $\alpha - \alpha^* = 2 \sim 4°$, the value of the augmented directional static stability, $C_{n_\beta}(\alpha) + K_4 C_{n_{\delta_r}}(\alpha)$, would achieve the level of C_{n_β} at low angles of attack, say at $\alpha = 0$ to 10°. The stability-axis yaw rate feedback gain K_7 was initially determined such that at Dutch roll frequency and above the augmented effective cross coupled damping N_p and L_r would be predominantly aerodynamic and the effect of inertial coupling due to the pitch rate would be minimized. These gains and others were finally determined using the six-degree-of-freedom nonlinear digital simulation. The nominal values along with the switching boundary are listed below:

Switching Boundary

$$\alpha^* = C_1 - C_2|\beta| - C_3\dot{\alpha} \quad , \quad |\beta| < 30°$$

$$= C_1 - 30C_2 - C_3\dot{\alpha} \quad , \quad |\beta| \geq 30°$$

and

$\dot{\alpha}$ may be replaced by

$$\dot{\alpha}(s) = \frac{s}{s + .25}\, q(s)$$

Departure Preventer Control Laws

$$\delta_{e_d} = K_1 (\alpha - \alpha^*) \qquad \text{if } \alpha - \alpha^* \geq 0$$

$$= 0 \qquad \text{if } \alpha - \alpha^* < 0$$

$$\delta_{a_d} = 0$$

$$\delta_{r_d} = \left(K_4 + \frac{K_5}{s}\right)\beta + \frac{K_7 s}{s+1}(r - \alpha p) \qquad \text{if } \alpha - \alpha^* \geq 0$$

$$= 0 \qquad \text{if } \alpha - \alpha^* < 0$$

with K_4 being a linear function of $\alpha - \alpha^*$.

TABLE I

SWITCHING BOUNDARY COEFFICIENTS
AND DEPARTURE PREVENTER GAINS

Parameters		Nominal Values
Switching Boundary	C_1	18 ~ 20 (deg)
	C_2	.13 ~ .20 (deg/deg)
	C_3	.10 ~ .30 (deg/deg/sec)
Departure Preventer	K_1	1.0 ~ 3.0 (deg/deg)
	K_4	$-.14\ (\alpha - \alpha^*)$ (deg/deg)
	K_5	-.5 (1/sec)
	K_7	1.5 (deg/sec/sec)

In mechanization of the breadboard of the departure preventer discussed above and the stall inhibitor, which will be discussed in Section IV, it was felt simpler to use a common switching law to activate and deactivate the two devices. However, since the stall inhibitor is a warning device, it was thought desirable to have it begin to function some 2 ~ 4 degrees in angle of attack earlier than the departure preventer. To accommodate these features so that their merit may be evaluated later in the man-in-the-loop ground simulation, the gains K_1 and K_4 were mechanized as follows.

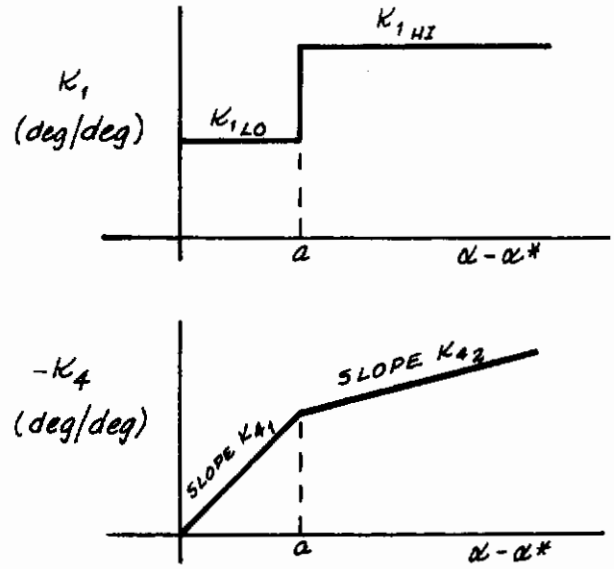

a = 2 to 4 deg

$K_{1_{LO}}, K_{1_{HI}}; K_{4_1}, K_{4_2}$ are adjustable

Details of the breadboard mechanization are described later in Section V.

3.3 DIGITAL SIMULATION AND SENSITIVITY STUDY

The A-7 aerodynamic data at high angles of attack were prepared in table form (see Appendix II) and incorporated in the existing nonlinear six-degree-of-freedom computer program of Calspan (References 14 and 15). Also incorporated in the program were the A-7D flight control system as described in Appendix I and the departure preventer control law discussed in the previous section. In simulating these analog flight control systems, some approximations and simplifications were employed. For example, for the computation involving dynamic elements such as the dynamics of the actuators and the shaping network, use was made of the discrete state transition method;* and differentiation was done using the simple rectangular or Euler method. No

*See Appendix II for details.

error analyses were attempted; however, these approximations were thought to be justifiable in view of the fairly small integration step used (Δt = .025 to .050).

Through use of the six-degree-of-freedom nonlinear digital simulation, many factors that may influence the performance of the departure preventer were evaluated. These are:

(1) Automatic roll damper cutoff

(2) Shifting the switching boundary

(3) Pitch AFCS authority increases

(4) Sensitivity to errors in α and β measurements

(5) Rudder effectiveness variation

(6) Turbulence effects

In conducting these evaluations, two fixed flight conditions at

G.W. = 31,000 lb

h = 21,200 ft

c.g. = 30% $\bar{c}$

V = 400 fps and 600 fps

were used. The control inputs used are shown in Figure 17. These inputs were not meant to be extreme and exhaustive. They were, however, pro-spin in nature and with sufficient pilot activity to permit evaluation of the possible transients associated with activation and de-activation of the departure preventer. For example, Figure 18 shows the responses of the simulated A-7D aircraft (with its existing flight control system operating) to control input 4B. As shown, the aircraft departed into a spin. With the departure preventer operating, however, the aircraft responses were smooth and without departure as shown in Figure 19.

The results of the sensitivity study are summarized in the following:

Effect of Automatic Roll Cutoff

The present basic AFCS of the A-7D aircraft will automatically disengage the roll axis augmentation when the angle of attack exceeds 22 units (approximately 18.7 degrees) thereby preventing the AFCS from producing adverse yaw to aggravate the departure. Moreover, with the present system, the pilot is trained to turn off the roll-axis AFCS manually as an additional precaution when the angle of attack exceeds 22 units. In the combat environment this will undoubtedly increase his workload. The departure prevention performance was therefore evaluated with and without automatic roll cutoff.

INPUT 3A

a. UHT STEP AND RUDDER STEP

F_{es} = 14 LB, $\delta_r = 6^o$

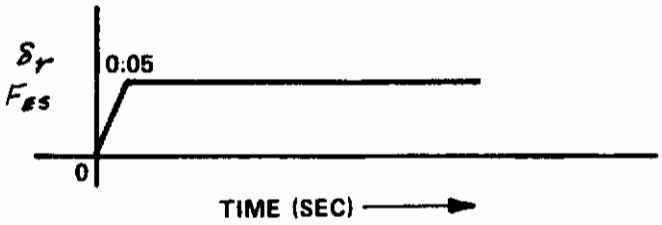

b. AILERON DOUBLET AT t = 0.5 SEC

F_{as} = 5 LB

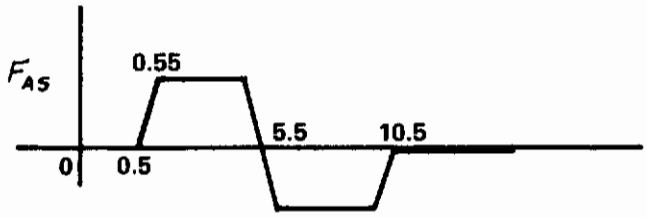

INPUT 4A

SAME AS INPUT 3A ABOVE EXCEPT F_{es} = 10 LB

INPUT 4B

a. UHT PULSE AND RUDDER PULSE

F_{es} = 100 LB, $\delta_r = 6^o$

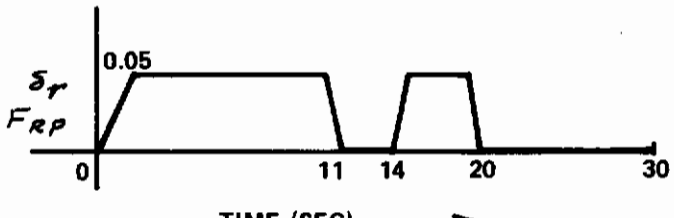

b. AILERON DOUBLETS

F_{as} = 5 LB

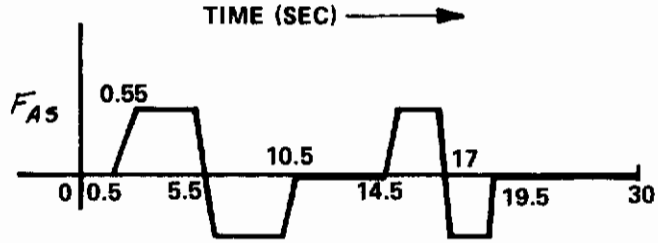

Figure 17 CONTROL INPUTS USED IN DIGITAL SIMULATION

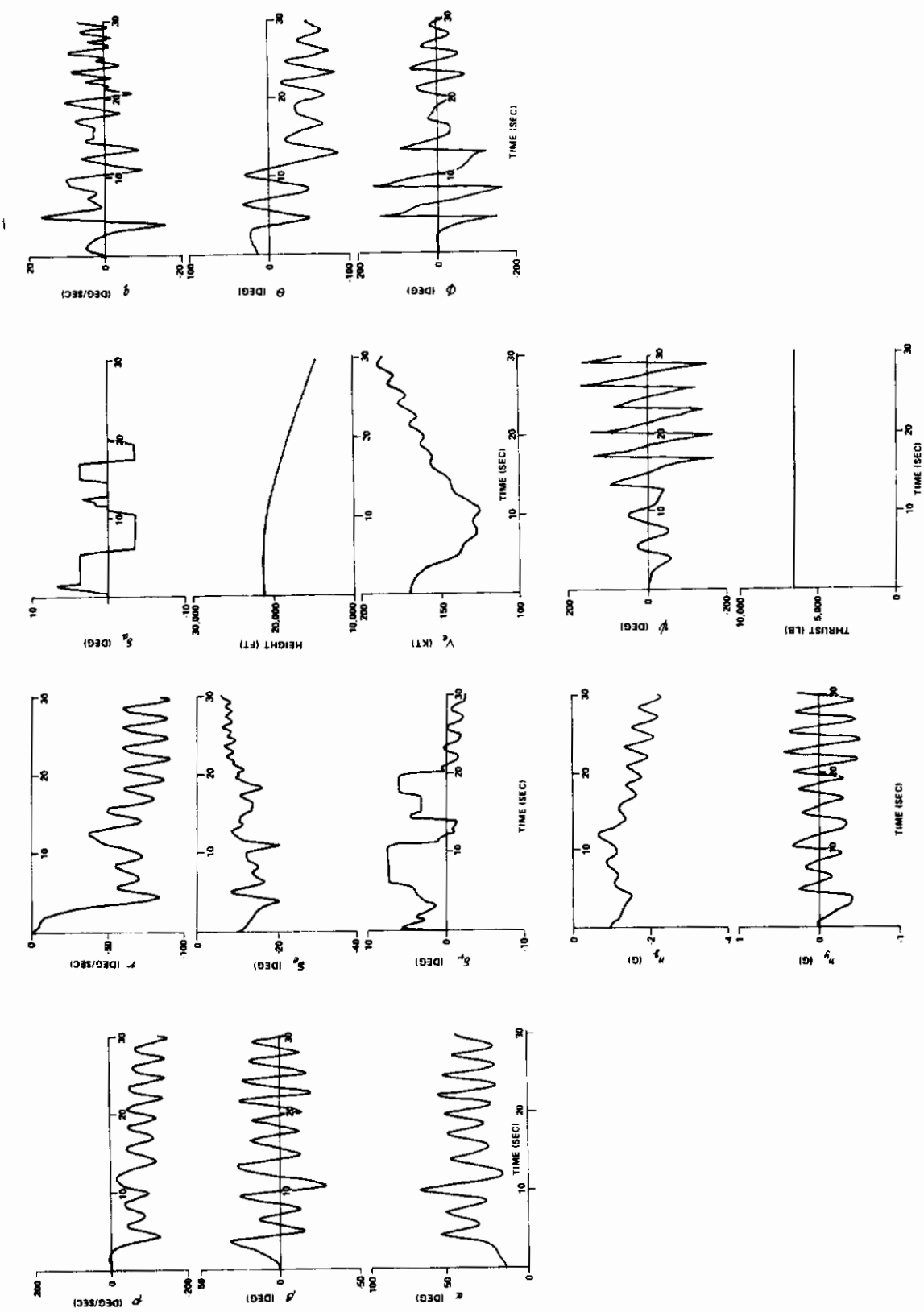

Figure 18 SIMULATED A-7D RESPONSES TO INPUT 4B (SEE FIGURE 17) - NO DEPARTURE PREVENTER

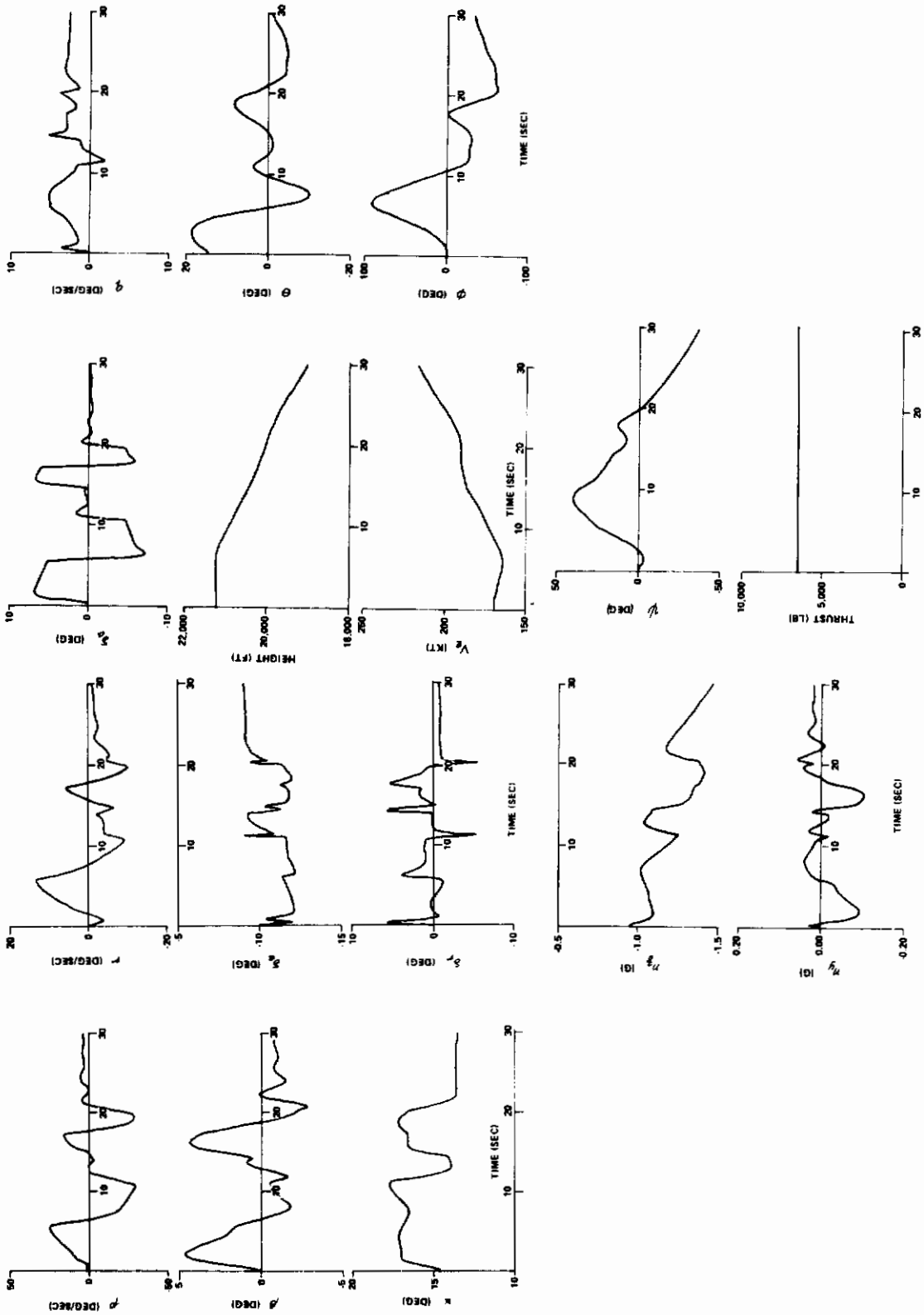

Figure 19 SIMULATED A-7D RESPONSES TO INPUT 4B WITH DEPARTURE PREVENTER ($\delta_{a_d} = 0$)

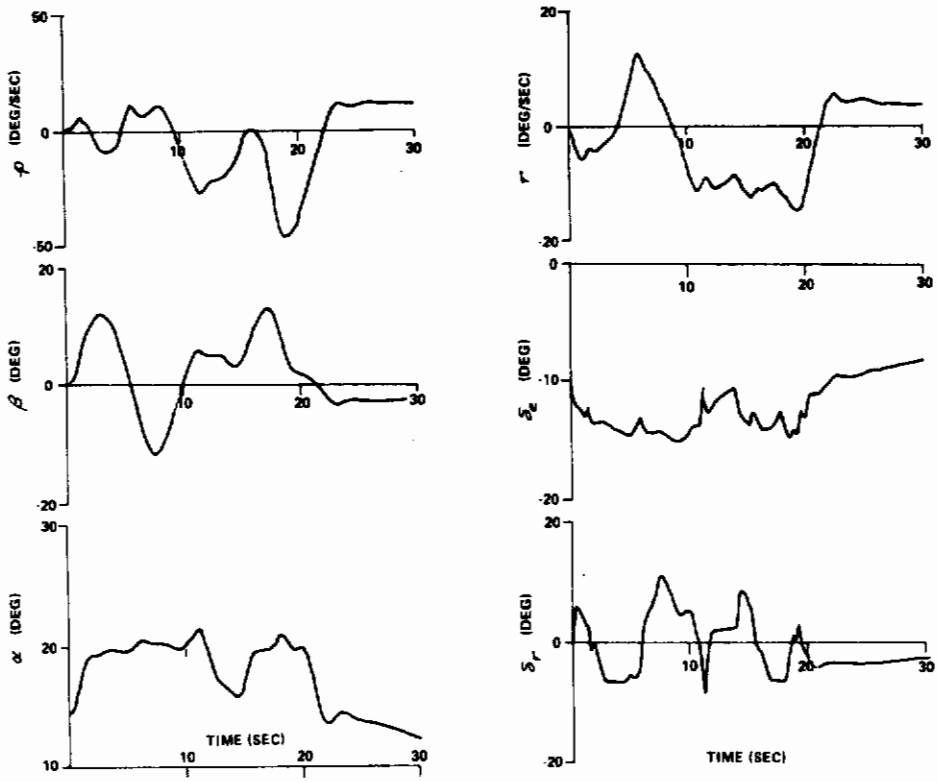

a) C_1 = 20 DEG, P.A. = ± 4 DEG

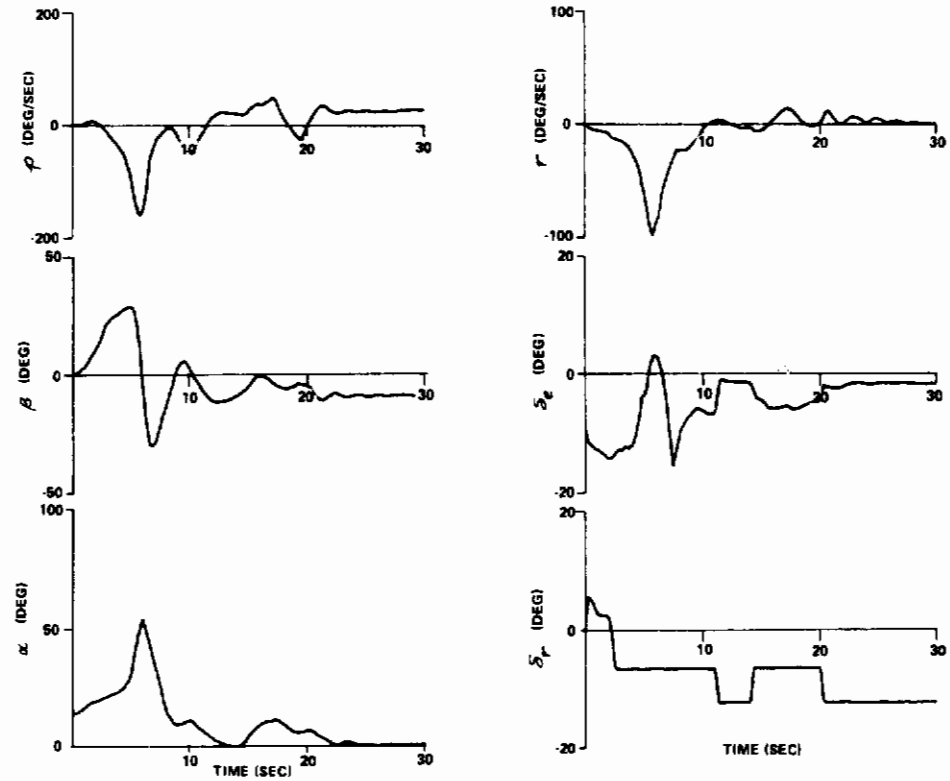

b) C_1 = 22 DEG, P.A. = ± 4 DEG

Figure 20 COMBINED EFFECT OF DEPARTURE PREVENTER AND PITCH AUTHORITY (INPUT 4B AND δ_{ad} = 0)

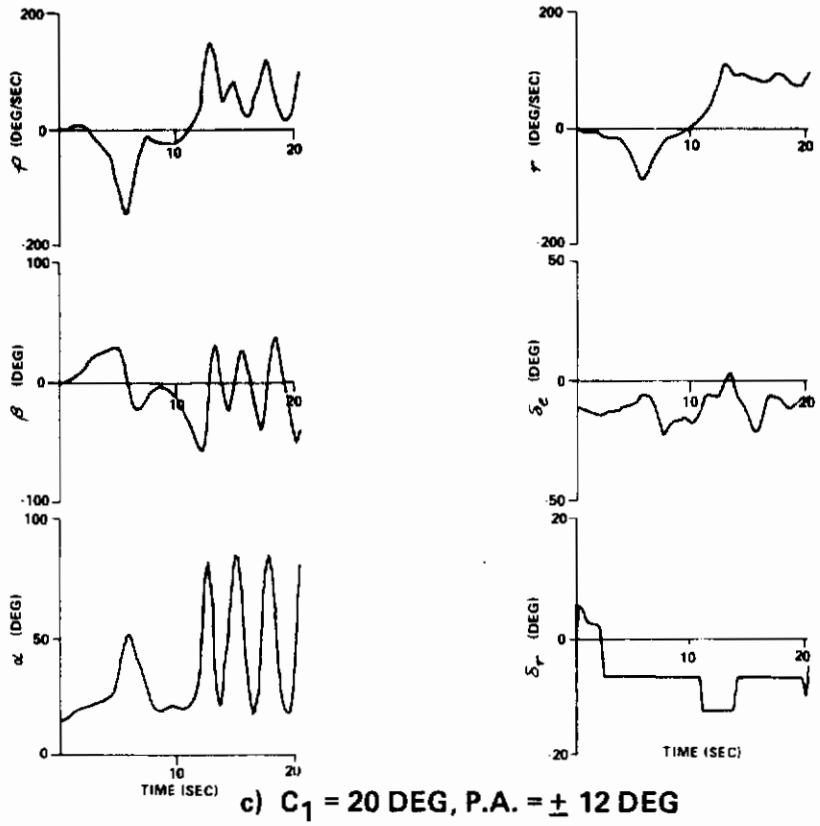

c) C_1 = 20 DEG, P.A. = ± 12 DEG

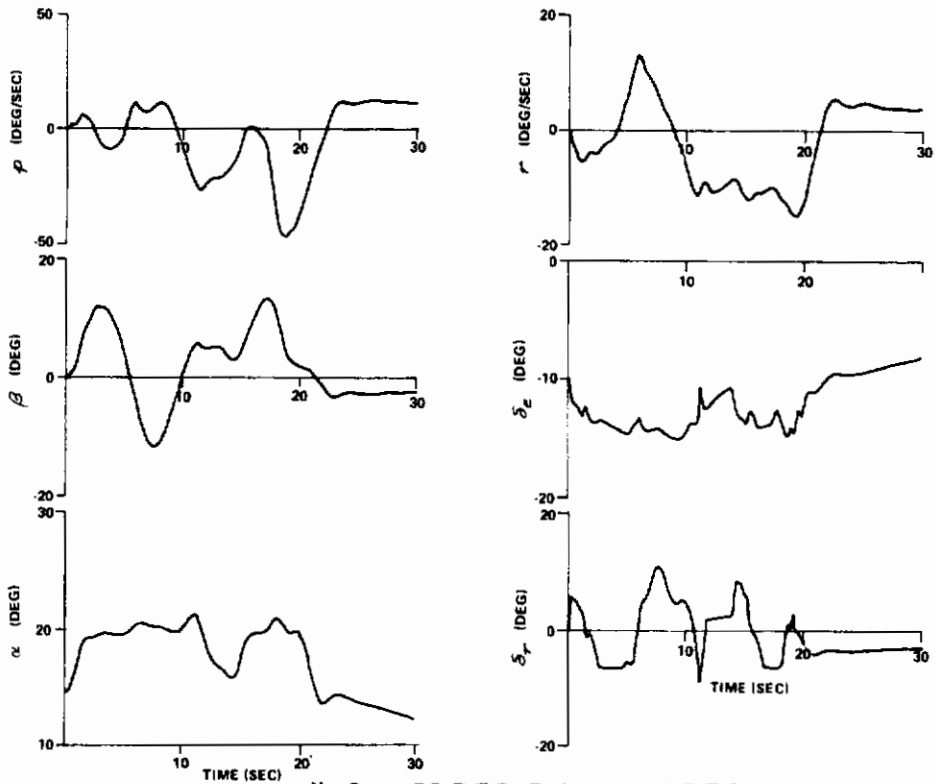

d) C_1 = 22 DEG, P.A. = ± 12 DEG

Figure 20 (Concluded) COMBINED EFFECT OF DEPARTURE PREVENTER AND PITCH AUTHORITY (INPUT 4B AND δ_{a_d} = 0)

Insignificant differences were noticed when the departure preventer was operative. It was therefore concluded that the automatic roll cutoff scheme was an unnecessary complication with the departure preventer.

Effect of the Switching Boundary and the Pitch AFCS Authority

The changes in the switching boundary and the AFCS authority have strong impact on the performance of the departure preventer, and their combined effects were evaluated through the digital simulation. For the switching boundary the ranges of parameters evaluated were C_1 = 16 to 30 degrees C_2 = 0.13 to 0.20 deg/deg, and C_3 = 0.1 ~ 0.3 deg/(deg/sec). Three levels of pitch AFCS authority were considered: $\pm$ 4° (approximately the existing value), $\pm$ 8°, and $\pm$ 12°. The yaw SAS is of high authority and therefore only the existing value ($\pm$ 12 degrees for cruise configuration) was used.

Some of the responses to the pilot control inputs of Figure 17 are shown in Figure 20a through 20d. For these cases C_2 and C_3 were set at 0.13 and 0.30 respectively. Shown in Figures 20a and 20b are the low authority responses, i.e., PA = $\pm$ 4°, with C_1 = 20° and 22° respectively. The responses in Figures 20c and 20d are for high pitch AFCS authority, i.e., PA = $\pm$ 12°, with C_1 = 20° and 22° respectively. Notice that for C_1 = 20° there is no departure for PA = $\pm$ 4° and PA = $\pm$ 12°. The aircraft experiences an departure and develops into a spin for C_1 = 22° and PA = $\pm$ 4°. For C_1 = 22° and PA = $\pm$ 12° the aircraft departs but recovers from the departure immediately however.

The result of these assessments was as follows: The upper limit for C_1 was approximately 22 degrees. For lower C_1 values the existing pitch AFCS authority appeared to be adequate. However, for C_1 values near the upper limit (22 degrees) the departure preventer required more than twice the nominal ± 4° pitch axis AFCS authority. This result was used as a guide in the final evaluation of the departure preventer on the ground-based simulator.

Sensitivity to α, β Errors

Partial evaluation of the sensitivity to errors in the α and β measurements was made by adjusting the coefficients C_1 and C_2 in the switching boundary and the gains K_1 and K_4. No sensor dynamics were included. The limited evaluation indicated that errors in the order of ± 10% for α and ± 20% for β appeared to have no severe effect on the performance of the departure preventer. Larger errors were not evaluated. However, in view of the paramount importance of these two state variables on the departure preventer system, further detailed evaluation is recommended.

Rudder Effectiveness

The departure preventer performance critically hinges on the use of the rudder. Moderate variations in the rudder effectiveness, on the order of ± 50% of the basic wind tunnel data were considered. Results indicated that with these variations, the departure preventer remained effective and worked satisfactorily.

Turbulence Effect

Turbulence simulation using Dryden models (Reference 16) was incorporated in the six-degree-of-freedom nonlinear computer program. For moderate turbulence, the performance of the departure preventer was satisfactory. It was approximately the same when either $C_{z_{\dot{\alpha}}}\dot{\alpha}$ or $C_{z_{\delta_{TOS}}}\delta_{TOS}q$ was included in the switching law. Because the pitch rate signal is readily available, the latter is preferred for the mechanization of the switching boundary. Section V will discuss how both schemes were mechanized in the breadboard of the departure preventer for the pilot-in-the-loop ground-based simulation.

SECTION IV

DETERMINATION OF DESIGN CRITERIA FOR THE STALL INHIBITOR

The stall inhibitor discussed in this report is basically a stall warning device which provides the pilot with the cues of the impending stall. A variety of stall warning devices such as pedal shakers, audio signals, stick pushers, etc. are presently in use. The A-7 for example uses a pedal shaker; however, as mentioned earlier, the pedal shaker is usually masked in the airframe buffet thus reducing its effectiveness as a stall warning device.

In the development of a stall inhibitor, three tasks are involved:

(1) To determine a suitable form of warning of the impending stall departure.

(2) To define a function that will actuate the inhibitor, and

(3) To perform pilot-in-the-loop evaluation to see if the device will actually function properly in predicting the impending stall departure and to see if pilots will accept the inhibitor and respond to its actuation in a desirable and useful manner.

The stall inhibitor investigated is a device which increases longitudinal stick forces as a function of sideslip angle and angle of attack. The same criteria function and values of coefficients as are used with the departure preventer are used to activate the stall inhibitor. That is:

for $\alpha - \alpha^* > 0$ provide an increment in F_{es}

for $\alpha - \alpha^* \leq 0$ no increment in F_{es}

$$\alpha^* = +18 - .2|\beta| - .1\dot{\alpha}$$

where α^*, α, β are in degrees

The manner in which an increment in F_{es} is generated is optional within the equipment as is described in Section V. Before the criteria were established for the design of the stall inhibitor, computer evaluations were made of the possible functional relations which could be used. This was done by incorporating possible configurations in the digital computer program that included the A-7 aerodynamics and flight control systems. Elevator force step inputs were introduced in trimmed flight at 14 degrees angle of attack. Several different sizes of step input were used. It was found that the added damping of the angle of attack rate term included in the expression for α^* was beneficial and powerful for stopping any "ringing" that resulted for large step inputs. It was further determined that the maximum angle of attack switching constant should be no greater than 18 degrees, or the system again became susceptible to "ringing" after large step inputs. (Hence it was reasonable to use the same switching boundary for both the stall inhibitor and the departure preventer.) The ranges of F_{es} increments for the stall

inhibitor were chosen to permit greater force increments than it is known a pilot would accept, and to be adjustable from zero to the maximum values. Both linear and functional increases in stick force are provided and a stick "kick" is provided. Both the increase in stick force and the stick kick are initiated at the switching boundary. The increase in stick force is a functional relation of angle of attack and the stick kick is a function of $\frac{d}{dt}(A-\alpha)^*$ after the switching boundary is crossed. The stick kick is a step increase in stick force, or some other chosen function of $\frac{d}{dt}(A-\alpha)$ and the reason for including it is from the consideration that a pilot under combat stress may not recognize the stiffer force gradient whereas the stick kick could be more discernible. The following depicts the concepts of the available stick force functions of the stall inhibitor in graphical form.

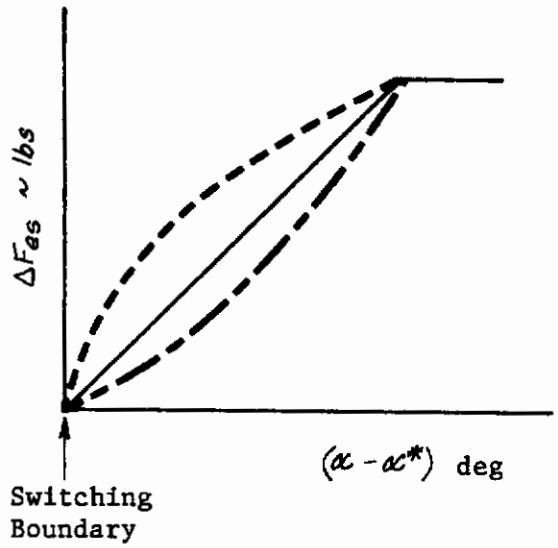

Figure 21 Stick Force Increment

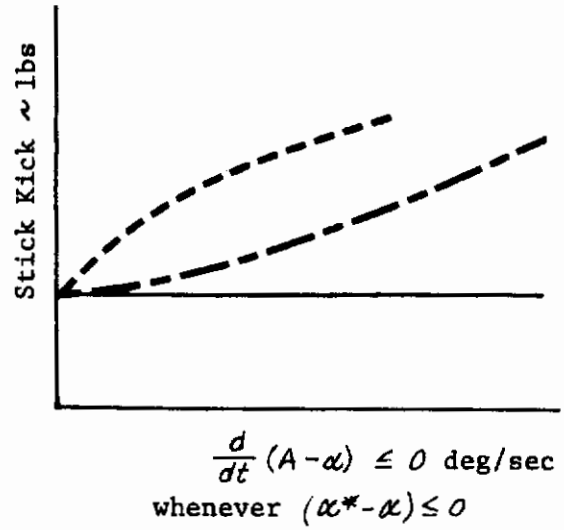

Figure 22 Stick Kick

---

* The quantity A is equal to α^* less the anticipation term $C_3\dot{\alpha}$.

SECTION V

DESCRIPTION OF STALL INHIBITOR - AUTOMATIC DEPARTURE PREVENTION DEVICE

This section describes the operation and mechanization of the electronic unit that was designed and fabricated as item 0001AA of the contract. The unit contains analog computation equipment that provides the following functions:

1) Actuation Monitor - A computation that determines when a selected combination of parameters exceed a specified value. At this point, the device becomes operative.

2) Stall Inhibitor - A voltage output is developed that can be used to increase the longitudinal stick force when the combination of parameters that indicate a stall or departure exceed a specified value.

3) Automatic Departure Preventer - This computation applies the necessary control functions to the flight control system to prevent the aircraft from departing into post-stall gyrations or spins.

Engineering data supplied with the unit and the information included in this section and Appendix III provide the necessary knowledge to test and use the equipment.

The unit was designed for use with an analog or hybrid computer. It has been successfully used for evaluations conducted on the Calspan Corporation ground-based simulator. At Calspan, it was used with a 100 volt hybrid computer; however, it uses 10 volt computing elements and requires an interface card to scale the 100 volt signals to a 10 volt level. This card may be removed and replaced with a jumper card supplied with the unit. The unit can then be interfaced directly with a 10 volt computer. Figure 23 is a photograph of the stall inhibitor - automatic departure preventer breadboards. The unit is housed in a standard 3/4 ATR case suitable for a simulator or experimental airborne application. The basic components in the unit are low-drift amplifiers, multipliers, electronic switches, coefficient potentiometers and a power supply. Data sheets for the specific devices used in the computer were supplied as a part of the equipment package. The computations are performed in standard analog fashion. Thus, the unit is essentially a programmed analog computer with adjustable potentiometers that can vary the coefficients and functions as desired.

Figures 24 through 27 are block diagrams of the computations performed by the stall inhibitor - automatic departure prevention device. The computations shown on each figure are the following:

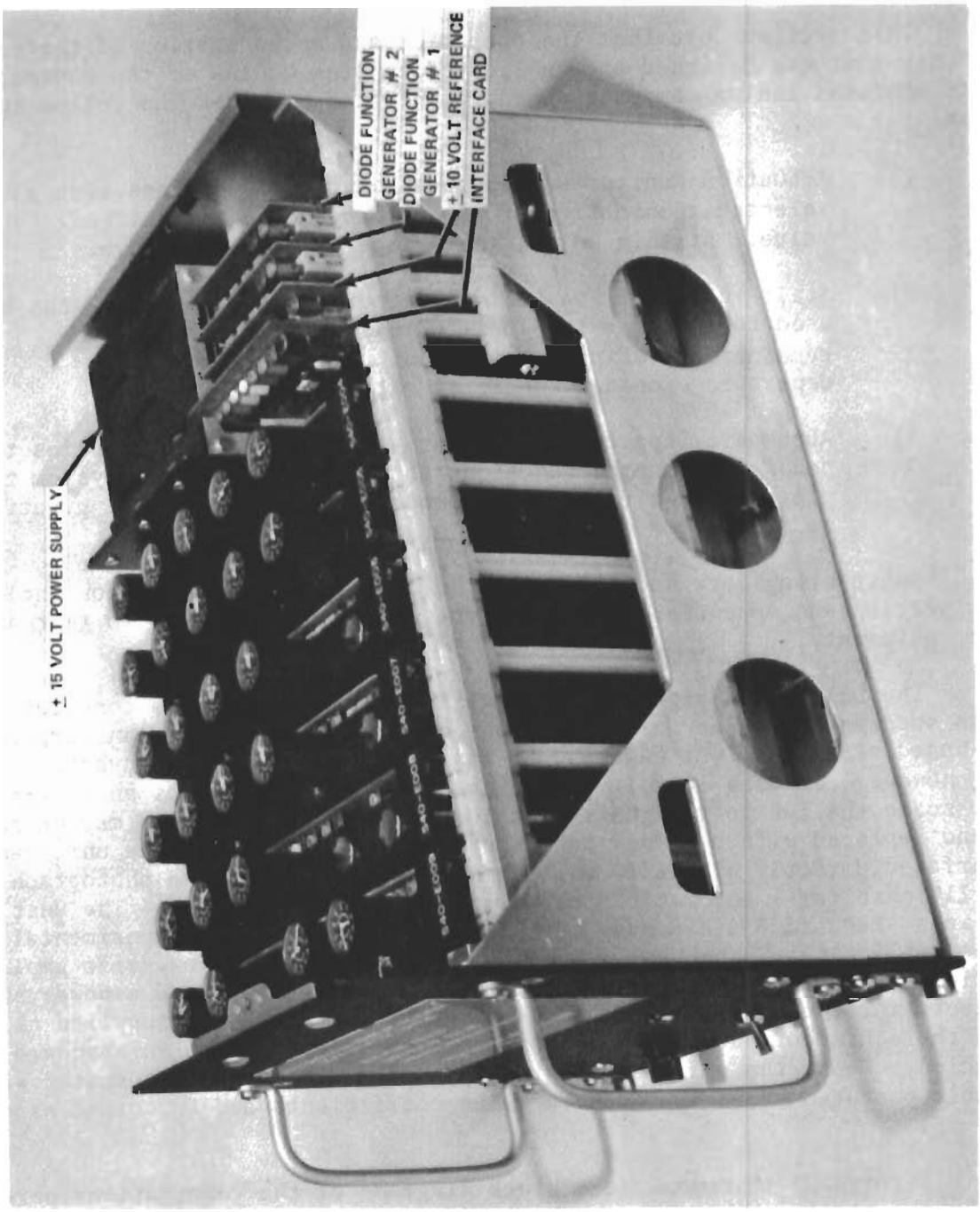

Figure 23 STALL INHIBITOR-AUTOMATIC DEPARTURE PREVENTION DEVICE

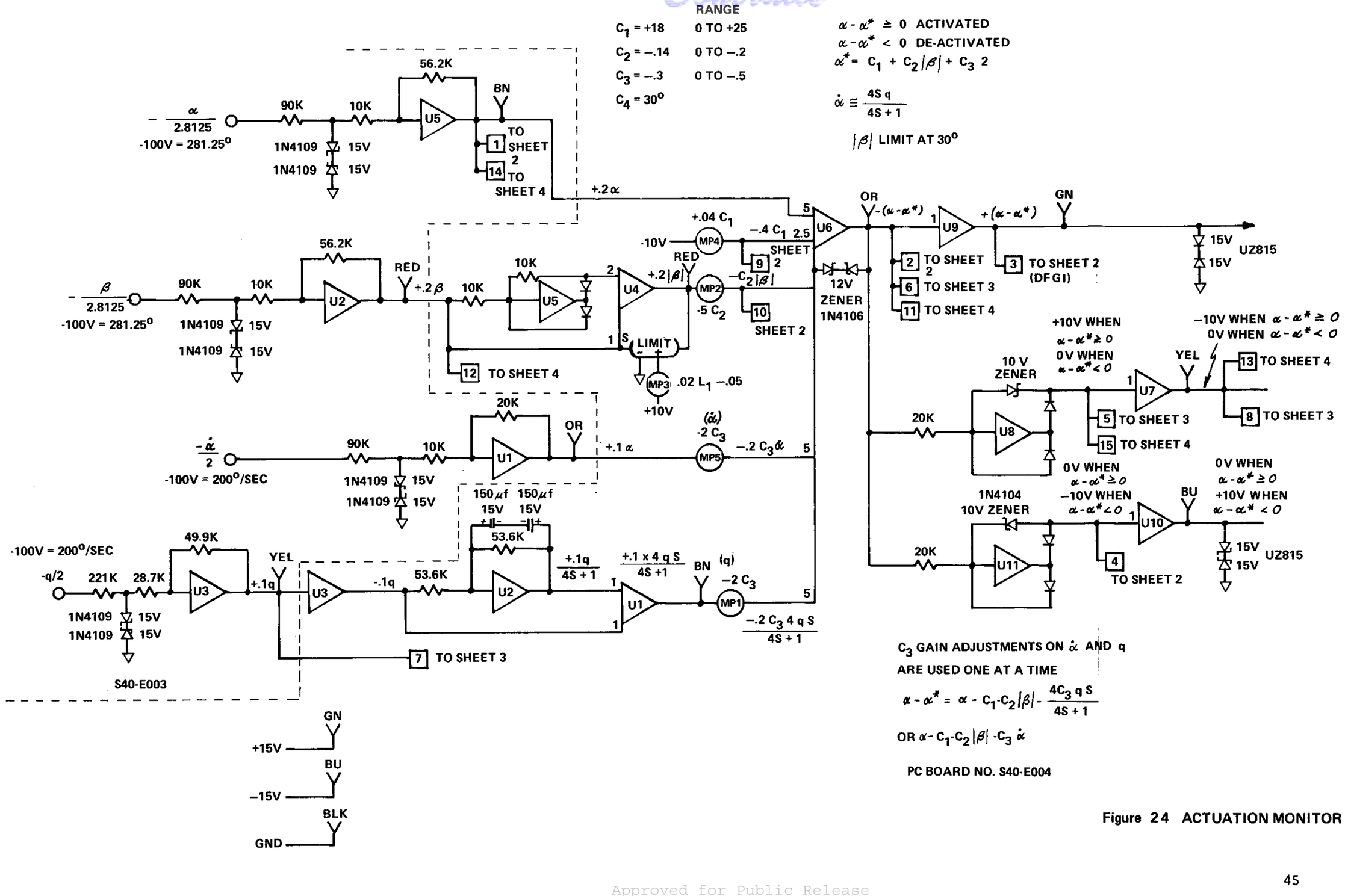

C_3 GAIN ADJUSTMENTS ON $\dot{\alpha}$ AND q ARE USED ONE AT A TIME

$$\alpha - \alpha^* = \alpha - C_1 - C_2|\beta| - \frac{4C_3\, q\, S}{4S+1}$$

OR $\alpha - C_1 - C_2|\beta| - C_3\dot{\alpha}$

PC BOARD NO. S40-E004

Figure 24 ACTUATION MONITOR SCHEMATIC

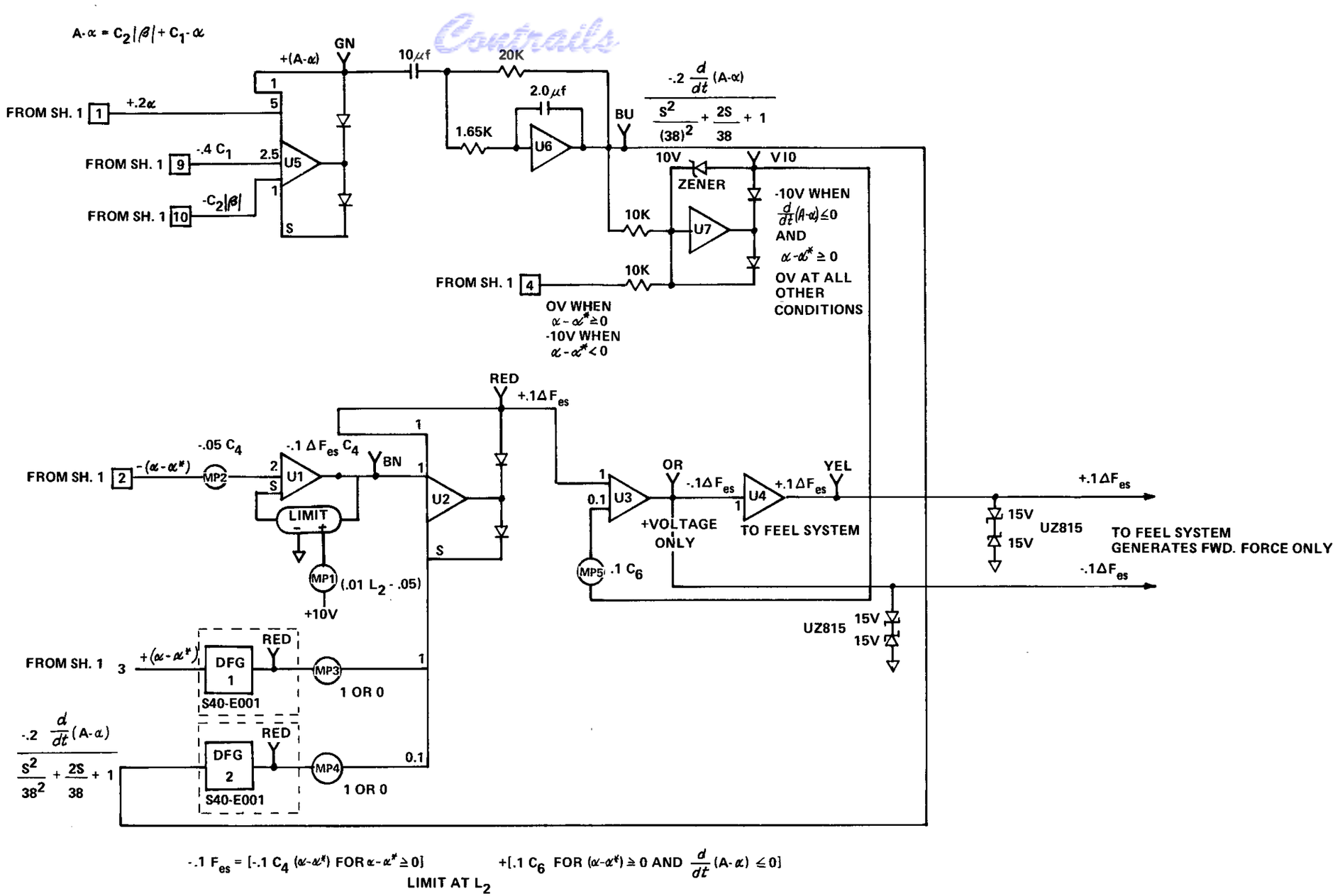

-.1 F_{es} = [-.1 C_4 (α-α*) FOR α-α* ≥ 0] +[.1 C_6 FOR (α-α*) ≥ 0 AND $\frac{d}{dt}$ (A-α) ≤ 0]

LIMIT AT L_2

C_4 0 TO -20 #/ DEG

C_5 0 TO 100 #

C_6 0 TO 10 #

P.C. BOARD NO. S40-E005

Figure 25 STALL INHIBITOR SCHEMATIC

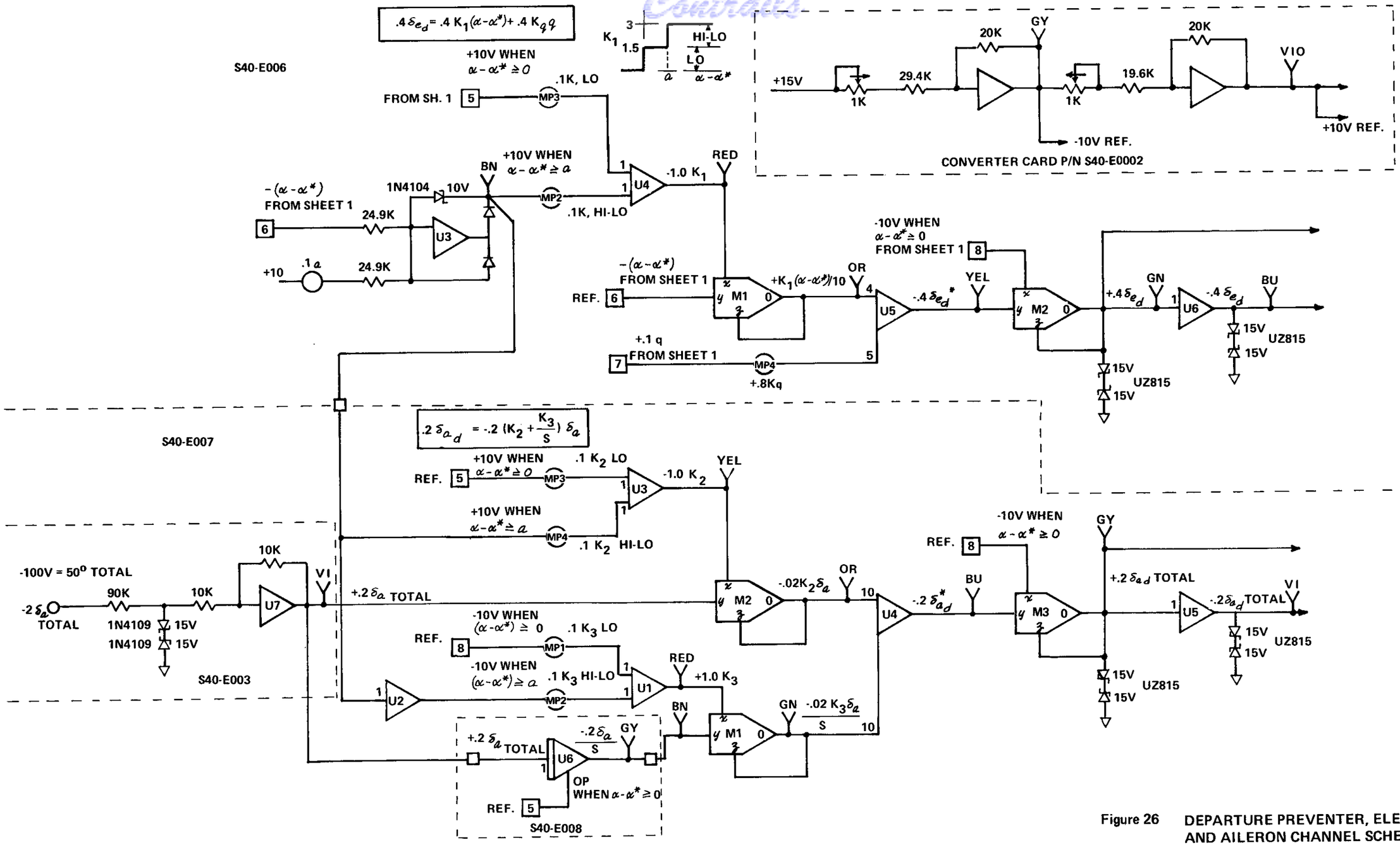

Figure 26 DEPARTURE PREVENTER, ELEVATOR, AND AILERON CHANNEL SCHEMATIC

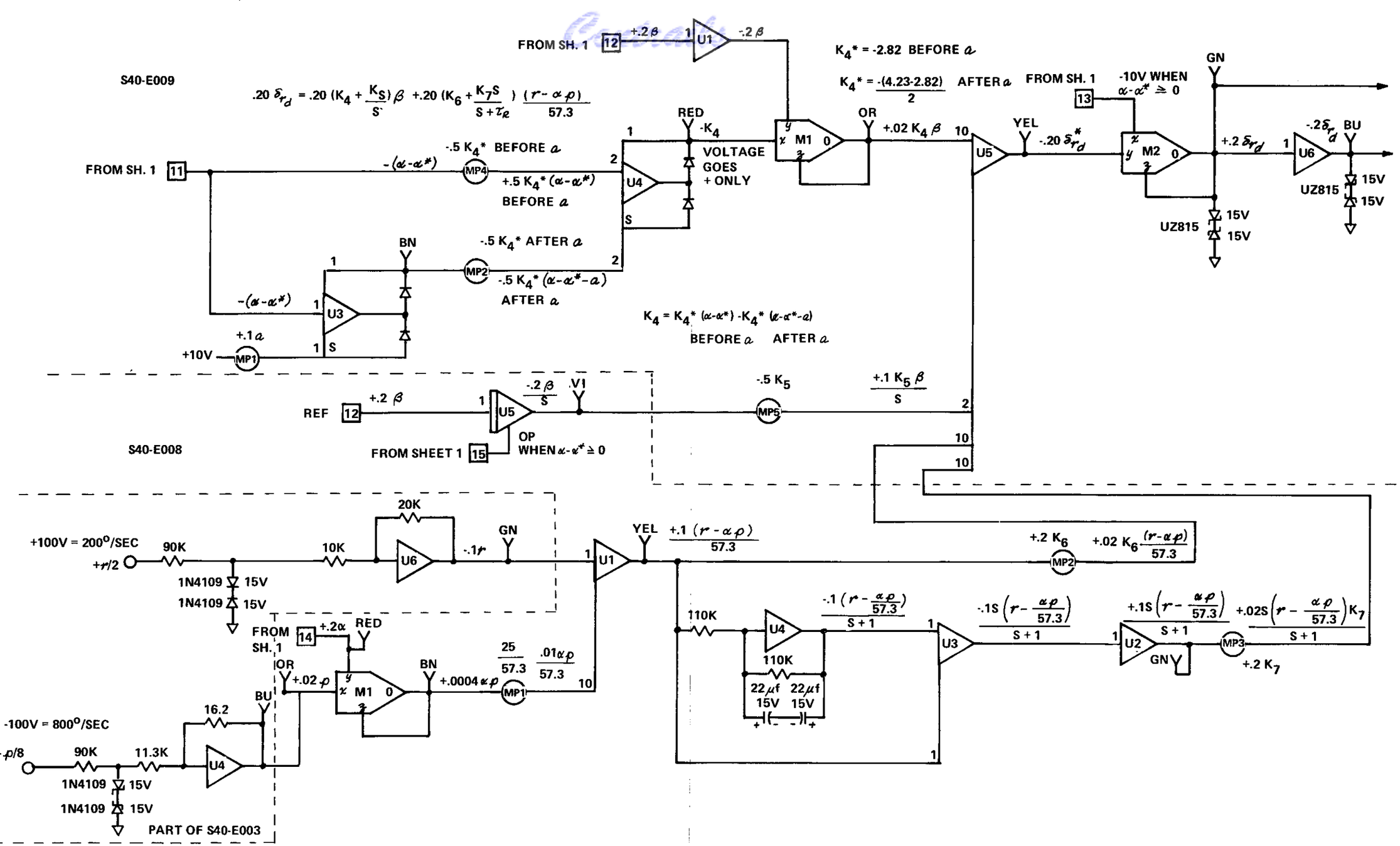

Figure 27 DEPARTURE PREVENTER AND RUDDER CHANNEL SCHEMATIC

Figure 24 - Actuation Monitor

Figure 25 - Stall Inhibitor

Figure 26 - Departure Preventer - Elevator and Aileron Channel*

Figure 27 - Departure Preventer - Rudder Channel

Scale factors and potentiometer coefficients are indicated by the following convention examples:

Scale Factor example: $\left[+ .2\ \alpha\right]$ = .2 volts/deg of angle of attack

or + 10 V = + 50 deg of angle of attack

Scale factors are indicated on all amplifier outputs and the lines leading into each amplifier.

Coefficient example: $\left[-5 C_z\right]$

The potentiometer settings are variable from 0 to + 1.0. Thus, in the example above, a value for C_z from zero to - 0.2 can be realized. For C_z equal to - 0.141 the potentiometer coefficient setting would be .705. The dial reading due to pot loading error can be determined from Figure 28. In this case it would be 732.

With the scale factors and coefficients expressed in this manner, the two may be multiplied together times the input gain of the amplifier. The result is the contribution of that signal (amplitude and sign) at the amplifier referred to the input.

The amplifiers invert the sign of all input signals; thus, the output of any amplifier is (-) the sum of all input signals. All multipliers are connected to provide the following function:

inputs		output	
$+X$	volts	$\frac{+XY}{10}$	volts
$+Y$	volts		

Complete schematics and front view layouts for each circuit card are part of the data package supplied with the equipment. A list of these drawings is given in Appendix III.

---

* An aileron channel is mechanized in this device. It may used if desired.

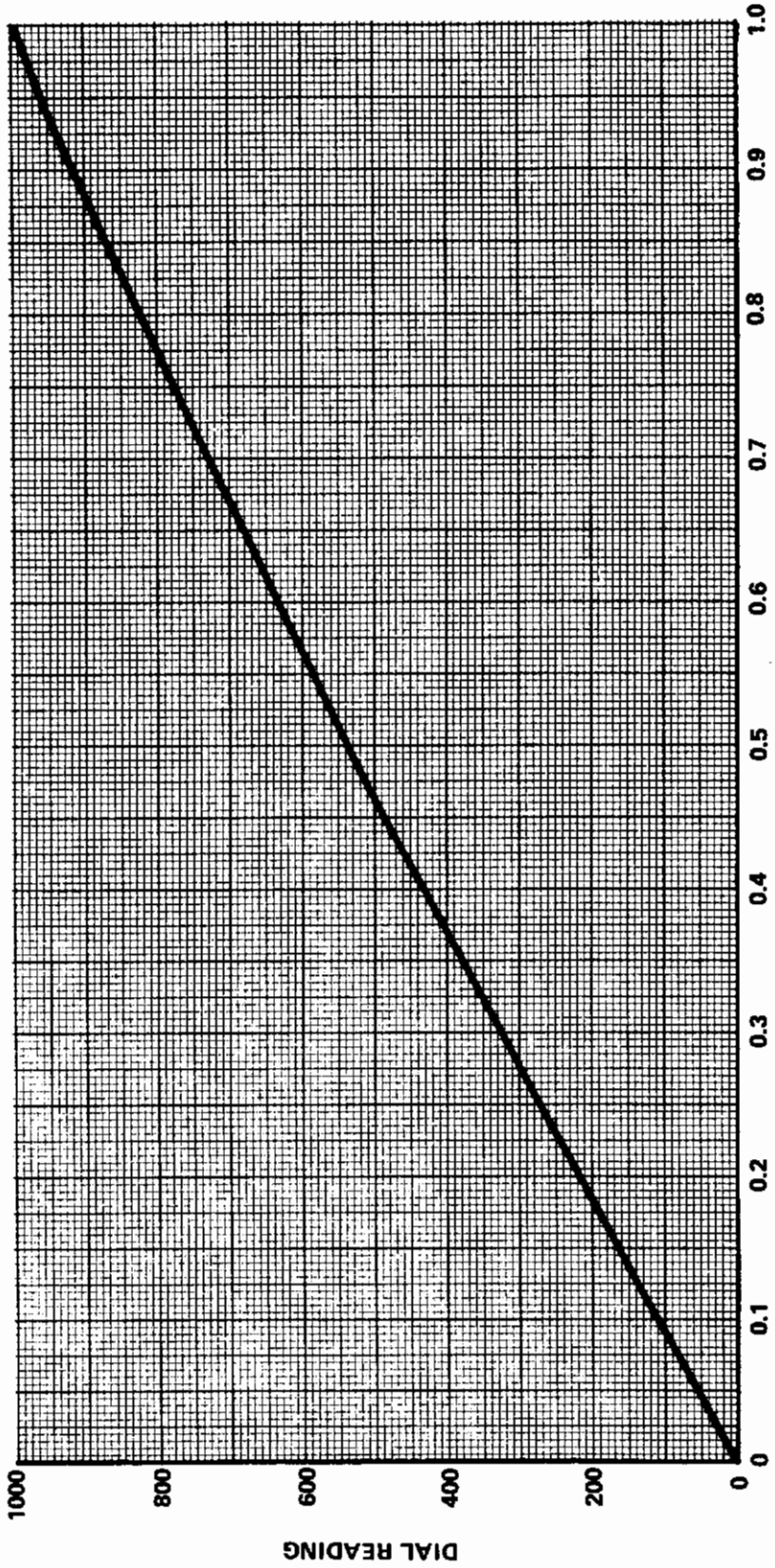

Figure 28 COEFFICIENT POTENTIOMETER LOADING CURVE

The following equations define the mechanization of the stall inhibitor - automatic departure prevention device.

Figure 24 - Actuation Monitor - The actuation monitor continuously computes the activating function $\alpha^*(t)$ and compares this signal with angle of attack, α. The stall inhibitor and departure preventer are activated if $\alpha - \alpha^* \geq 0$. If $\alpha - \alpha^* < 0$ neither device is activated. $\alpha - \alpha^*$ is defined in terms of the mechanization as follows. Factors are written in the order they are encountered while moving downstream, and variable coefficients (pots) are indicated by brackets.

$$\alpha - \alpha^* = .2\alpha 5 - 10\left[.04C_1\right] 2.5 + .2|\beta|\underset{\text{LIMIT AT } L_1}{\left[-5C_2\right]} + .1\dot{\alpha}\left[-2C_3\right]5$$

$$+ \left[\frac{.4s}{4s+1}\right]q\left[-2C_3\right]5$$

or

$$\alpha - \alpha^* = \alpha - 25\left[.04C_1\right] + .2|\beta|\underset{\text{LIMIT AT } L_1}{\left[-5C_2\right]} + .5\dot{\alpha}\left[-2C_3\right]$$

$$+ \frac{2s}{4s+1}\left[-2C_3\right]q$$

Each coefficient and limit is defined and is adjustable through the following range:

Potentiometer Coefficient or Limit	Units	Coefficient Range
$+ .04C_1$	degrees	$0 \leq C_1 \leq 25$
$- 5C_2$	degree/degree	$0 \geq C_2 \geq -0.2$
$.02L_1 - .05$	degrees	$2.5 \leq L_1 \leq 52.5$
$- 2C_3$ ($\dot{\alpha}$)	degree/degree/sec	$0 \geq C_3 \geq - 0.5$
$- 2C_3$ (q)	degree/degree/sec	$0 \geq C_3 \geq - 0.5$

Note: the q term may be substituted for the $\dot{\alpha}$ term. Thus, only one of the C_3 potentiometers should be set to the desired value at any one time. The other C_3 potentiometer should be set to zero.

Signals generated in this computation are used in the stall inhibitor and automatic departure prevention mechanization.

Figure 25 - Stall Inhibitor - This device generates a voltage that can be used to increase the longitudinal stick force as a function of the actuation monitor signal, $\alpha-\alpha^*$ plus the rate of change of a criterion function, $A-\alpha$. Linear and nonlinear forms of this function change have been mechanized. The linear mechanization is defined by the following equations:

$$-.1\Delta F_{ES} = (\alpha-\alpha^*)\left[-.05C_4\right]2 - (-10)\left[.1C_6\right]$$

LIMIT AT L_2

$$A-\alpha = -.2\alpha(5) + .4C_1(2.5) + C_2|\beta|$$

LIMIT AT L_1

VALUE OF $-.1\Delta F_{ES}$

	$\alpha-\alpha^* < 0$	$\alpha-\alpha^* \geq 0$
$\frac{d}{dt}(A-\alpha) > 0$	0	$(\alpha-\alpha^*)\left[-.05C_4\right]2$
$\frac{d}{dt}(A-\alpha) \leq 0$	0	$(\alpha-\alpha^*)\left[-.05C_4\right]2-(-10)\left[.1C_6\right]$

$\frac{d}{dt}(A-\alpha)$ is obtained by differentiating $A-\alpha$ but only when $A-\alpha$ is negative. An approximate scheme was used in the differentiating as shown in Figure 25.

Each coefficient and limit is defined and is adjustable through the following ranges:

Potentiometer Coefficient or Limit	Units	Coefficient Range
$-.05C_4$	pounds/degree	$-20 \leq C_4 \leq 0$
$.1C_6$	pounds	$0 \leq C_6 \leq 10$
$.01L_2 - .05$	pounds	$5 \leq L_2 \leq 105$
C_1, C_2, C_3	defined on page 51	

In the nonlinear mechanization, two function generators are provided to create the following equation:

$$-.1\Delta F_{es} = -f_1(\alpha - \alpha^*) + f_2 \frac{d}{dt}(A-\alpha)\Big/.1$$

with the switching conditions as shown in Figures 21 and 22. f_1 and f_2 are five fixed-break-point, variable-slope diode function generators that are programmable for positive voltage inputs and generate only positive voltage outputs. For all negative inputs, their output is zero. This feature prevents generation of aircraft nose-up pro-stall control inputs.

The output of the stall inhibitor is a voltage that can be used to command a stick force through a feel system. This signal would be summed with the pilot-applied force. The amplifier outputs of the stall inhibitor can only produce a negative or a forward force.

Figures 25 and 26 - Departure Prevention Device - The automatic departure preventer applies the necessary control functions to the aircraft elevator, aileron, and rudder flight control surfaces to prevent the aircraft from departing. Mechanization of the elevator channel is shown in Figure 25. The equation that describes this mechanization is the following:

$$.4\delta_{e_d} = +\frac{K_1}{10}(\alpha - \alpha^*)4 + .1q\left[+.8K_q\right]5$$

when $\alpha - \alpha^* \geq 0$

$$K_1 = 0, \qquad \alpha - \alpha^* < 0$$

$$K_1 = +10\left[.1K_{1_{LO}}\right], \qquad 0 \leq \alpha - \alpha^* < a$$

$$K_1 = +10\left[.1K_{1_{LO}}\right] + 10\left[.1K_{1_{HI-LO}}\right], \quad \alpha - \alpha^* \geq a$$

The K_1 function is shown in Figure 29.

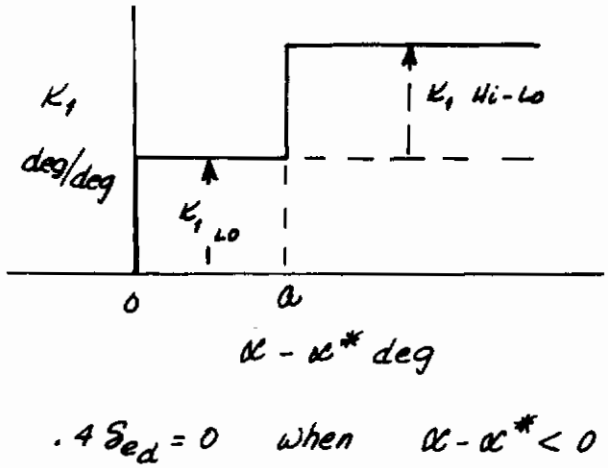

Figure 29. Description of K_1 Function

The coefficients for the elevator channel are adjustable through the following ranges:

Potentiometer Coefficient	Units	Coefficient Range
$+.1\ K_{1\ Lo}$	degrees/degree	$0 \leq K_1 \leq 10$
$+.1\ K_{1\ Hi-Lo}$	degrees/degree	$0 \leq K_1 \leq 10$
$+\ .8\ K_q$	degrees/degree/sec	$0 \leq K_q \leq 1.25$
$+\ .1\ a$	degrees	$0 \leq a \leq 10$

The output of this channel is an electrical signal that drives the elevator flight control system whenever $\alpha - \alpha^* \geq 0$.

The equation that describes the mechanization of the aileron channel* is the following:

$$+.2\,\delta_{a_d} = -.02K_2\delta_a 10 - \frac{.02K_3}{s}\delta_a 10$$

when $\alpha - \alpha^* \geq 0$

* An aileron channel is mechanized in the device, although it was not used in the pilot-in-the-loop evaluation.

The integrator does not start to integrate until $\alpha-\alpha^*$ exceeds zero. If $\alpha-\alpha^*$ becomes less than zero, the integrator resets to zero output.

$$+.2\delta_{a_d} = 0 \quad \text{when} \quad \alpha-\alpha^* < 0$$

$$K_2 = 0 \qquad \alpha-\alpha^* < 0$$

$$K_2 = +10\left[.1K_{2_{LO}}\right] \qquad 0 \le \alpha-\alpha^* < a$$

$$K_2 = +10\left[.1K_{2_{LO}}\right] + 10\left[.1K_{2_{HI-LO}}\right] \qquad \alpha-\alpha^* \ge a$$

$$K_3 = 0 \qquad \alpha-\alpha^* < 0$$

$$K_3 = +10\left[.1K_{3_{LO}}\right] \qquad 0 \le \alpha-\alpha^* < a$$

$$K_3 = +10\left[+1K_{3_{LO}}\right] + 10\left[.1K_{2_{HI-LO}}\right] \qquad \alpha-\alpha^* \ge a$$

K_2 and K_3 take the form shown in Figure 30.

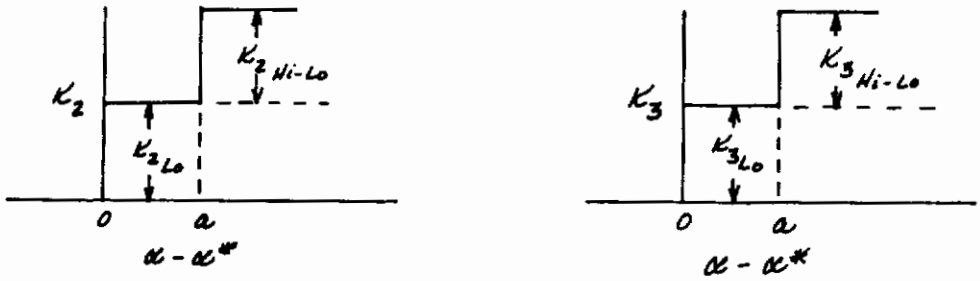

Figure 30. Description of K_2 and K_3 Functions

The coefficients in the aileron channel are adjustable through the following ranges:

Potentiometer Coefficient	Units	Coefficient Range
+ .1 $K_{2\ Lo}$	degree/degree	$0 \le K_{2\ Lo} \le 10$
+ .1 $K_{2\ Hi-Lo}$	degree/degree	$0 \le K_{2\ Hi-Lo} \le 10$
+ .1 $K_{3\ Lo}$	degree/degree second	$0 \le K_{3\ Lo} \le 10$
+ .1 $K_{3\ Hi-Lo}$	degree/degree second	$0 \le K_{3\ Hi-Lo} \le 10$

The aileron departure prevention channel provides an output signal to the aileron flight control system whenever $\alpha-\alpha^* \geq 0$.

The mechanization for the rudder channel of the departure preventer is shown in Figure 26 and can be described by the following equation:

$$+.2\delta_{r_d} = .02K_4\beta(10) - \frac{.2\beta}{s}\left[-.5K_5\right]2 + .1\left(\frac{r-\alpha p}{57.3}\right)\left[.2K_6\right]10$$

$$+ .1\delta \frac{\left(\frac{r-\alpha p}{57.3}\right)}{s+1}\left[.2K_7\right]10$$

when $\alpha - \alpha^* \geq 0$

The integrator does not start to integrate until $\alpha-\alpha^*$ exceeds zero. If $\alpha-\alpha^*$ becomes less than zero, the integrator resets to zero output.

$+.2\delta_{r_d} = 0$ when $\alpha-\alpha^* < 0$

$$K_4 = 0 \qquad \alpha-\alpha^* < 0$$

$$K_4 = -(\alpha-\alpha^*)\left[-.5K_{4_{BEFORE\ a}}\right]2 \qquad 0 \leq \alpha-\alpha^* < a$$

$$K_4 = -(\alpha-\alpha^*)\left[-.5K_{4_{BEFORE\ a}}\right]2 + (\alpha-\alpha^*-a)\left[-.5K_{4_{AFTER\ a}}\right]2, \quad \alpha-\alpha^* \geq a$$

K_4 can only be zero or negative as shown in Figure 31.

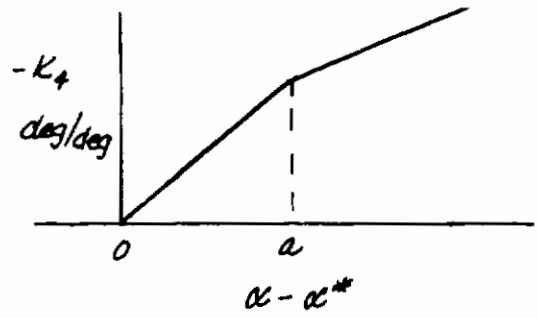

Figure 31. Description of K_4 Function

The coefficients in the rudder channel are adjustable through the following ranges:

Coefficient	Units	Coefficient Range
$-.5\ K_4$ Before a	degree/degree	$-2 \leq K_4$ Before a ≤ 0
$-.5\ K_4$ After a	degree/degree	$-2 \leq K_4$ After a ≤ 0
$-.5\ K_5$	degree/degree/sec	$-2 \leq K_5 \leq 0$
$+.2\ K_6$	degree/degree/sec	$0 \leq K_6 \leq 5$
$+.2\ K_7$	degree/degree/sec	$0 \leq K_7 \leq 5$
25/57.3	25 x radians/degree	0.436 or 0

The rudder channel output of the departure preventer provides a signal to the rudder flight control system whenever $\alpha - \alpha^* \geq 0$.

Table II lists all inputs and outputs of the stall inhibitor - departure prevention device.

TABLE II

STALL INHIBITOR AND AUTOMATIC DEPARTURE PREVENTER SIGNALS

INPUT SIGNALS

100 Volt Computer Interface Card	10 V Computer Interface Card
$-\alpha/2.8125$	$+ .2\ \alpha$
$-\beta/2.8125$	$+ .2\ \beta$
$-\dot{\alpha}/2$	$+ .1\ \dot{\alpha}$
$- p/8$	$+ .02p$
$- q/2$	$+ .1q$
$+ r/2$	$- .1r$
$- 2\ \delta_a$ Total	$+ .2\ \delta_a$ Total

OUTPUT SIGNALS

$+ (\alpha - \alpha^*)$

$+ .4\ \delta_{e_d}$

$- .4\ \delta_{e_d}$

$+ .2\ \delta_{a_d}$ Total

$- .2\ \delta_{a_d}$ Total

$+ .2\ \delta_{r_d}$

$- .2\ \delta_{r_d}$

$+ .1\ \Delta F_{es}$

$- .1\ \Delta F_{es}$

+ 10 V when $\alpha - \alpha^* < 0$, 0V when $\alpha - \alpha^* \geq 0$

SECTION VI

PILOT-IN-THE-LOOP EVALUATION

6.1 THE A-7 SIMULATION

The Calspan ground-based simulator that was used for this study is a fixed-base simulator with an outside view display and a full instrument panel display. The aileron and elevator control is a standard stick with a two-degree-of-freedom electrohydraulic feel system. The rudder pedals are loaded with a mechanical spring. The elevator-aileron system is able to simulate break-out forces and hysteresis characteristics and control system dynamics. Summing points are provided to permit signals for simulation of bobweights, etc.

A full instrument panel is provided with aircraft and engine instruments, all of which have the appearance of standard aircraft instruments, see Figure 32. Full maneuvering capability is simulated in that the equations are scaled for the large motions and rates and accelerations attained in a spin and there are no attitude ambiguities in the solutions.

For an outside view display, a "line drawing view" is computer-generated and presented on a large CRT with intensity modulation, see Figure 33. A high-resolution TV camera views the oscilloscope presentation and transmits it to a 1000 line, high-intensity TV projection tube which projects the image on the rear of a translucent screen. The screen is in front of the simulator. The field viewed by the pilot is $\pm 30^{o}$ horizontal, 37^{o} vertically up and 7^{o} vertically down.

For the computations, a hybrid computer facility is used. It consists of a Honeywell DDP 116 digital computer with 8K core and two COMCOR Ci5000 analog computers, see Figure 34. The aerodynamic data and equations of motion are solved by the digital computer. The control system dynamics and associated nonlinear functions are solved on analog computers which also drive the instruments. In addition to these computers, considerable Pace analog computer equipment was used.

A flyable target airplane image was generated for the heads-up pursuit tracking. The target airplane aerodynamics are simplified and only a stick is needed to manually fly the target airplane. The target airplane image represented a delta wing aircraft (no specific aircraft), presented to the pursuing pilot always in proper perspective. To aid in interpretation of the attitude of the target airplane, its right wing was formed with dashed lines and the image was intensity modulated so that the parts of it that were geometrically furthest from the viewer were dimmer than those parts which were to appear as closest.

The thrust data were taken from Reference 7 for the TF 41-F-1 engine. For purposes of interpolation, additional points of thrust versus RPM were needed, and so they were assumed as idle thrust of a few hundred pounts at 55% RPM and zero thrust at zero percent RPM. To enter the thrust data, Mach

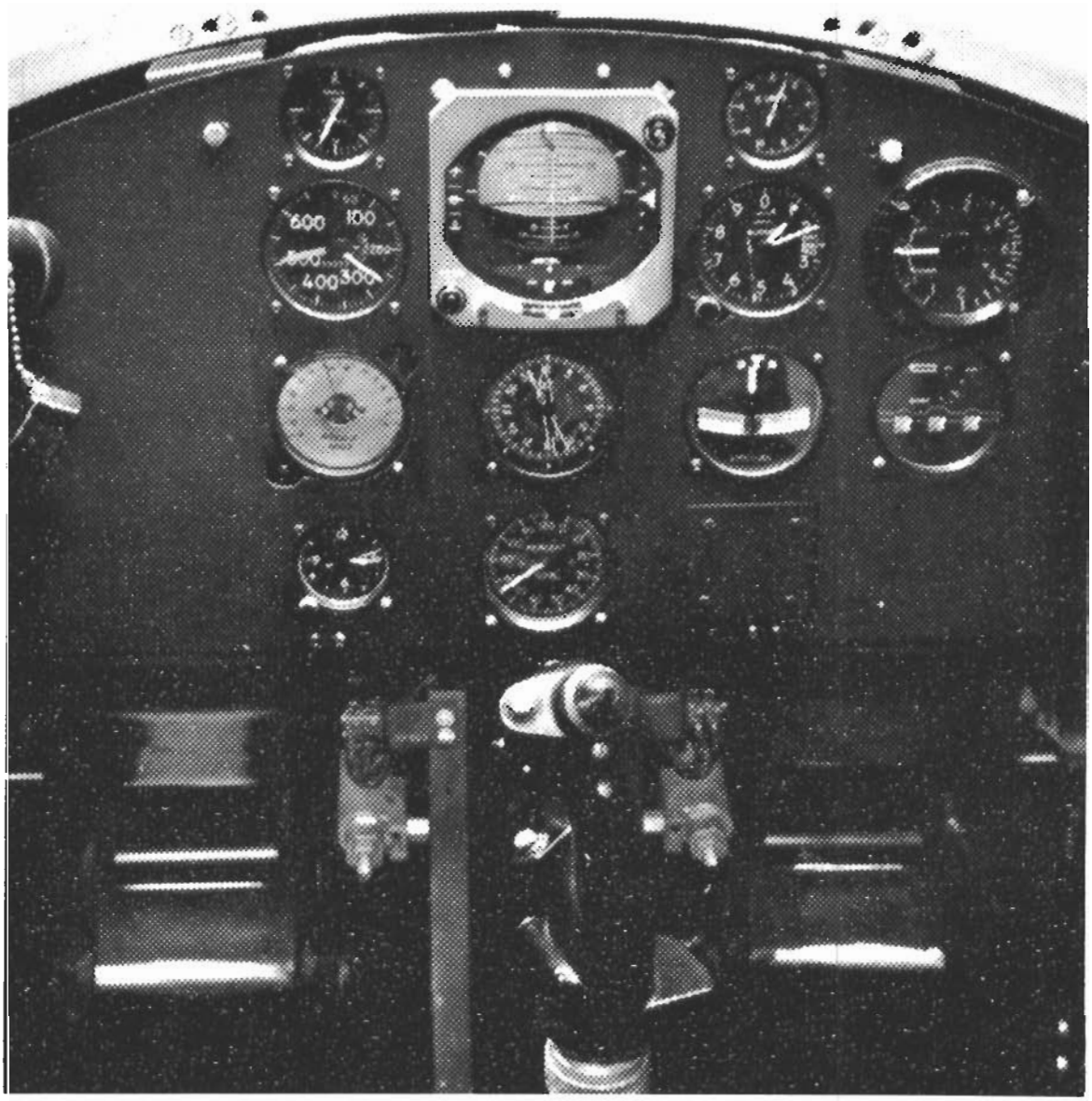

Figure 32 INSTRUMENT PANEL

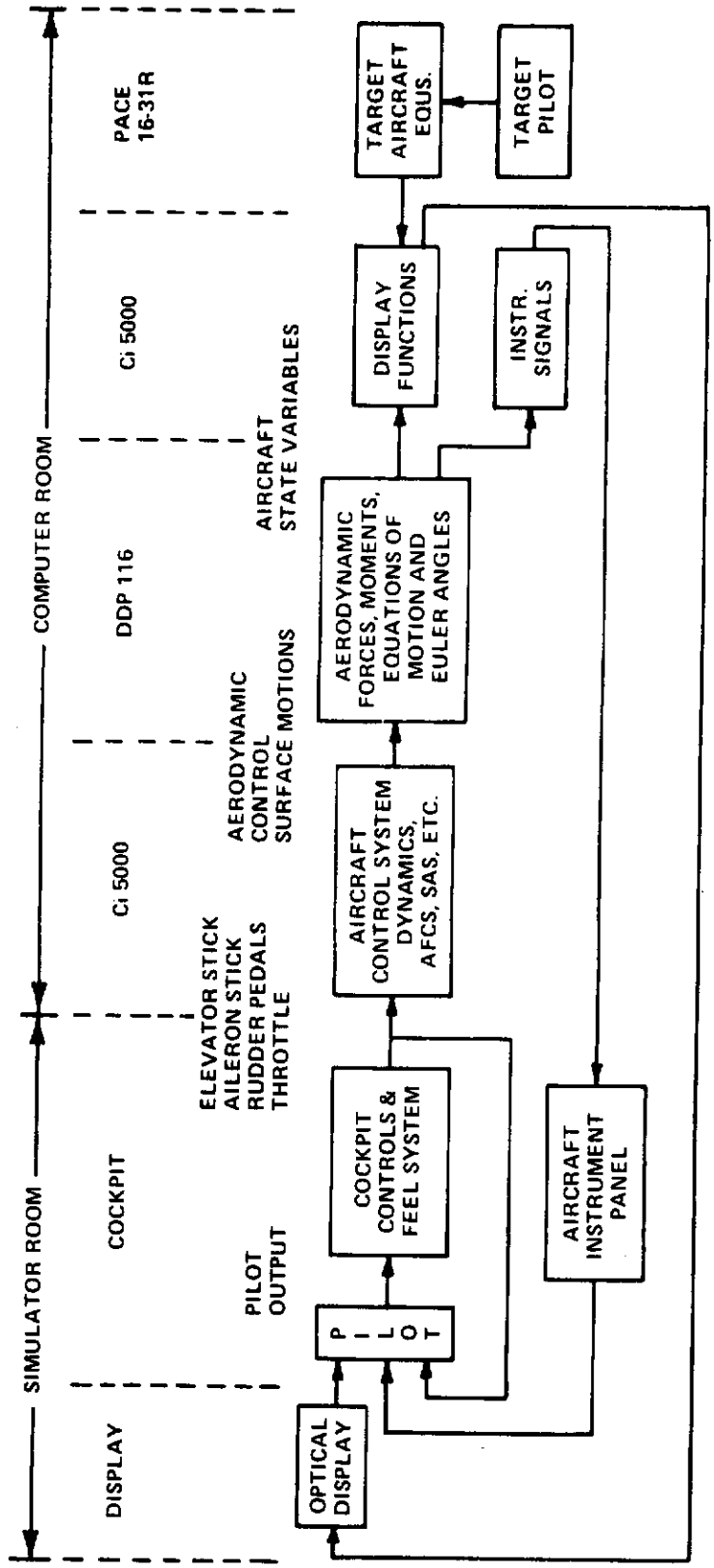

Figure 33 INFORMATION FLOW – CALSPAN FLIGHT SIMULATOR

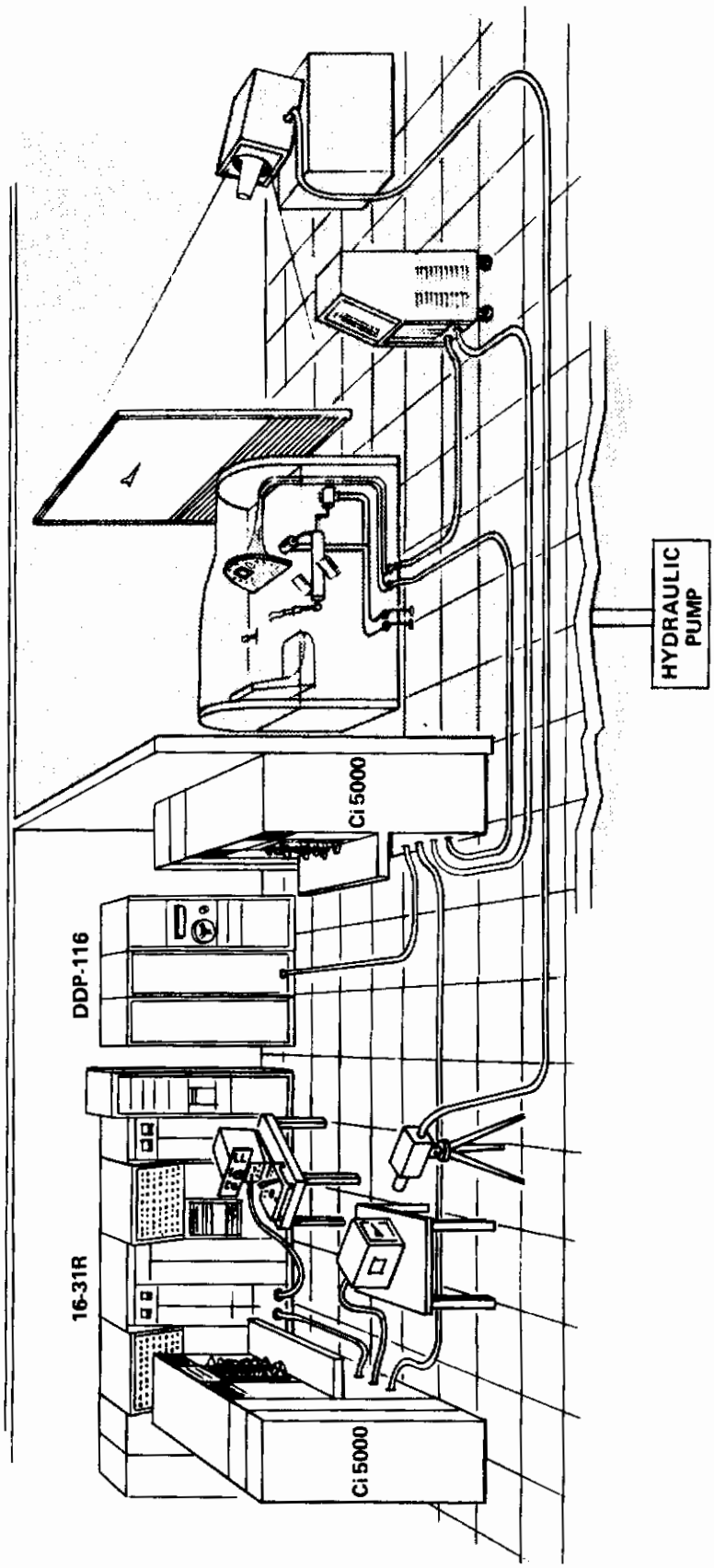

Figure 34 CUTAWAY VIEW OF GROUND-BASED FLIGHT SIMULATOR

number was approximated by

$$M = \frac{V}{1030}$$

The thrust data are shown in Figure 35. The linearized data depicted by dashed lines were used in the tabulation for the digital computer.

A COMCOR Ci5000 analog computer was used in conjunction with the electronics of the electrohydraulic feel system to simulate the characteristics of the A-7 mechanical and AFCS flight control systems. Only those portions of the AFCS which are operative in typical maneuvering flight were simulated. For instance the carrier landing, bombing, etc., modes of the AFCS were not to be used in the evaluations of the stall inhibitor/departure preventer and so they were not simulated. Those systems which were simulated are shown in block diagram form in Figures 9, 10, and 11. The equations of motion and the A-7D aerodynamic data used are given in Appendix II.

6.2 EXPERIMENT PROCEDURES, EVALUATION AND RESULTS

A rigorous pre-evaluation of the stall inhibitor/departure preventer was performed prior to any formal evaluations. These pre-evaluations examined the characteristics of the device and determined the most efficacious gain settings to prevent departures while not reducing the pilot's capabilities with the simulated A-7 airplane. Initially many maneuvers were flown, purposely entering the departure region and also using pro-spin control inputs. During this phase many gain levels were explored until departure-free maneuvering was attained. Then a more formal series of pre-evaluation runs was made according to a planned sequence.

First, stalls were performed with "coordinated" controls. These included one-g stalls and accelerated stalls with peak load factors of 7.5 g. For the accelerated stalls the airplane did not usually reach the departure angle of attack at the peak g. Therefore accelerated stalls were also performed by doing wind-up turns wherein g was maintained at the desired level and speed was adjusted to obtain departure angles of attack.

Then the series of stalls was repeated by aggravating the departure conditions first by increasing pitch rate as the departure angle of attack was reached, then by increasing roll rate as the departure condition was reached and finally by increasing both pitch rate and roll rate together as the departure condition was reached.

To complete the pre-evaluations, the departure region entries were made, for all acceleration levels, with aileron and rudder controls purposely uncoordinated.

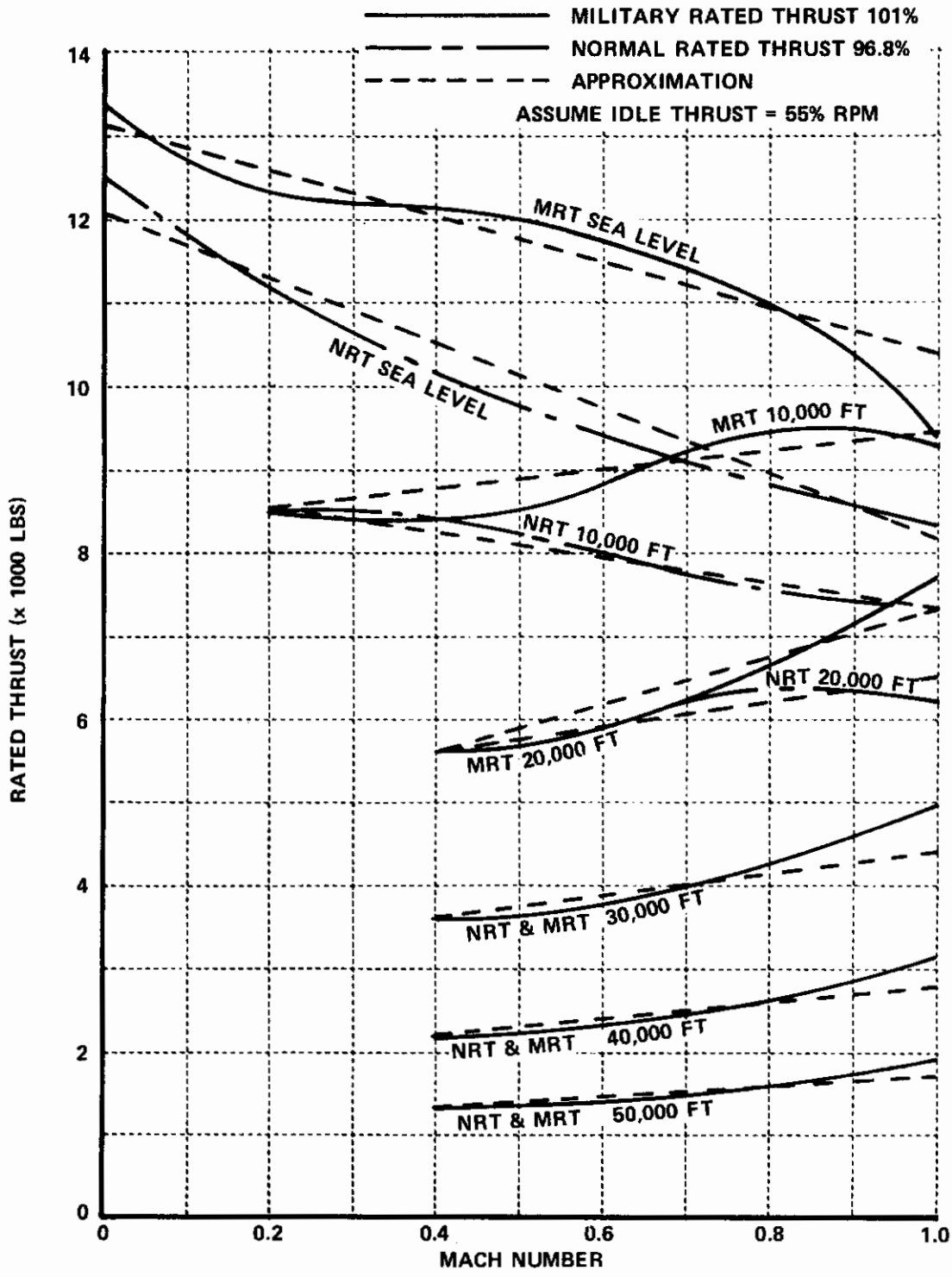

Figure 35 GROSS THRUST OF TF-41-A-1 ENGINE (A-7D STANDARD DAY)

These tests were performed with a simulation of the A-7 flight control system included in the total simulation. However, the pitch and normal acceleration bobweight was not activated because it was found to sometimes give undesirable stick nibbles which were strongly disliked by the pilot. Not using the bobweight did not affect the departure conditions of the basic, simulated A-7 in any way other than decreasing the longitudinal stick forces.

As a result of the pre-evaluation tests, the following characteristics were chosen for the formal evaluation:

A. Switching Boundary:

$$\alpha^* = c_1 - c_2|\beta| - c_3\dot{\alpha}$$

where c_1 = Switching boundaries at 18° and 20° and 22° angle of attack for zero sideslip

c_2 = A switching boundary slope of 0.20 deg/deg

c_3 = 0.1 deg/deg/sec

and $c_3\dot{\alpha}$ may be replaced by $c_3 \frac{s}{s+.25} q$

B. Stall Inhibitor

1. Linear slope at 3 lb per degree of angle of attack, up to a limit of 30 lb, starting at switching boundary.

2. A stick kick of 1 lb at the switching boundary.

C. Departure Preventer (See Section III)

$$\delta_{e_d} = 1.0(\alpha - \alpha^*)$$

$$\delta_{a_d} = 0$$

$$\delta_{r_d} = \left(K_4 - \frac{.5}{s}\right)\beta + \frac{1.5s}{s+1}(r - \alpha p)$$

where

$$K_4 = -.14(\alpha - \alpha^*)$$

Notice that $K_1 = 1.0$ was obtained by setting $K_{1_{LO}} = 1.0$, and $K_{1_{HI-LO}} = 0$ (see Figure 29); $K_4 = -.14\ (\alpha - \alpha^*)$ was obtained using a = 2° and setting the two line segments at the same slope of - .14 (see Figure 31).

The rating scale and comment card for the formal evaluations were as follows:

Rating Scale:

A. Much improved over A-7, can use full capability of airplane with confidence.

B. Better than A-7, but with some shortcomings.

C. No improvement over A-7.

D. Worse than A-7.

Plus and minuses may be used with the ratings.

Comment Card:

1. Does stall inhibitor provide sufficient warning?

2. Can you override the stall inhibitor reasonably?

3. Does departure preventer operate smoothly and satisfactorily?

4. Do you have confidence in the total system?

Each question, as answered, is to be elaborated upon to give the "whys" and "wherefores".

As noted from the relative rating scale, the pilots made comparisons to the normal A-7 as simulated. To keep the pilots "calibrated" for these comparisons they were given the normal A-7 configuration, on the average, every third or fourth run. Two pilots were used for the formal evaluations and they were each given practice sessions prior to the beginning of their evaluation sessions.

The background of the two pilots is summarized as follows:

	Pilot 1	Pilot 2
Ratings	Commercial pilot, single and multi-engine land; Rotorcraft-Helicopter; Instrument (including helicopter)	Commercial pilot, single and multi-engine land; Instrument, Instrument Instructor
Flight Time	Total: 3400 hours High performance jet - 2600 hours (including F4B and F3B) Total carrier landing - 300 hours plus Helicopter - 550 hours (including operational experience in SH3A) X-22A V/STOL - 60 hours C-130 Turbo prop - 250 hours	Total: 9520 hours Reciprocating engine twins - 6760 hours Small, single engine - 2500 hours Helicopter - 160 hours Fighter - 100 hours
Other Experience	Extensive experience as both an evaluation pilot and safety pilot in variable stability airplanes.	Extensive experience as both an evaluation and safety pilot in variable stability airplanes such as X-22A, T-33, TIFS, B-26 and as an evaluation pilot in simulators.

The evaluation runs were done in a random order. The planned evaluation matrices were as follows:

		Switching Boundary 1 : C_1 = 18°											
		Departure Preventer with elevator AFCS authority of ± 4.8°				Departure Preventer with elevator AFCS authority of ± 9.6°				Departure Boundary with elevator AFCS authority of ± 14.4°			
		ON		OFF		ON		OFF		ON		OFF	
		Stall Inhibitor		Stall Inhibitor		Stall Inhibitor		Stall Inhibitor		Stall Inhibitor		Stall Inhibitor	
Pilot	Eval.	ON	OFF	ON	OFF *	ON	OFF	ON	OFF *	ON	OFF	ON	OFF*
1	1												
	2												
	3												

In the matrix, the starred runs were all normal airplanes with an elevator AFCS authority of 4.8 degrees.

An identical matrix was made for Switching Boundary 2, C_1 = 20°, and it was planned that each pilot would experience the same matrices of runs. However, after each pilot had performed approximately twenty-five runs randomly chosen from both matrices, they each complained that nothing new would be determined and they wondered why the evaluations should be continued. Indeed, their ratings and comments were stable and unchanging as to effects of the experiment parameters to the extent that the test directors could correctly presuppose the ratings and comments for each configuration. Changes were made to the evaluation matrices which will be explained a little later after the following discussion of the conduct of the evaluation runs.

For the evaluation runs, a pursuit task was performed. The target airplane was initially two miles directly ahead of the pursuing airplane and both airplanes were at the same altitude of 21,200 feet and identical airspeeds of 270 KIAS in trimmed flight. The pursuing pilot would fly the simulated A-7 to a relatively close (100 to 300 ft) position behind the target airplane at which time the target airplane was maneuvered in climbing turns which the pursuit pilot followed. This resulted in a scissors maneuver between the two airplanes and a gradual loss of airspeed that took the pursuing aircraft into the departure region. Because of the close formation, the pursuing pilots flew "visually" with greater concentration upon the target than upon their instruments. Yet, the angle of attack and normal acceleration meters were at the top of the instrument panel and could easily be included in the pilot's scan at his discretion.

After the pre-experiment learning period and several runs of the evaluation, Pilot 1 began performing a specific maneuver at the beginning of each run. He would dive below the target airplane to pick up speed and then zoom up on the target. As the pursuit airplane airspeed decreased and its angle of attack increased, Pilot 1 could discern whether or not he had the stall inhibitor and whether or not he had the departure preventer. Pilot 2 did not perform the same maneuver at hand-off, but he performed steep turns and such maneuvers as to allow him to determine the same information.

For the major set of evaluations, the following parameters were chosen:

SB_i - Switching boundary (1 or 2); the angle of attack at which the stall inhibitor or departure preventer or both became active for $\beta = 0$. SB_1; $C_1 = 18^o$; SB_2; $C_1 = 20^o$ with $\alpha^* = C_1 - .2|\beta| - 0.1\dot{\alpha}$.

$DP_{a,b,c}$ - Departure preventer with three different values of elevator SAS authority limits.

DP_a has an elevator AFCS authority limit of ± 4.8°

DP_b has an elevator AFCS authority limit of ± 9.6°

DP_c has an elevator AFCS authority limit of ± 14.4°

SI - Stall inhibitor, either on or off

The departure preventer operates through the AFCS system, and during the pre-evaluations it was seen that the strength of the departure preventer depended upon the elevator AFCS authority. In order to evaluate the tradeoff between increased flight envelope size and increased control authority, three values of elevator AFCS authority were chosen.

During the pre-evaluations it appeared that the stall inhibitor was primarily a nuisance, particularly because the departure preventer opened the maneuver boundary of the simulated A-7 to the full aerodynamic stall region of the airplane and the stall inhibitor reduced the pilots' capability in this extended region. Because of the short time available for the formal evaluations it was decided to concentrate on the departure preventer rather than the stall inhibitor.

The results of the primary formal evaluation stabilized very rapidly as is indicated by the relative ratings which are presented in Table III. There are several points of interest as gleaned from the pilots' comments.

From the ratings it appears that the pilots were insensitive to the difference in switching boundary. They were able to discern the difference in switching boundary, but except for one case the difference had an insignificant effect on the rating. The one case is the rating of B from Pilot 1 for the configuration with SB_2, DP_b on, SI off. This configuration was evaluated directly after Pilot 1 had rated the same configuration but for SB_1 A+. In his comments, Pilot 1 made a direct comparison between the two configurations and noted the airplane was more "rolly" at the high angles of attack for the twenty-degree switching boundary case. However, this difference was not noticed without the direct comparison of back-to-back configurations.

Another interesting aspect of the relative rating data is the indicated double ratings from Pilot 2 for every case in which both the stall inhibitor and departure preventer were active. The B rating in parenthesis for each case was given during the formal evaluations wherein the pilot comments indicate that Pilot 2 very much disliked the "stick pusher" because "it is not the kind of stall warning a pilot wants" and because "it makes the nose move." Yet, because the departure preventer worked "very well" and kept the airplane from rolling off he rated the combination with a B. He, however, did not try pulling much "g" to track the target with the stall inhibitor working. After the formal evaluations were completed, Pilot 2 did a run with both the stall inhibitor and the departure preventer operating purposefully to investigate using greater "g". His comments were as follows: "Run N for November - this was one (with) the departure preventer device plus the stick pusher. It does the same as in my previous comments, but (previously) I didn't pull as much g as I might have. If you don't pull very much g, the fact that it doesn't roll off is good, the pumping of the stick which prevents you from putting the nose on the target is a disadvantage but perhaps not too serious. However, if the tactical situation demands more g, then this configuration becomes unacceptable due to the pumping of the stick and the motion of the nose and that bad feature is not counter-balanced by the presence of the good feature that it won't roll off. We still like the anti-roll off feature, we still like the departure preventer, but the stick pusher is really unacceptable (and) it makes it worse than the normal airplane. I think that if you were considering that the things like 4 g were what you would use, and I guess they are, then all the ratings for the stall preventer plus stick pusher would go from bravo down to delta." - End of comments.

The "stick pusher" in the above paragraph of comments was the stall inhibitor and not the longitudinal bobweight. In fact, for all of the evaluations discussed so far, the longitudinal bobweight was not activated. It was not activated because, as mentioned earlier, during the pre-evaluations the bobweight was found to sometimes give undesirable stick "nibbles" and be detrimental. No reason could be found and we were reluctant to use the bobweight because of its inconsistent operation.

As the formal evaluations proceeded, the test conductors quickly became aware that the pilots' comments and ratings were consistent and very stable. Each pilot, on his own volition and after each performed between

twenty and twenty-five runs, remarked that he could immediately tell what kind of airplane he had and that as soon as he recognized the airplane characteristics then his comments and rating were known to him. Therefore, unless there was something new to be seen and evaluated, there was little sense in continuing. The pilots' remarks were clearly valid and reasonable. Because of the attained stability of comments and ratings, an opportunity to deviate from the planned matrix was taken in order to expand the formal evaluations.

Both pilots performed runs to evaluate the stall inhibitor/departure preventer with an active pitch bobweight, see Table IV. During these runs, none of the disturbing nibbles occurred. Pilot 1's ratings were consistent with those of his earlier, primary evaluations for the 18 degrees angle of attack switching boundary (SB_1). However, for the twenty degrees switching boundary, Pilot 1 upgraded his ratings for the stall inhibitor on some cases because although the stall inhibitor still caused the nose to oscillate, the effect of the inhibitor seemed to be lessened. Pilot 2 simply did not appreciate the bobweight under any circumstances because it made the stick move, even at low angles of attack, and reduced his tracking ability throughout the flight envelope. Pilot 2's background does not include extensive experience with bobweights and because the rating of C applied to the normal A-7 without bobweight his dislike for bobweights caused him to downrate the A-7 with bobweight as contrasted with the A-7 without bobweight.

With the expanded opportunity to investigate the stall inhibitor/departure preventer, a further characteristic of the stall inhibitor was addressed. During the primary, formal evaluations a one pound stick kick for a positive angle of attack rate at the switching boundary was incorporated in the stall inhibitor. A further evaluation of the stall inhibitor without the stick kick was made by Pilot 1 to see if there would be a reduction or elimination of the PIO tendencies caused by the stall inhibitor. This was done for all twelve configurations with the stall inhibitor on and was intermixed with other configurations. There was no change in either the ratings or the pilot's comments from the cases with the full stall inhibitor.

The A-7 has an AFCS cut-out in the lateral mode for angles of attack above eighteen degrees. Pilot 2 did ten evaluations where the automatic roll cut-out feature was inactivated. Again, these evaluations were intermixed with other configurations. No changes in pilot comments or pilot ratings were observed.

Because a pitch rate gyro is a more common instrument on airplanes than is an angle-of-attack rate measurement device, a procedure was developed for substituting a filtered pitch rate signal for the angle-of-attack rate signal used in the calculation of the switching boundary. This substitution was evaluated by Pilot 2 in ten runs of alternating between the pitch rate and the angle of attack rate signals for the departure preventer at different levels of elevator AFCS authority. The pilot was told that direct comparison between runs was intended. There was no difference discernible to the pilot between the pitch rate signal and the angle of attack rate signal. No runs

with simulated turbulence were made and it is expected that the pitch rate signal would be preferred in a turbulence environment.

During the pre-evaluations, several values of the angle of attack switching boundary constant (C_f) were investigated and it was established that values of 18° and 20° were most effective. Values of 22° and greater were progressively less effective. Recall that for the simulated A-7, departure generally occurs between 21° and 22° angle of attack at zero sideslip. Four formal evaluations were made with the angle of attack switching constant at 20°, 22° and 25°. For the 22° case, both the maximum and minimum values of elevator AFCS authority were used and for the 25° case the maximum elevator AFCS authority was used. For the 22° case, the pilot noticed that for the high angles of attack the airplane can "roll off into what has the appearance of a rather gentle spin (but) recovery is easy. Just relax the stick a little bit and the roll returns." Because the "spin" was gentle and the recovery very easy, the pilot did rate these an A. The 25° case was seen to be very similar to the normal airplane configuration and was rated C.

In summary, the departure preventer, for all AFCS authority levels, worked smoothly and very satisfactorily and it, by itself, was highly preferred. With just the departure preventer, the pilots could maneuver freely with great confidence and use the full capability of the airplane right into the aerodynamic stall. The departure preventer thus expands the maneuver envelope of the simulated A-7 and it prevents the yaw slice characteristics of the typical A-7 stall. It further prevents departure and will keep the simulated airplane under control in a complete aerodynamic stall if the angle-of-attack switching constant is 20° or less.

The stall inhibitor, stick pusher characteristic was not at all acceptable because of the PIO tendencies it induced.

TABLE III

RELATIVE RATINGS (*IS NORMAL AIRPLANE)

		SB_1											
		DP_a				DP_b				DP_c			
PILOT	RUN	ON		OFF		ON		OFF		ON		OFF	
		SI		SI		SI		SI		SI		SI	
		ON	OFF	ON	OFF	ON	OFF	ON	OFF	ON	OFF	ON	OFF
1	1	D	A+	D-	C*	D	A+	B	C*	D	A+	D-	C*
	2	D	A+	D-	C*	D-	A+	D	C*	D	A	D-	B*
2	1	(B) D	A	D	C*	(B) D	A	D	C*	(B) D	A		C*
		SB_2											
1	1	D	A+	D-	C*	D	A+	B	C*	D	A+	C-	C*
	2	D	A	D-	C*	D	B	D-	C*	D	A+	D-	C*
2	1	(B) D	A	D	C*	(B) D	A	D	C*	(B) D	A	D	C*
SUMMARIZED COMMENTS FROM BOTH PILOTS													
Primary reason for rating		Preventer is great, but PIO, no confidence	Great, smooth, can use full capability of airplane with confidence	PIO, no confidence	Seems no different than normal A-7	Preventer is great, but PIO, no confidence	Great, smooth, can use full capability of airplane with confidence	PIO, no confidence	Seems no different than normal A-7	Preventer is great, but PIO, no confidence	Great, smooth, can use full capability of airplane with confidence	PIO, no confidence	Seems no different than normal A-7

TABLE IV

LONGITUDINAL BOBWEIGHT ACTIVE*

RELATIVE RATINGS

			DP_a			
			ON		OFF	
	PILOT	RUN	STALL INHIBITOR		STALL INHIBITOR	
			ON	OFF	ON	OFF
SB_1	1	1	D	A	D	C
	2	1	D	D	D	D
SB_2	1	2	B	A	C	C
	2	2	D	D	D	D

* In this series, several runs of the normal A-7, (without bobweight) as it was used in the primary evaluations, were made and they were rated C by both pilots.

SECTION VII

CONCLUSIONS AND RECOMMENDATIONS

7.1 CONCLUSIONS

The analytical and experimental studies of the program led to the following conclusions:

1. The simplified departure boundary, which is characterized by only the two major parameters, the angle of attack α and the angle of sideslip β, have been shown to be desirable and adequate for use in the design of the departure preventer for the A-7D aircraft.

2. A switching law based upon the $\alpha - |\beta|$ departure boundary and the time rate of change of α (or its substitute using pitch rate passing through a high pass filter) for activation and deactivation has provided a natural means to design a departure preventer and stall inhibitor. The nonlinear longitudinal control law is a function of the magnitude of the sideslip as well as of the longitudinal state variables, and the nonlinear directional control law is a function of the angle of attack as well as of the lateral-directional state variables. Furthermore, the concept permits these devices to be deactivated outside the dangerous stall departure region.

3. The evaluation pilots consider the departure preventer, which when activated automatically commands the longitudinal control (UHT) and the directional control (rudder), has been shown to be very desirable. It works smoothly, and it permits the pilot to use an expanded maneuvering capability of the aircraft with confidence.

4. The stall inhibitor, which increases the longitudinal stick force when activated, has been shown through the pilot-in-the-loop evaluation to be detrimental. Although it does warn the pilot of the impending stall, the stall inhibitor hinders the pilot from using the maximum maneuvering capability of the aircraft because of the strong PIO tendency, regardless of whether the departure preventer is operating or not.

7.2 RECOMMENDATIONS

In view of the fact that the breadboard of the departure preventer has been mechanized as a flightworthy special-purpose analog computer, it is recommended that the departure preventer be evaluated in flight in the A-7 aircraft. Other recommendations are given below:

1. It is felt that, in view of its generality, the procedure used in the design of the departure preventer for the A-7D aircraft should be applicable to other aircraft, fighter or not. It is strongly recommended that the proposed procedure and the breadboard be applied to other contemporary fighter aircraft such as F-4, F-111, F-14 or others, and then perhaps to transport class aircraft.

2. The present $\alpha - |\beta|$ departure boundary was based on low subsonic data. The dependency of the boundary on Mach number should be determined and incorporated in the boundary.

3. If better flight test data of the A-7 at high angle of attack becomes available, near-stall characteristics should be identified and correlated to modify, as required, the coefficients and gains in the switching law and the departure preventer.

4. Possible replacement of the sideslip by some inertia measurement such as n_y would be desirable because of the difficulty of measuring sideslip.

5. Limited study of sensitivity of performance of the departure preventer to errors in α and β has been done in this program. However, more extensive sensitivity study including the sensor dynamics is recommended. It may also be beneficial to obtain better estimates of α and β by blending air and inertia measurements.

6. The specific characteristics of the A-7 wherein the factors which induce the departure prior to the aerodynamic stall and the fact that control effectiveness is retained into the stall permit the departure preventer to be a stability augmentation device for the A-7. Other aircraft may not have the same sequence of factors even though they exhibit the same factors as the A-7. Both the sequence of factors as well as the factors themselves can affect the philosophy of approach to the design of a "departure preventer" system. It is recommended that a pilot-in-the-loop study be performed to determine pilot acceptance of different philosophies of design criteria for stall inhibitor/departure preventer devices as these philosophies are affected by both the factors and sequence of factors that lead up to the "stall" and the departure of an airplane.

APPENDIX I

A-7D FLIGHT CONTROL SYSTEM SIMULATION

For the studies required on Contract F33615-72-C-1162, the flight control system of the A-7D airplane must be simulated to a reasonable extent. The following represents the resulting simulation. Reference 7 is excerpted without quotation marks.

The hydraulic system for the A-7D is supplied by two independent power control (PC) systems, PC1 and PC2. Each of the basic power control systems provides the design rates of control surface motion, but only 50% of the design operating hinge moments. The nominal design rates of control surface motion and nominal design hinge moments with both power control systems operating in tandem are as follows:

Aileron	100 deg/sec	3000 ft-lb
Spoiler-Slot-Deflector	200 deg/sec	1025 ft-lb
Unit Horizontal Tail	25 deg/sec	27250 ft-lb/side
Rudder	75 deg/sec	3150 ft-lb

LONGITUDINAL CONTROL SYSTEM

To provide good speed control in the landing approach and good longitudinal control at sensitive flight conditions, a nonlinear stick-to-surface relationship (variable gain mechanical linkage) is incorporated. Longitudinal stick position vs. horizontal tail deflection is presented in Figure I-1. A parallel trim system is incorporated and the shallowest part of the stick-to-surface gain is set at the sensitive flight condition.

Longitudinal Feel System

The longitudinal feel system consists of:

1. a dual rate feel spring
2. two bobweights
3. two viscous dampers.

Variations of F_{es} with speed are obtained from the feel spring because of stick motion. The variation of F_{es} with δ_{es} (spring contribution only) is shown in Figure I-2.

The dual bobweight system provides a static force gradient of 2.75 pounds per g, and a dynamic force gradient of 9.6 pounds per radian per(second)^2 pitch acceleration. The forward bobweight is on the stick and the aft bobweight

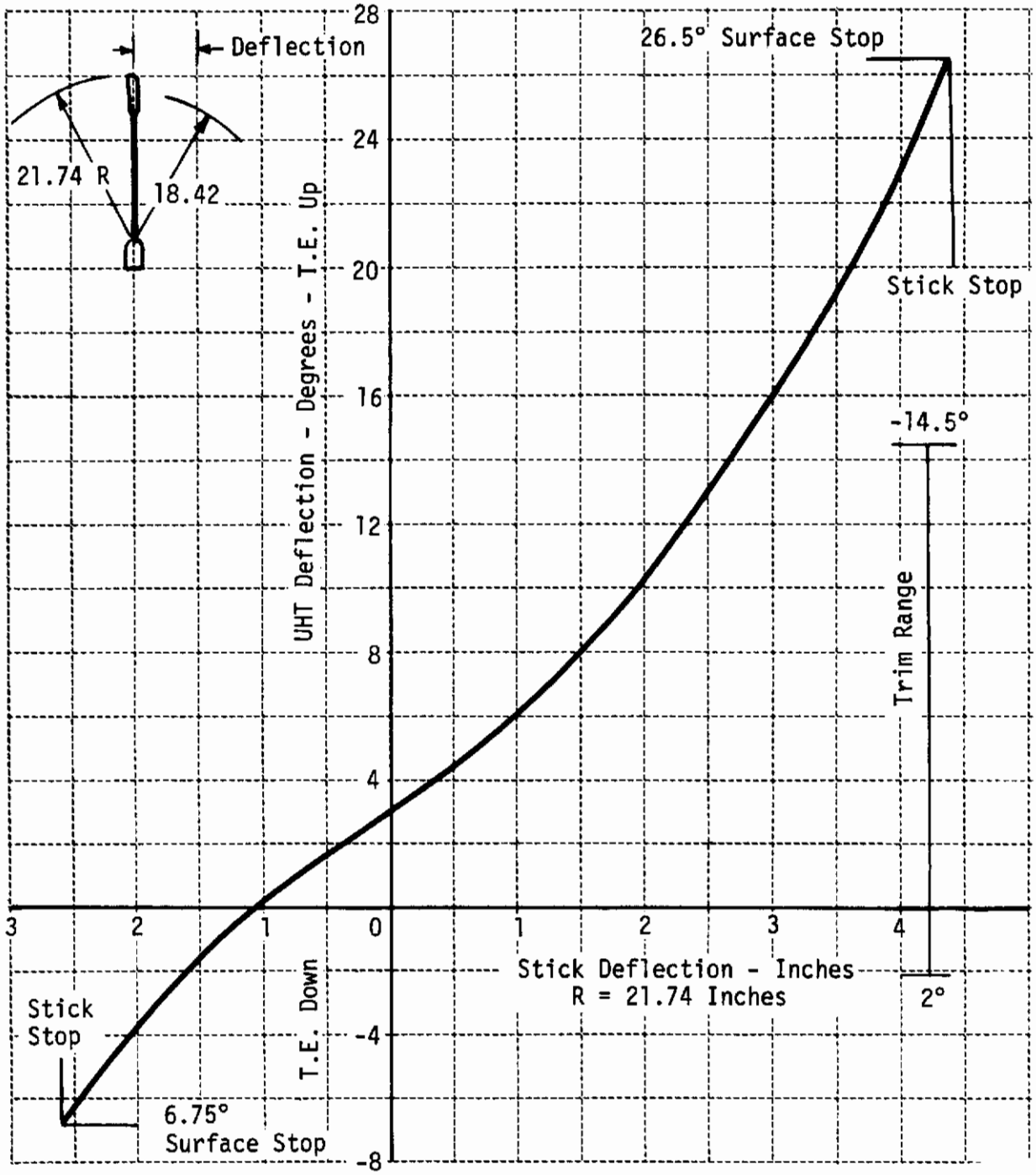

Figure I-1 Unit Horizontal Tail Deflection Vs. Stick Position
(Taken from Figure 8.3 of Reference 7)

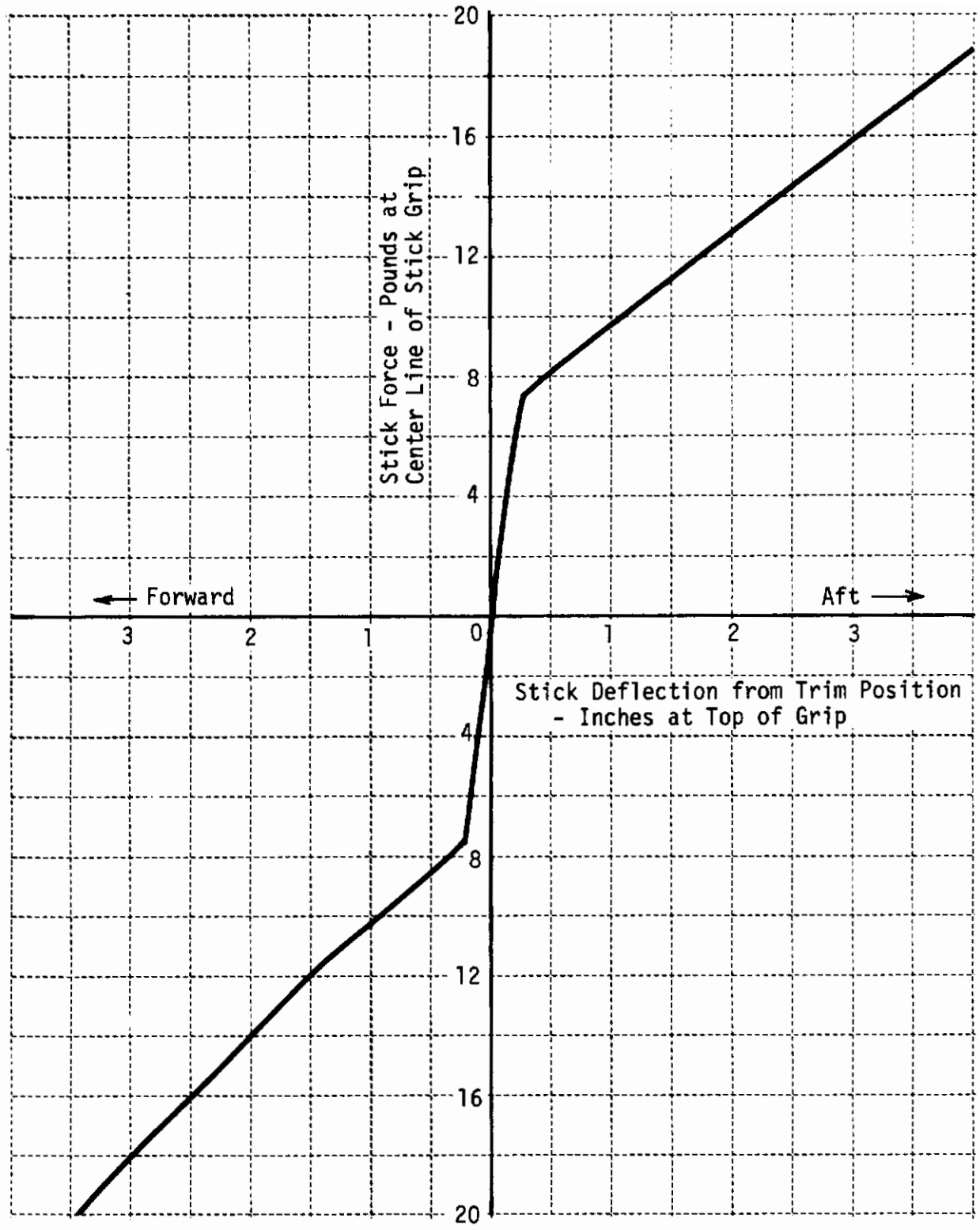

Figure I-2 Longitudinal Stick Force at One "g" Vs. Longitudinal Stick Deflection From Trim (Taken from Figure 8.4 of Reference 7)

is in the vertical fin. Steady-state stick force vs. normal load factor for representative cases is presented in Figures I-3 and I-4.

Viscous dampers provide stick force proportional to stick velocity at 2 pounds per inch per second measured at the stick grip.

Balance springs are used to balance bobweight forces at 1 g flight and for preloading the pushrod system.

Longitudinal Stick Force Trim

The trim system is a parallel, beep system which trims the stick. therefore stick position at all times reflects the surface position except for transient series AFCS inputs.

minimum trim rate - 1.6 deg of surface/sec occurring at minimum slope of variable gain

maximum trim rate - 3.8 deg of surface/sec occurring at steepest slope of variable gain

UHT can be positioned 2^{o} (TED) to -14.5^{o} (TEU) with trim.

LATERAL CONTROL SYSTEM

The lateral control surfaces consist of:

1. outer panel aileron
2. inboard panel spoiler-slot-deflector.

Both surfaces are activated at all times. At low speeds, the ailerons provide powerful roll control. At high speeds the aileron looses effectiveness because of elasticity and the spoiler alone is capable of providing spec roll power.

A small deadspot in spoiler motion, ± 2 degrees of aileron travel, is provided near stick neutral so that the spoiler does not break out for small inputs. Figure I-5 shows lateral stick position versus roll control surface deflections.

Lateral trim is provided by the ailerons alone to prevent trim drag from the spoilers.

The lateral stick stops are set to give a stick throw of 2.81 inches. The aileron stops are set at ± 25^{o} and the spoiler stops are set at 60^{o}. The lateral stick throw of 2.81 inches commands ± 16^{o} ailerons and 35.15^{o} of spoiler. The difference between the surface available with stick displacement and that available at the surface stops is available for the AFCS in the CONT AUG mode.

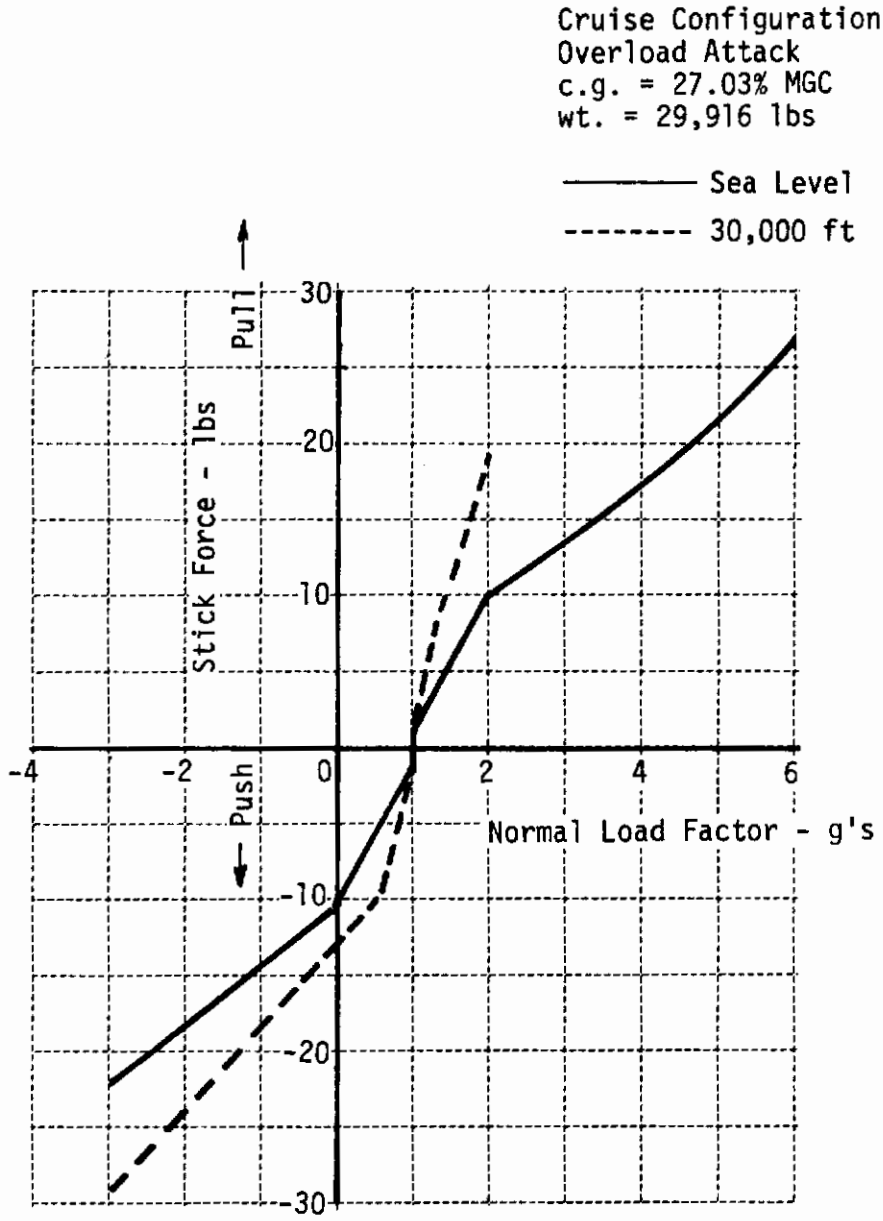

Figure I-3 Stick Force Required to Pull Normal Load Factors From Trimmed Level Flight at Mach Number = 0.60
(From Figure 5.29 of Reference 7)

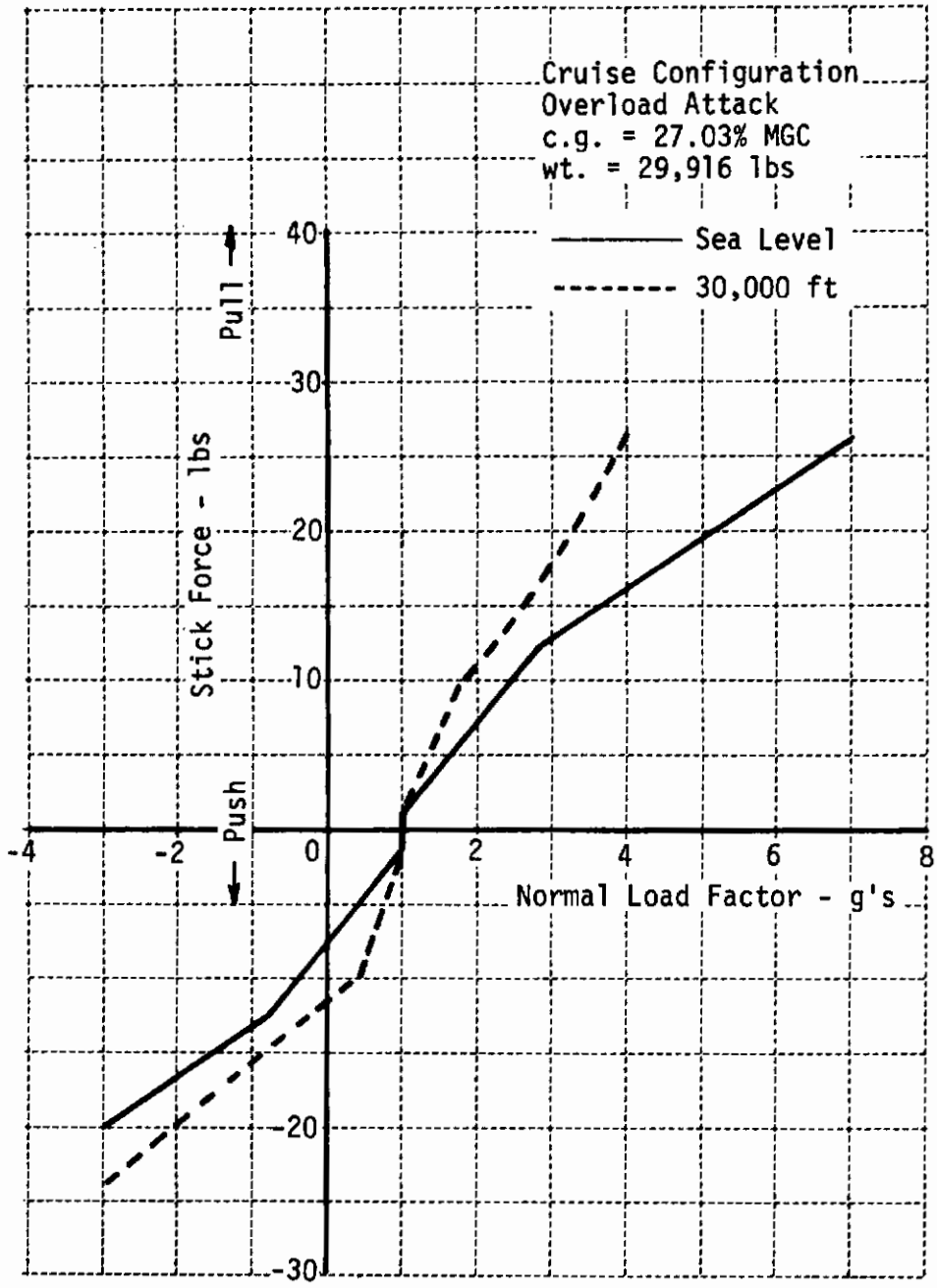

Figure I-4 Stick Force Required to Pull Normal Load Factors From Trimmed Level Flight at Mach Number = 0.9 (From Figure 5.31 of Reference 7)

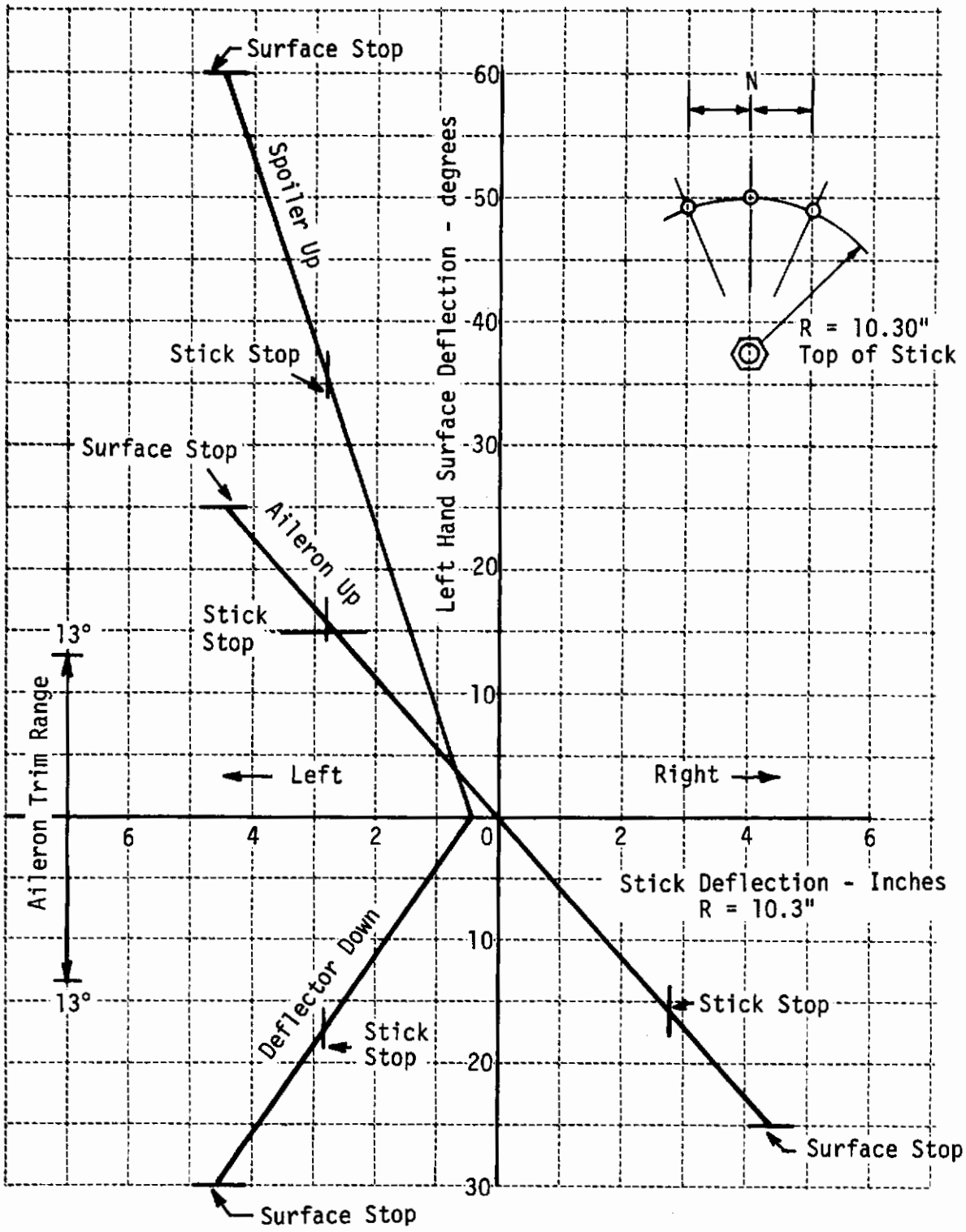

Figure I-5 Lateral Control Surface Deflection Vs. Lateral Stick Deflection
(From Figure 8.8 of Reference 7)

Lateral Stick Forces

Lateral stick forces are provided by a linear spring and a viscous damper. Figure I-6 shows the spring rate. The viscous damper provides 0.5 lbs/in./sec at the stick grip. AFCS signals are not fed back to the stick.

A bobweight is included to improve the mass balance of the pushrod system. A breakout force of 1 lb is provided.

Lateral Trim

Lateral trim is a beep, series system. Trim authority is ± 13° of aileron (single aileron) with a maximum rate of 1 deg/sec. The stick stays in neutral for all trim positions.

AFCS

There is no artificial stability augmentation in roll with the auto pilot in OFF or in STAB (yaw damper only) position.

DIRECTIONAL CONTROL SYSTEM

The directional control system has a constant mechanical advantage system. Rudder control available in cruise configuration is ±6° and for landing is ±24°. See Figure I-7. Trim is ±5°.

Directional Feel System

Pedal forces are produced by linear springs. See Figure I-8. Gradients change at opening of landing gear doors.

Directional Trim

Pedals stay neutral with rudder trim.

Yaw Damper and ARI

Stability augmentation about the yaw axis and an aileron-rudder interconnect (ARI) are provided when the STAB switch is in the STAB position. The rudder is deflected proportional to the aileron deflection from roll trim, with the gain programmed by the UHT position. See Figure I-9.

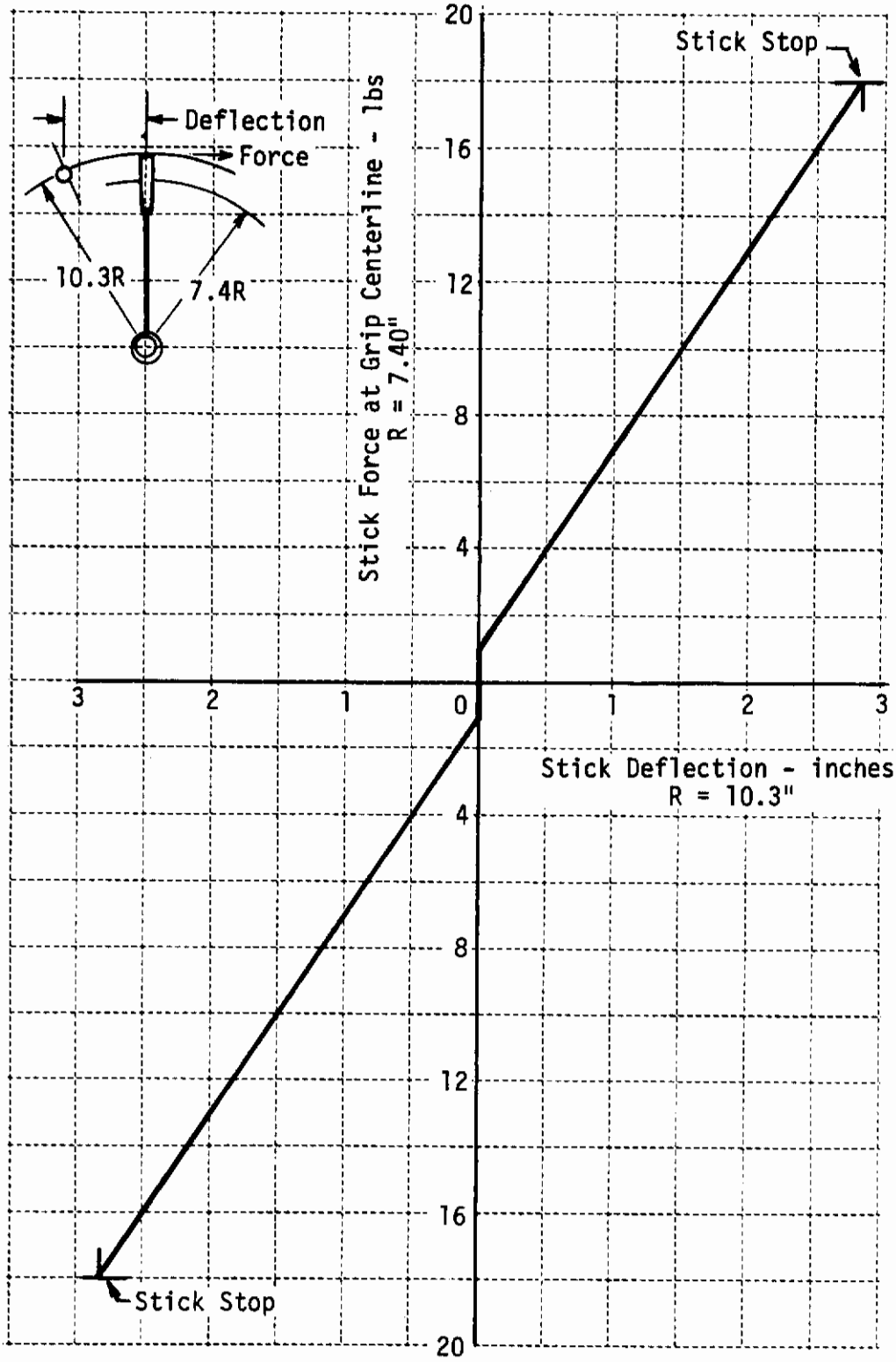

Figure I-6 Lateral Stick Force Vs. Lateral Stick Position
(From Figure 8.9 of Reference 7)

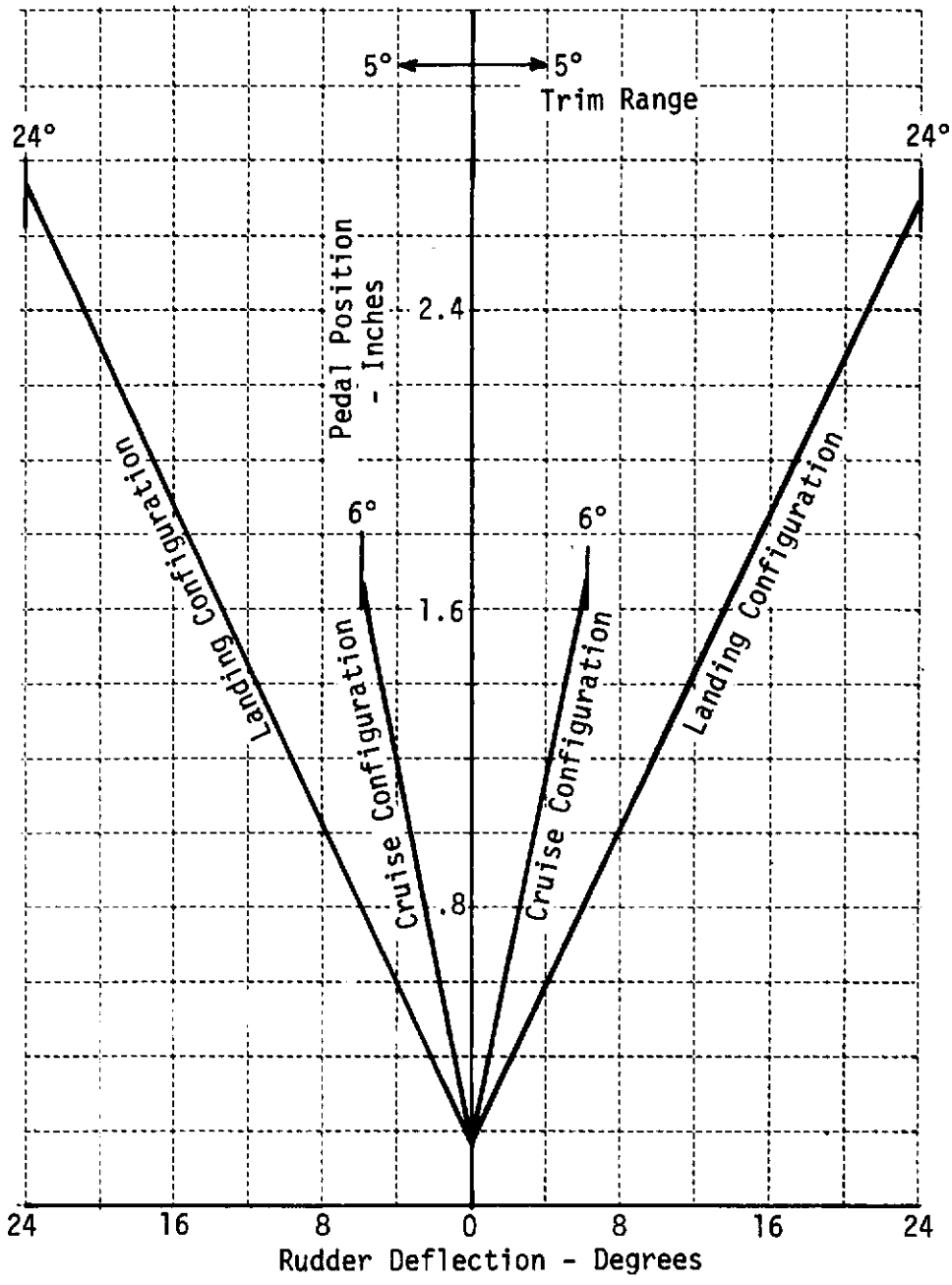

Figure I-7 Rudder Pedal Position Vs. Rudder Deflection
(From Figure 8.12 of Reference 7)

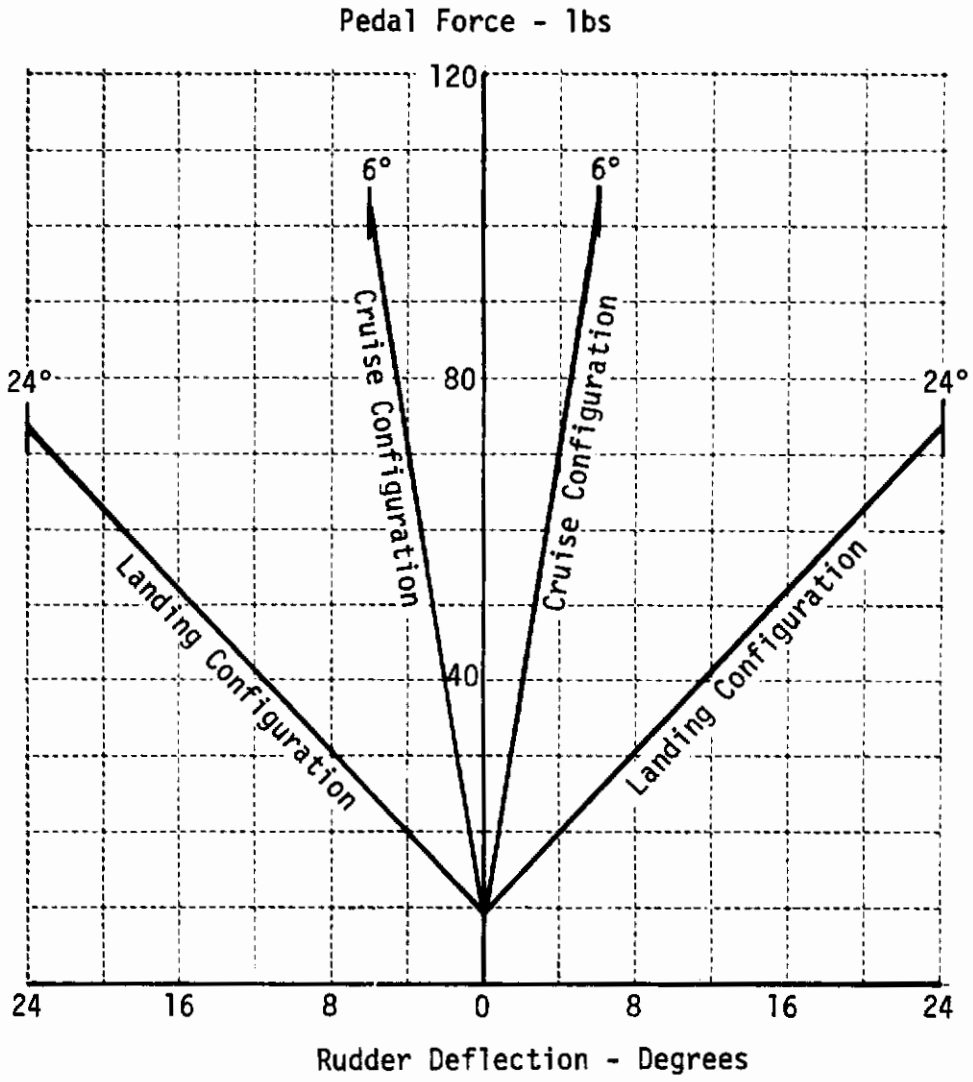

Figure I-8 Rudder Pedal Force Vs. Rudder Deflection
(From Figure 8.13 of Reference 7)

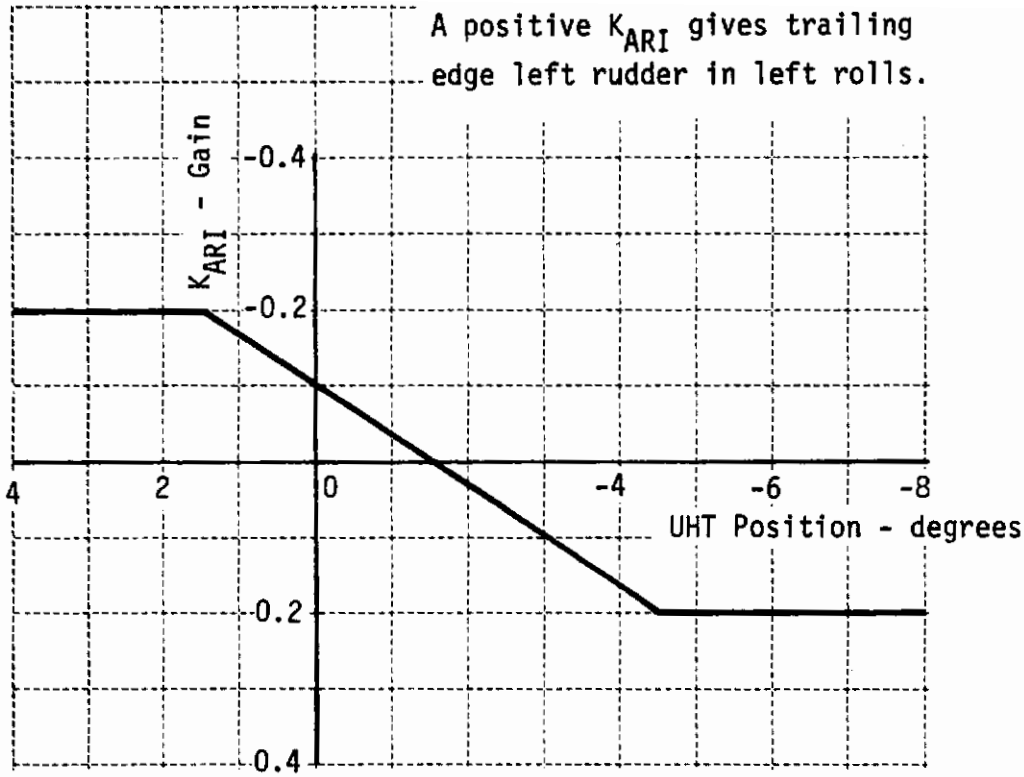

Figure I-9 UHT Position Vs. ARI Gain
(From Figure 8.14 of Reference 7)

Automatic Flight Control System

The functions available are:

stability augmentation	-	STAB
control augmentation	-	CONT AUG
attitude hold	-	ATT HOLD (not applicable)
heading hold	-	HDG (not applicable)
navigation	-	NAV (not applicable)
altitude hold	-	ALT (not applicable)

a position labeled PATH is not used.

CONT AUG

This consists of pitch rate, normal acceleration and stick force signals fed to series actuators for the longitudinal case. See Figures I-10 and I-10a with only those functions required being reproduced herein.

For the roll axis, stick force steering and roll rate damping are provided. (There is a versine function of bank angle fed to the longitudinal control axis to automatically hold the nose up during turns, but it is believed that this is not operative for the CONT AUG mode.) See Figure I-11 and I-11a.

STAB

Block diagrams of the yaw axis are shown in Figures I-12 and I-12c. Yaw rate damping, yaw trim and an aileron-rudder interconnect (ARI) are provided in STAB. A signal proportional to aileron position less the aileron deflection for roll trim is multiplied by a gain schedule $[f(\delta_e)]$ to command rudder for the ARI.

AFCS actuator output capability in terms of surface rates and authorities at no load conditions and neutral rigging are:

	max rate, deg/sec	nominal authority - deg
UHT(AFCS)	23.6	±4.8
Rudder (AFCS)	72	±14
Aileron (AFCS)	80	±10
Spoiler (AFCS)	237	21
Deflector (AFCS)	119	10.5

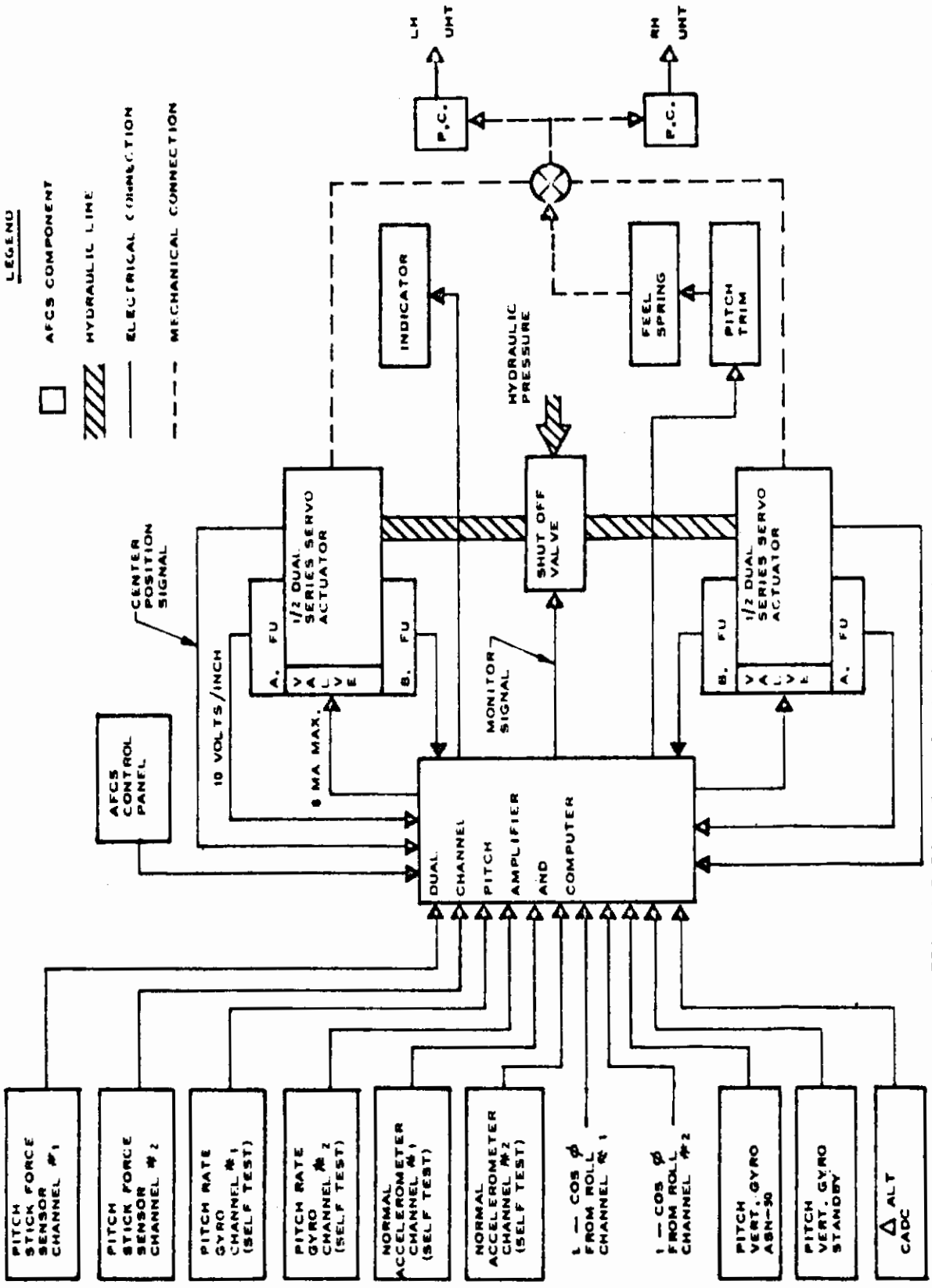

FIGURE I-10 PITCH AXIS BLOCK DIAGRAM
(FROM FIGURE 8.16 OF REFERENCE 7)

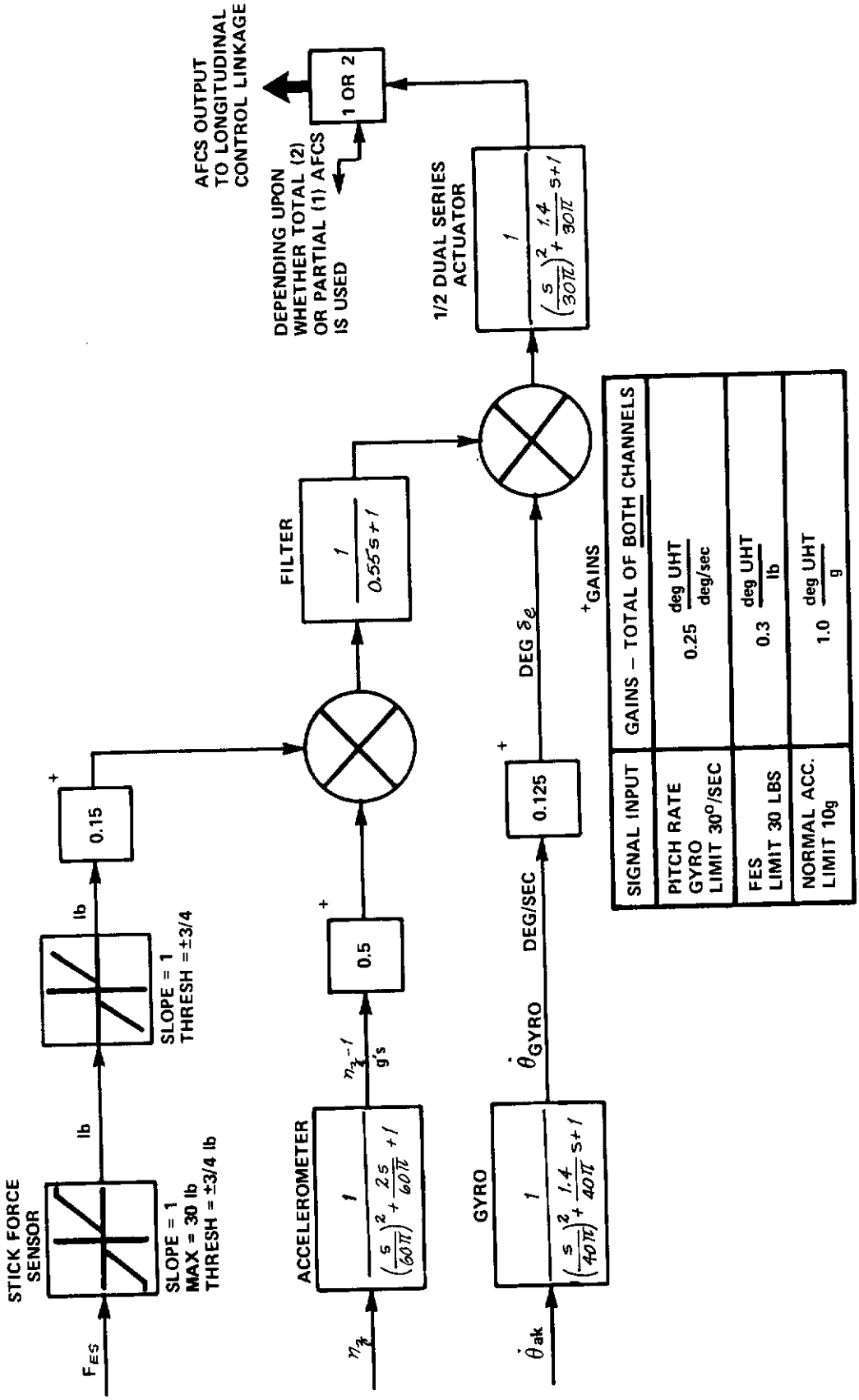

SIGNAL INPUT	GAINS – TOTAL OF BOTH CHANNELS
PITCH RATE GYRO LIMIT 30°/SEC	0.25 $\frac{\text{deg UHT}}{\text{deg/sec}}$
FES LIMIT 30 LBS	0.3 $\frac{\text{deg UHT}}{\text{lb}}$
NORMAL ACC. LIMIT 10g	1.0 $\frac{\text{deg UHT}}{\text{g}}$

Figure I-10a Pitch Axis Block Diagram: Cruise Configuration
(Reference 13, Figure 4.3 and Table 4.3)

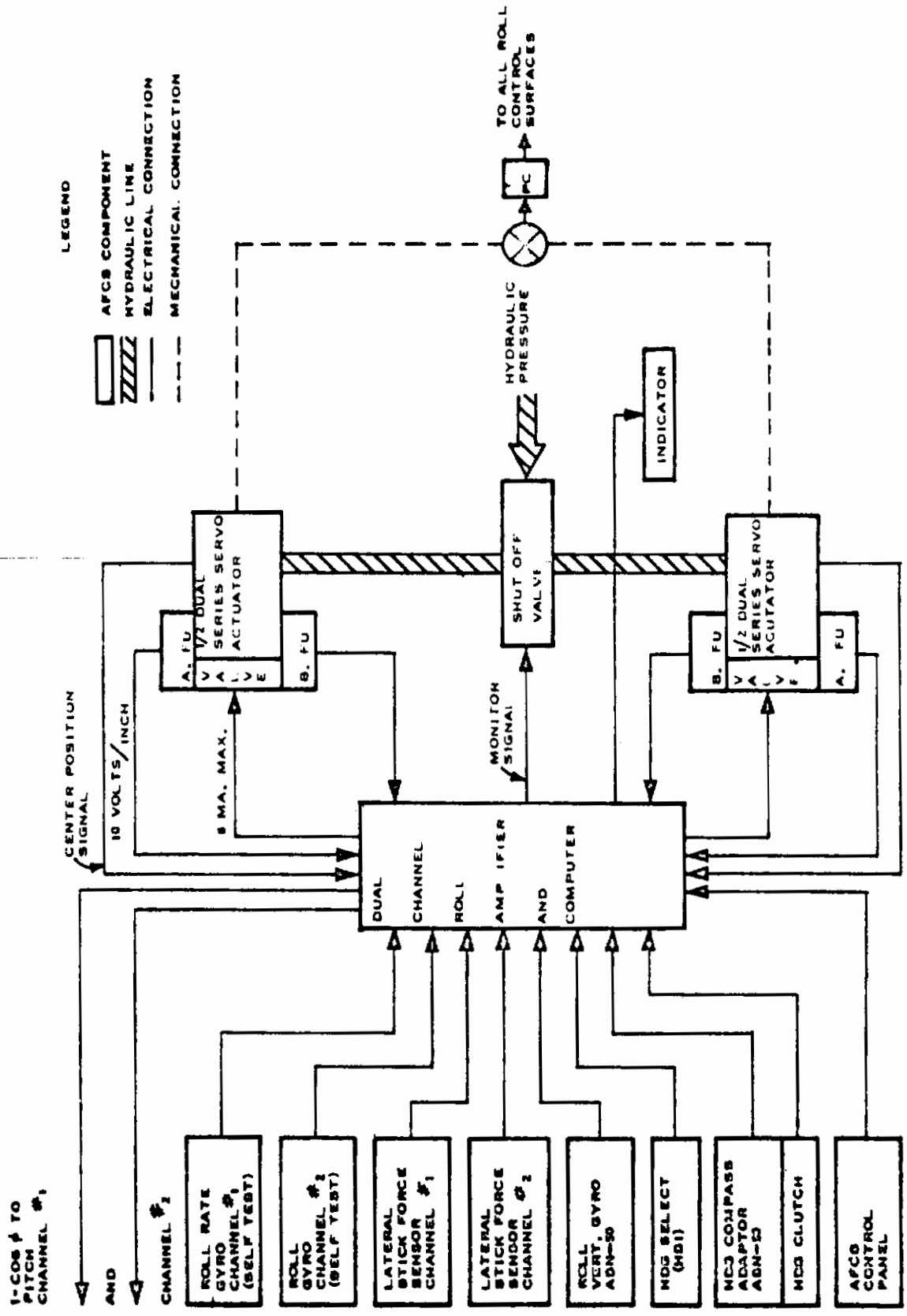

FIGURE I-11 ROLL AXIS BLOCK DIAGRAM
(FROM FIGURE 8.17 OF REFERENCE 7)

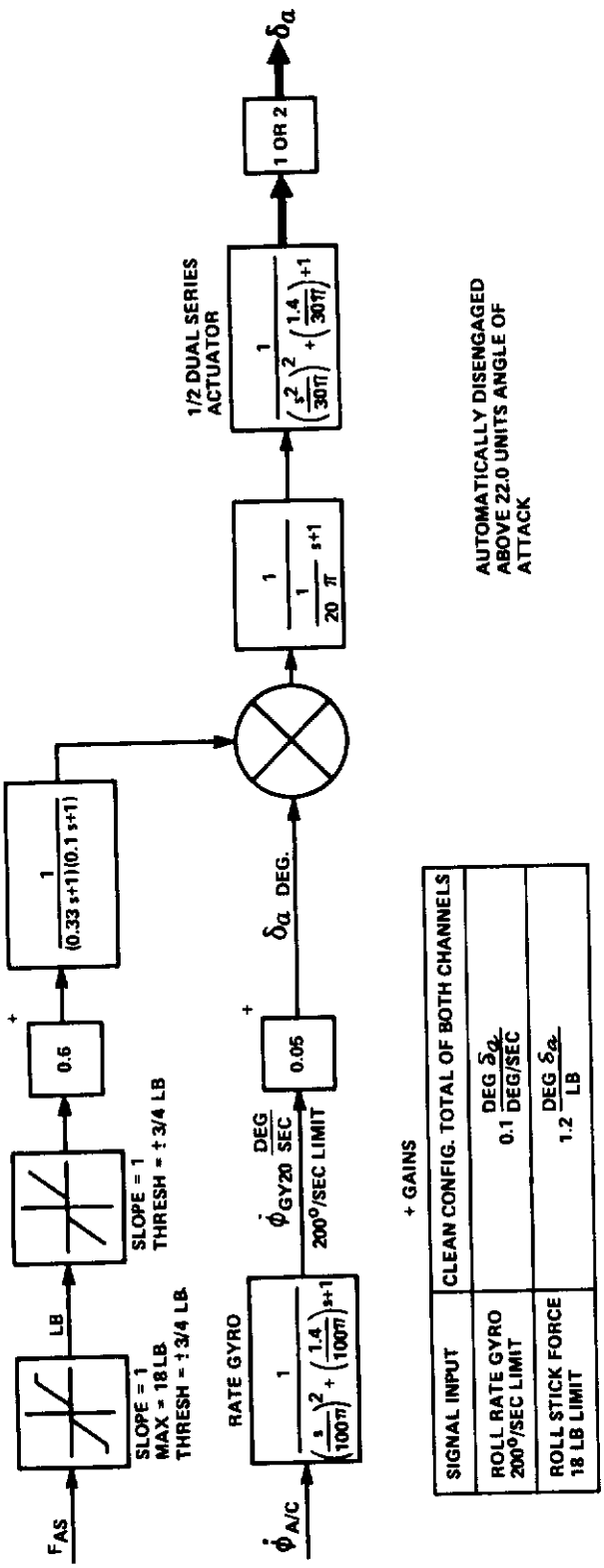

+ GAINS

SIGNAL INPUT	CLEAN CONFIG. TOTAL OF BOTH CHANNELS
ROLL RATE GYRO 200°/SEC LIMIT	0.1 $\frac{DEG\ \delta_a}{DEG/SEC}$
ROLL STICK FORCE 18 LB LIMIT	1.2 $\frac{DEG\ \delta_a}{LB}$

Figure I-11a Roll Axis Block Diagram: Cruise Configuration
(Reference 13, Figure 4.2 and Table 4.2)

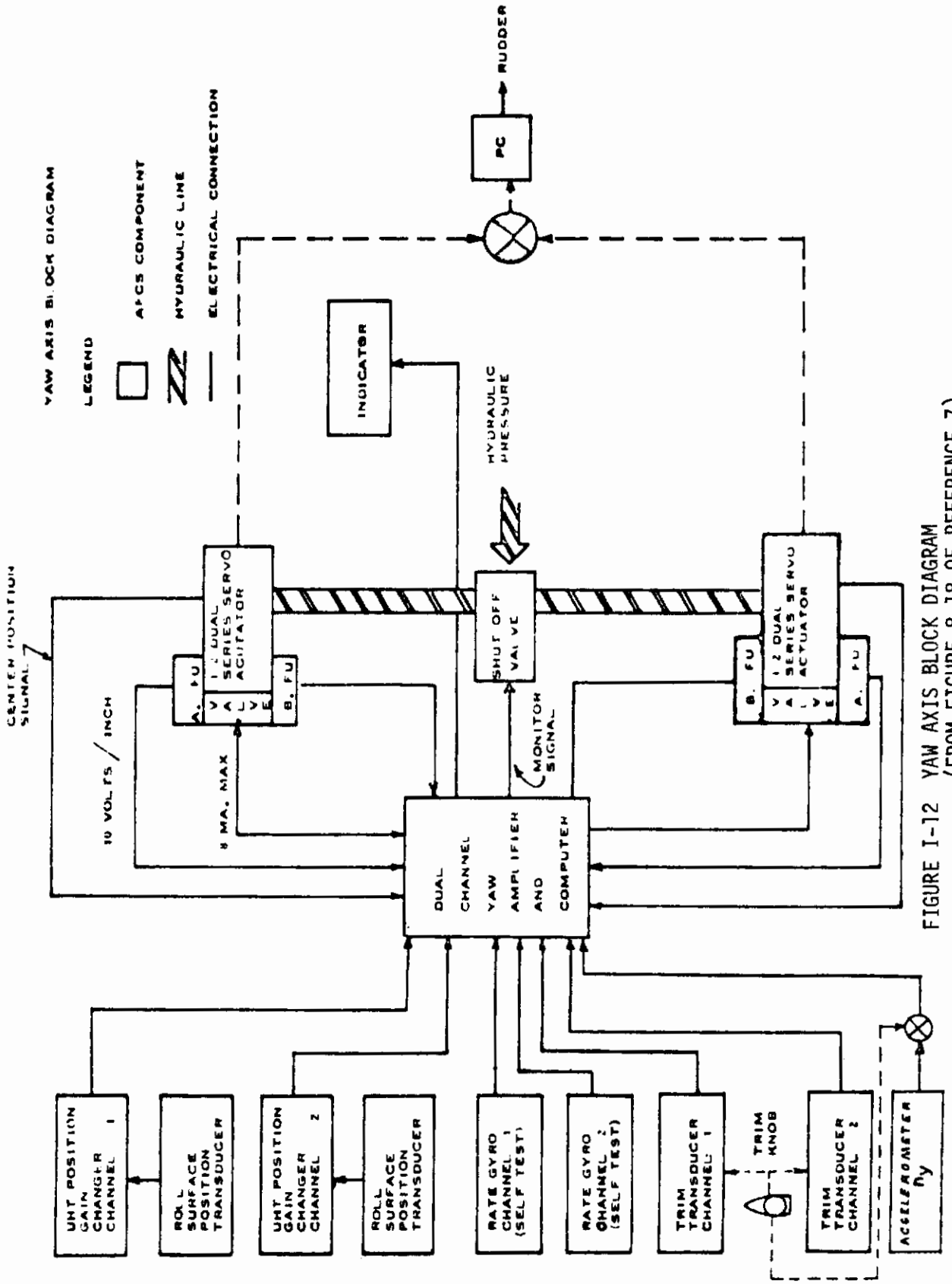

FIGURE I-12 YAW AXIS BLOCK DIAGRAM
(FROM FIGURE 8.18 OF REFERENCE 7)

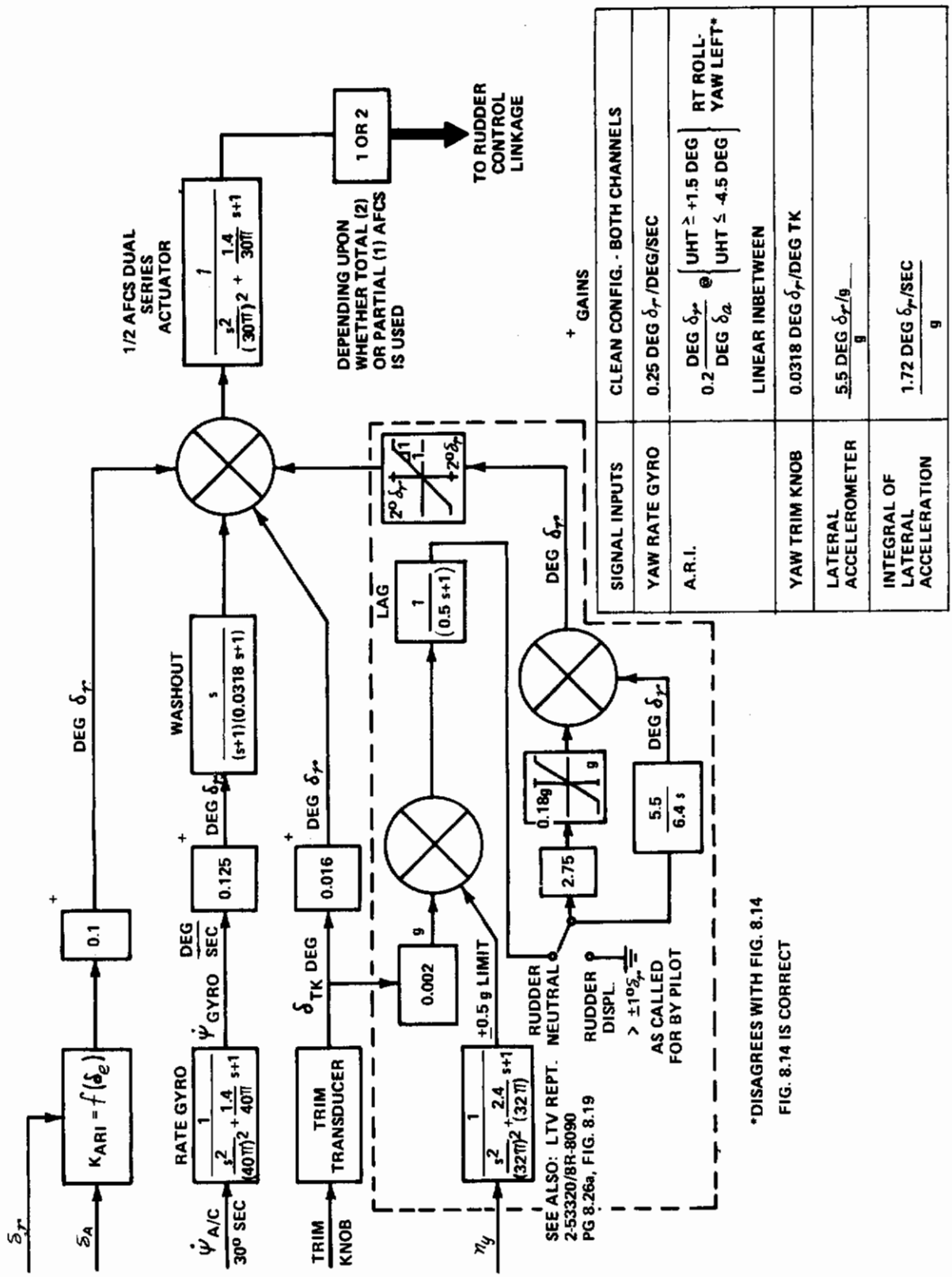

SIGNAL INPUTS	CLEAN CONFIG. - BOTH CHANNELS	
YAW RATE GYRO	0.25 DEG δ_r/DEG/SEC	
A.R.I.	$0.2 \frac{\text{DEG } \delta_r}{\text{DEG } \delta_a}$ @ UHT ≥ +1.5 DEG UHT ≤ -4.5 DEG LINEAR INBETWEEN	RT ROLL-YAW LEFT*
YAW TRIM KNOB	0.0318 DEG δ_r/DEG TK	
LATERAL ACCELEROMETER	$\frac{5.5 \text{ DEG } \delta_r/g}{g}$	
INTEGRAL OF LATERAL ACCELERATION	$\frac{1.72 \text{ DEG } \delta_r/\text{SEC}}{g}$	

Figure I -12a Yaw Axis AFCS Block Diagram: Cruise Configuration
(Reference 13, Figure 4.1 and Table 4.1)

The spoiler and deflector are mechanically linked together and both are operated by the same power control actuator. Furthermore, all of the spoiler-deflector aerodynamic data are given with respect to only the spoiler. We can, in effect, forget there is a deflector.

By referring to report "LTV Report No. 2-51724/8R-8111" originally issued 4 April 1969 but revised and re-issued in May 1971, the following table* of maximum control rates is made.

Control Surface	No Load Maximum Rate (Deg/Sec) of Surface	Position for Maximum Rate
Aileron (AFCS)•	78	neutral
Spoiler (AFCS)✘	208	neutral
Deflector (AFCS)°	104	neutral
Aileron (PC)	142	neutral
Spoiler (PC)	432	neutral
Deflector (PC)	216	neutral
UHT (AFCS)✝	23.6	-3°
UHT (PC)	98.8	-3°
Rudder (AFCS)†	72	neutral
Rudder (PC)	140.5	neutral
FIA	100	

* From control system schematics on pages 21, 51, and 86.
† A table on page 27 gives 75°/sec
✝ A table on page 90 gives 25°/sec
✘ A table on page 60 gives 200°/sec
• A table on page 56 gives 100°/sec
° A table on page 60 gives 100°/sec.

The immediately preceding table of rate limits is the one to be used. The AFCS outputs are added or subtracted to the mechanical control system linkage. There is no feedback to the pilots' controls of the AFCS outputs. To assure no feedback in the aileron system, there is a Feel Isolation Actuator (FIA) that is a hydraulic actuator placed midway in the mechanical linkage and ahead of the point at which the AFCS outputs are added.

The roll axis of the AFCS can produce pro-spin aileron in response to the yaw and roll motions at the stall. Therefore, the roll axis of the AFCS is disengaged automatically when the airplane reaches 22.0 units angle of attack. The ailerons produce adverse yaw and if the ailerons are applied at the stall then the airplane may depart into a spin. The ailerons should not be used until 200 knots indicated airspeed is reached. (See Reference 7.)

For the digital simulation, the preceding information is simplified to what is required and is presented in Figures I-13, I-14, and I-15. A similar procedure may be used for incorporating the power control (PC) actuators and the FIA actuator rate limits.

The fixed-base, ground simulator should use AFCS systems as shown in Figures I-13, I-14, and I-15 except that the straight-through, mechanical control commands must represent the mechanical systems in the airplane. For the ground simulator, the command loops are shown in Figures 9, 10, and 11.

For both the ground-based simulator and the digital simulation, the r_b and p_b rate gyros are misaligned from the z_b and x_b axes by 2.5 degrees. Thus:

$$r_{b_{\text{rate gyro}}} = r_b \cos 2.5^\circ - p_b \sin 2.5^\circ$$

$$p_{b_{\text{rate gyro}}} = p_b \cos 2.5^\circ + r_b \sin 2.5^\circ$$

The yaw rate gyro limits are at ± 30 deg/sec with different airplanes. However, LTV says that the limit can vary from ± 10 deg/sec to ± 30 deg/sec with different airplanes. Also, LTV says the n_y loop of Figure I-12a actually degrades stability.

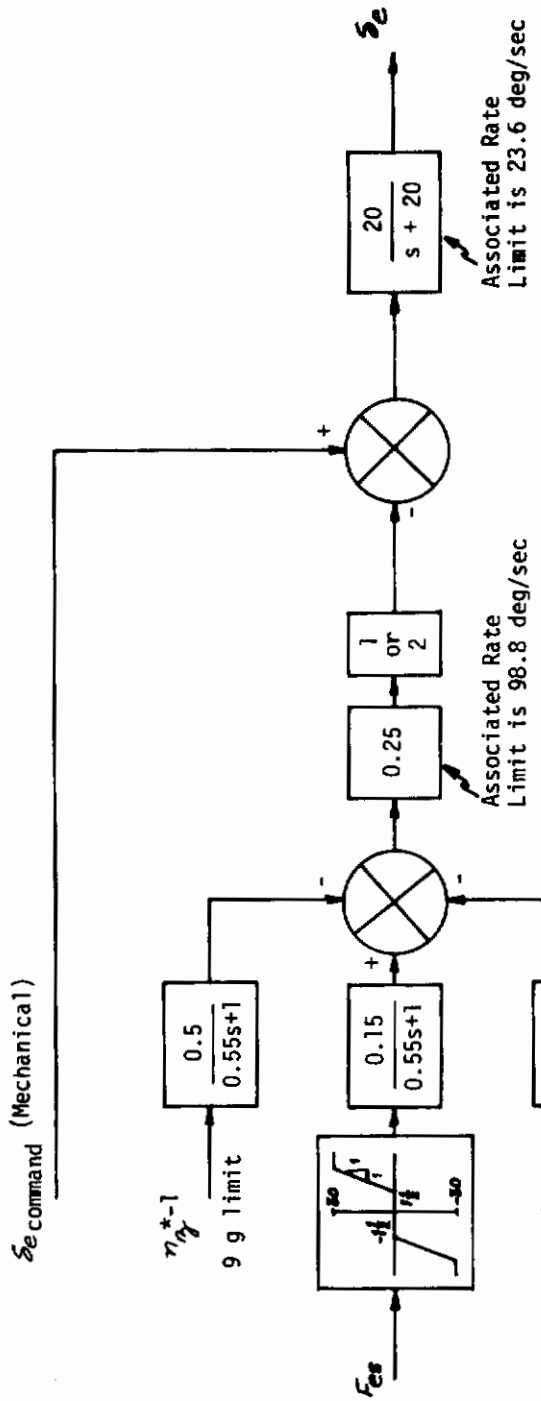

Figure I-13 Recommended Pitch Axis Digital Simulation

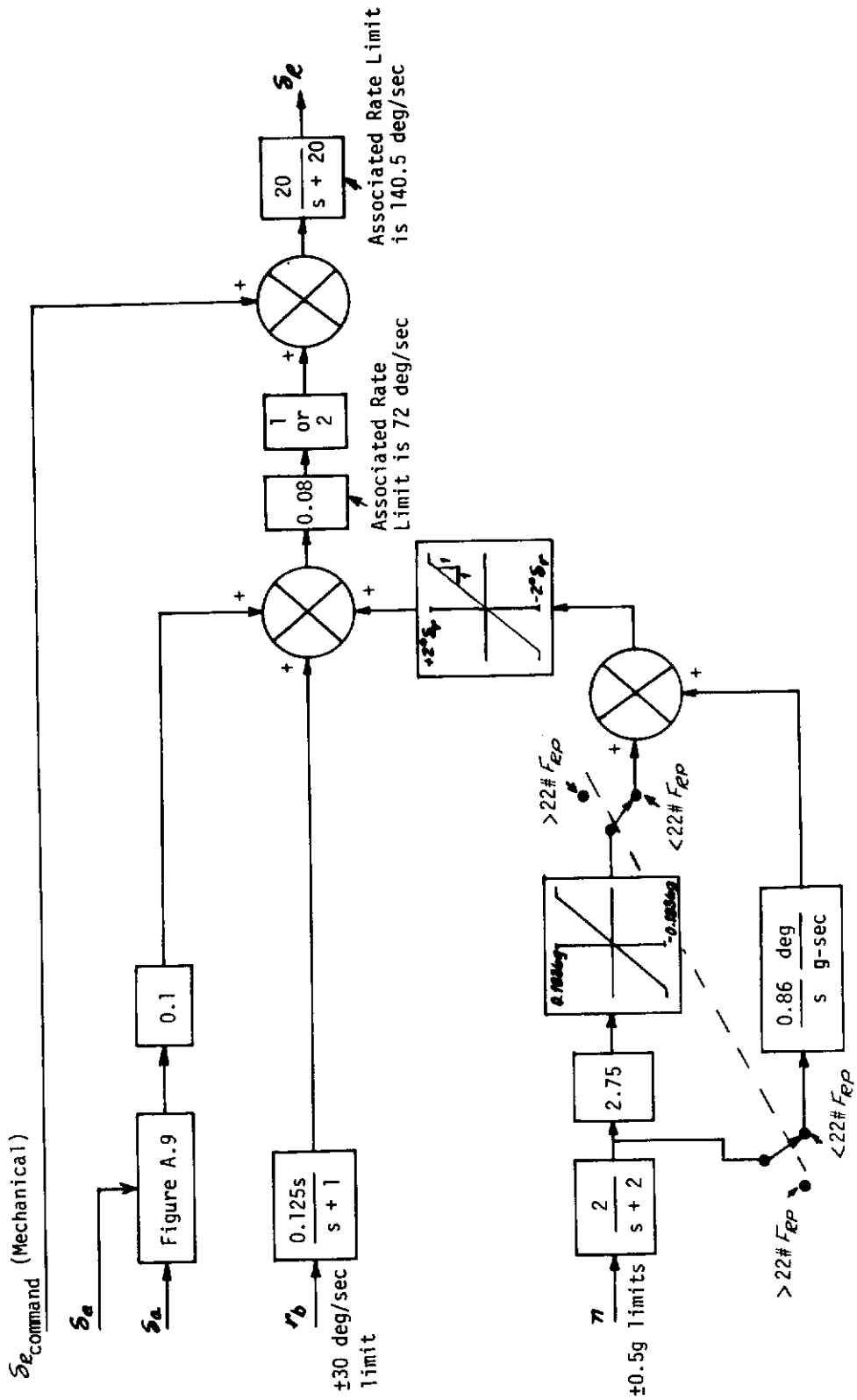

Figure I-14 Recommended Yaw Axis Digital Simulation

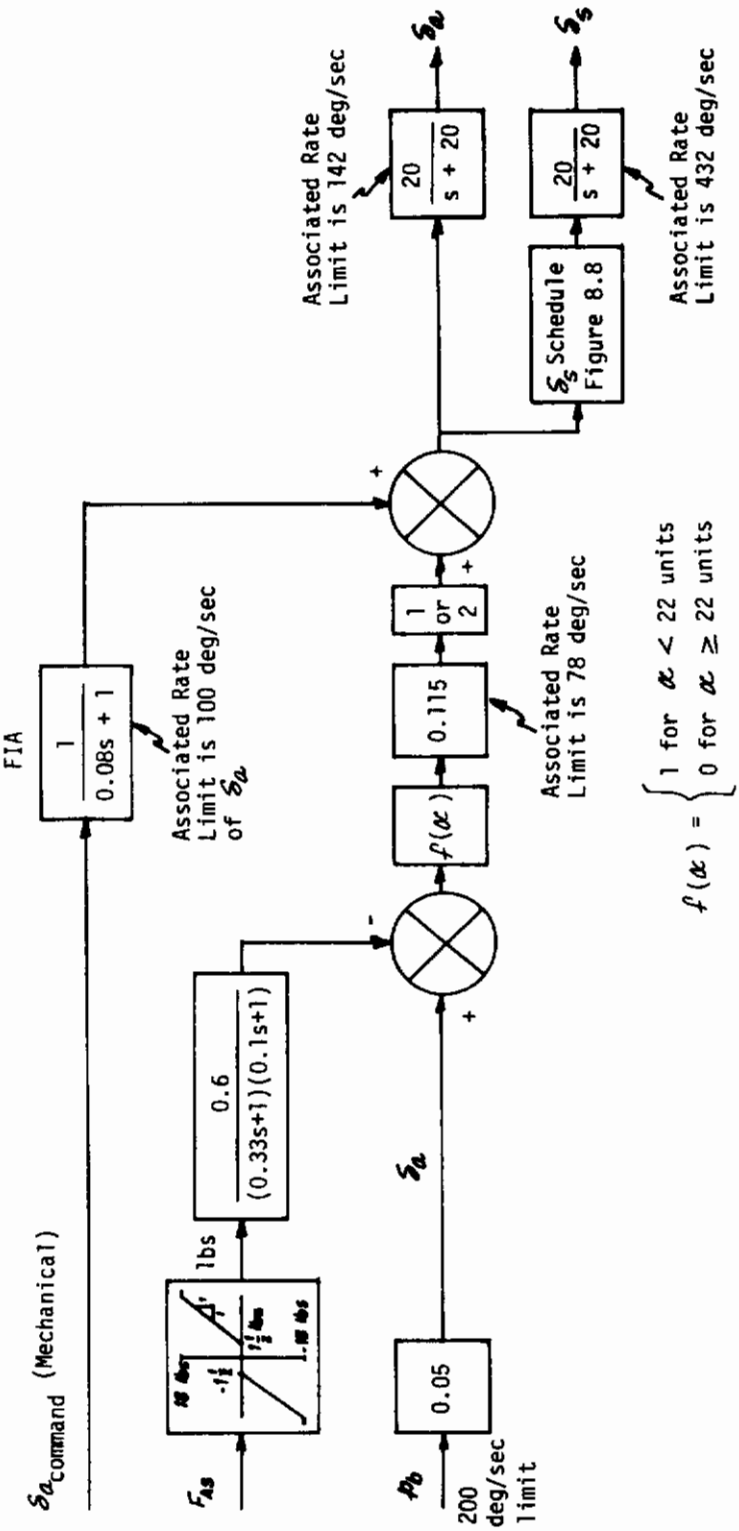

Figure I-15 Recommended Roll Axis Digital Simulation

APPENDIX II

EQUATIONS OF MOTION

A complete set of equations of motion is used in the simulator. These equations are in body axes. The Euler angles are computed through use of quaternions to overcome the gimbal lock problems. Thus, full maneuvering capability is provided without any ambiguities.

1. EULER EQUATIONS OF MOTION

$$\dot{V} = \frac{1}{m}(F_A + F_G) - W_x V$$

$$\dot{\omega} = I^{-1}(M_A - W_x I_\omega)$$

where

$$I = \begin{bmatrix} I_x & 0 & -I_{xy} \\ 0 & I_y & 0 \\ -I_{xy} & 0 & I_z \end{bmatrix}, \quad W_x = \begin{bmatrix} 0 & -r & q \\ r & 0 & -p \\ -q & p & 0 \end{bmatrix}$$

$$V = (u, v, w)^T, \quad \omega = (p, q, r)^T$$

$$F_A = \begin{bmatrix} X \\ Y \\ Z \end{bmatrix} = \bar{q} S \begin{bmatrix} C_x \\ C_y \\ C_z \end{bmatrix} + \begin{bmatrix} T_x \\ 0 \\ T_z \end{bmatrix}$$

$$F_G = mg \begin{bmatrix} \ell_{13} \\ \ell_{23} \\ \ell_{33} \end{bmatrix} = mg \begin{bmatrix} -\sin\theta \\ \sin\phi\cos\theta \\ \cos\phi\cos\theta \end{bmatrix}$$

$$M_A = \begin{bmatrix} L \\ M \\ N \end{bmatrix} = \bar{q} S \begin{bmatrix} b & 0 & 0 \\ 0 & \bar{c} & 0 \\ 0 & 0 & b \end{bmatrix} \begin{bmatrix} C_l \\ C_m \\ C_n \end{bmatrix} + \begin{bmatrix} 0 \\ -Td \\ 0 \end{bmatrix} + \begin{bmatrix} -YZ_a + ZY_a \\ XZ_a - ZX_a \\ YX_a - XY_a \end{bmatrix}$$

where the last matrix converts C_ℓ , C_m , C_n data for a given c.g. position to any c.g. position to be investigated. x_a, y_a , z_a are measurements of the reference c.g. location with respect to new c.g. location in body axes system. Also, for A-7 aircraft the aerodynamic coefficients are given in stability-axis system. These data are converted into body-axis data using

$$\begin{bmatrix} C_x \\ C_y \\ C_z \end{bmatrix} = \begin{bmatrix} \cos\alpha & 0 & -\sin\alpha \\ 0 & 1 & 0 \\ \sin\alpha & 0 & \cos\alpha \end{bmatrix} \begin{bmatrix} C_{x_s} \\ C_{y_s} \\ C_{z_s} \end{bmatrix}$$

$$\begin{bmatrix} C_l \\ C_m \\ C_n \end{bmatrix} = \begin{bmatrix} \cos\alpha & 0 & -\sin\alpha \\ 0 & 1 & 0 \\ \sin\alpha & 0 & \cos\alpha \end{bmatrix} \begin{bmatrix} C_{l_s} \\ C_{m_s} \\ C_{n_s} \end{bmatrix}$$

$$C_{x_s} = -C_D(\alpha, \delta_e) - \Delta C_D(\alpha, \delta_s)$$

$$C_{y_s} = C_{y_s}(\alpha, \delta_e, \beta) + \Delta C_y(\alpha, \delta_a) + \Delta C_y(\alpha, \delta_s) + C_{y_{\delta_r}}(\alpha)\delta_r +$$

$$+ \frac{b}{2V}\left\{\left[C_{y_{p_s}}(\alpha)\cos\alpha - C_{y_{r_s}}(\alpha)\sin\alpha\right]p + \left[C_{y_{p_s}}(\alpha)\sin\alpha + C_{y_{r_s}}(\alpha)\cos\alpha\right]r\right\}$$

$$C_{z_s} = -\left[C_L(\alpha, \delta_e) + \Delta C_L(\alpha, \delta_a) + \Delta C_L(\alpha, \delta_s)\right]$$

$$C_{l_s} = C_{l_s}(\alpha, \delta_e, \beta) + \Delta C_l(\alpha, \delta_a) + \Delta C_l(\alpha, \delta_s) + C_{l_{\delta_r}}(\alpha)\delta_r +$$

$$+ \frac{b}{2V}\left\{\left[C_{l_{p_s}}(\alpha)\cos\alpha - C_{l_{r_s}}(\alpha)\sin\alpha\right]p + \left[C_{l_{p_s}}(\alpha)\sin\alpha + C_{l_{r_s}}(\alpha)\cos\alpha\right]r\right\}$$

$$C_{m_s} = C_m(\alpha, \delta_e) + \Delta C_m(\alpha, \delta_a) + \Delta C_m(\alpha, \delta_s) +$$

$$+ \frac{\bar{c}}{2V}\left[C_{m_{q_s}}(\alpha, \delta_e)\,q + C_{m_{\dot{\alpha}}}(\alpha, \delta_e)\,\dot{\alpha}\right]$$

$$C_{n_s} = C_{n_s}(\alpha, \delta_e, \beta) + \Delta C_n(\alpha, \delta_a) + \Delta C_n(\alpha, \delta_s) + C_{n_{\delta_r}}(\alpha)\delta_r +$$

$$+ \frac{b}{2V}\left\{\left[C_{n_{p_s}}(\alpha)\cos\alpha - C_{n_{r_s}}(\alpha)\sin\alpha\right]p + \left[C_{n_{p_s}}(\alpha)\sin\alpha + C_{n_{r_s}}(\alpha)\cos\alpha\right]r\right\}$$

These aerodynamic data were digitized from Reference 12 and were given in Reference 17.

2. KINEMATIC EQUATIONS

The trajectory of the aircraft c.g. with respect to an earth reference system, x_e, y_e, h, is calculated by integrating

$$V_e \triangleq \begin{bmatrix} \dot{x}_e \\ \dot{y}_e \\ -\dot{h} \end{bmatrix} = (L_{B\text{-}E})^T V$$

where

$$L_{B\text{-}E} \triangleq \begin{bmatrix} \ell_{11} & \ell_{12} & \ell_{13} \\ \ell_{21} & \ell_{22} & \ell_{23} \\ \ell_{31} & \ell_{32} & \ell_{33} \end{bmatrix} \triangleq \begin{bmatrix} \cos\theta\cos\psi & \cos\theta\sin\psi & -\sin\theta \\ \sin\theta\sin\phi\sin\psi - \cos\phi\sin\psi & \sin\theta\sin\phi\sin\psi + \cos\phi\sin\psi & \sin\phi\cos\theta \\ \sin\theta\cos\phi\cos\psi + \sin\phi\sin\psi & \sin\theta\cos\phi\sin\psi - \sin\phi\cos\psi & \cos\phi\cos\theta \end{bmatrix}$$

3. QUATERNION SYSTEM

$$\frac{d}{dt}\begin{bmatrix} \lambda_0 \\ \lambda_1 \\ \lambda_2 \\ \lambda_3 \end{bmatrix} = \frac{1}{2}\begin{bmatrix} 0 & -p & -q & -r \\ p & 0 & r & -q \\ q & -r & 0 & p \\ r & q & -p & 0 \end{bmatrix}\begin{bmatrix} \lambda_0 \\ \lambda_1 \\ \lambda_2 \\ \lambda_3 \end{bmatrix} + K\epsilon\begin{bmatrix} \lambda_0 \\ \lambda_1 \\ \lambda_2 \\ \lambda_3 \end{bmatrix}$$

where

$$\epsilon = 1 - \sum_{i=0}^{3} \lambda_i^2$$

and K is a positive constant for error correction (K = 2 was used in the

ground simulator). The initial conditions for the quaternions, λ_i, are calculated from the initial Euler angles ψ_o, θ_o, ϕ_o by the following equations

$$\lambda_0 = \cos\frac{\psi_o}{2}\cos\frac{\theta_o}{2}\cos\frac{\phi_o}{2} + \sin\frac{\psi_o}{2}\sin\frac{\theta_o}{2}\sin\frac{\phi_o}{2}$$

$$\lambda_1 = \cos\frac{\psi_o}{2}\cos\frac{\theta_o}{2}\sin\frac{\phi_o}{2} - \sin\frac{\psi_o}{2}\sin\frac{\theta_o}{2}\cos\frac{\phi_o}{2}$$

$$\lambda_2 = \cos\frac{\psi_o}{2}\sin\frac{\theta_o}{2}\cos\frac{\phi_o}{2} + \sin\frac{\psi_o}{2}\cos\frac{\theta_o}{2}\sin\frac{\phi_o}{2}$$

$$\lambda_3 = \sin\frac{\psi_o}{2}\cos\frac{\theta_o}{2}\cos\frac{\phi_o}{2} - \cos\frac{\psi_o}{2}\sin\frac{\theta_o}{2}\sin\frac{\phi_o}{2}$$

The quaternions are then converted into directional cosines, ℓ_{ij}, by

$$\ell_{11} = \lambda_0^2 + \lambda_1^2 - \lambda_2^2 - \lambda_3^2 \qquad \ell_{12} = 2(\lambda_1\lambda_2 + \lambda_3\lambda_0) \qquad \ell_{13} = 2(\lambda_1\lambda_3 - \lambda_2\lambda_0)$$

$$\ell_{21} = 2(\lambda_1\lambda_2 - \lambda_3\lambda_0) \qquad \ell_{22} = \lambda_0^2 + \lambda_2^2 - \lambda_1^2 - \lambda_3^2 \qquad \ell_{23} = 2(\lambda_2\lambda_3 + \lambda_1\lambda_0)$$

$$\ell_{31} = 2(\lambda_1\lambda_3 + \lambda_2\lambda_0) \qquad \ell_{32} = 2(\lambda_2\lambda_3 - \lambda_1\lambda_0) \qquad \ell_{33} = \lambda_0^2 + \lambda_3^2 - \lambda_1^2 - \lambda_2^2$$

The Euler angles are calculated from the direct cosines as follows:

$$\theta = \sin^{-1}(-\ell_{13})$$

$$\phi = \tan^{-1}(\ell_{23}/\ell_{33})$$

$$\psi = \tan^{-1}(\ell_{12}/\ell_{11})$$

In the simulator, the aerodynamic data and equations of motions are solved by a small digital computer (Honeywell DDP 116). The control system dynamics and associated nonlinear functions are solved on an analog computer (COMCOR Ci 5000). However, during the preliminary design of the departure preventer, a six-degree-of-freedom digital simulation was done on an IBM 370/165 wherein the control system dynamics were computed by discretization of the continuous system, known as the discrete transition method. The method is now briefly described in the following.

Discrete Transition Method

Consider a linear time-invariant continuous system

$$\dot{x} = Ax + Bu \quad , \qquad x(0) = x_0$$

The well-known solution is

$$x(t) = e^{At}x(0) + e^{At}\int_0^t e^{-A\tau}Bu(\tau)\,d\tau$$

If all the components of the control vector $u(t)$ between any two consecutive sampling instants $KT \le t < (K+1)T$, are approximated by a constant, i.e., $u(KT)$ (assuming the sampling interval T is "small enough"), then the above equation may be written as

$$x\left[(K+1)T\right] = e^{AT}x(KT) + e^{AT}\int_0^T e^{-A\tau}Bu(KT)\,d\tau$$

or

$$x\left[(K+1)T\right] = G(T)\,x(uT) + H(T)\,u(KT)$$

where

$$G(T) = e^{AT}$$

$$H(T) = \left[\int_0^T e^{A\tau}\,d\tau\right]B$$

The above difference equation thus gives an approximate solution of the continuous equation at discrete points of time, $t = KT$, $K = 0, 1, 2, \ldots$.

APPENDIX III

CALIBRATION AND ADJUSTMENT OF THE STALL INHIBITOR - AUTOMATIC DEPARTURE PREVENTION DEVICE

The unit was designed using high quality components and has been found to be extremely reliable. Since the unit is essentially an analog computer, with many possible coefficient potentiometer settings and diode function generator (DFG) functions, any built-in test function would be cumbersome and ineffective. However, it is possible to perform a static check by use of methods similar to those employed on any analog computer. External input signals can be applied to the computer and the coefficient potentiometers varied to desired settings. The amplifier, multiplier, and diode function generator outputs can then be measured and compared with pre-computed values. A digital voltmeter, low frequency oscillator and an oscilloscope are required for the calibration and adjustments described in the following paragraphs.

Trim potentiometers and test points are provided to measure and adjust the power supply, reference supply, and multiplier trim. These voltages and trims have been properly set, but may vary slightly with time. Adjustment of the plus and minus 15 volt power supply voltage is done by trim potentiometers located inside the power supply module. To perform this adjustment, the module must be removed from the rack and powered through the extension cable supplied with the equipment. The cover of the module must be removed to provide access to the internal adjustment potentiometers. Test points for the plus and minus 15 volts are located on PC Board S40-E004. (The + 15 volts must be adjusted first.) The plus and minus 10 volt reference used in the unit appear as outputs of two amplifiers located on Card S40-E002. These reference voltages can be measured at test points and adjusted with trim potentiometers located on this card. (The -10 volt reference must be adjusted first.)

The Analog Devices model 426 multiplier used in the unit has external adjustments for output null, Y feed through, and X feed through. Each multiplier is labelled per location on the circuit cards and should not be interchanged. If a multiplier must be replaced, the replacement multipliers should be adjusted for offset and feed through. Test points are provided to measure the X, Y, and XY/10 output of each multiplier. Inputs to each multiplier can be varied by adjusting input voltages to the computer and coefficient potentiometers to arrive at desired X and Y voltages. The external adjustments for each multiplier should be made in the following order:

Offset

1) Adjust the X and Y inputs to zero with an appropriate input voltage or coefficient potentiometer.

2) Adjust the output balance potentiometer until the output voltage is zero.

Feed Through

1) Adjust the Y input to zero with an appropriate input voltage or coefficient potentiometer setting.

2) Apply an input voltage into an appropriate channel such that the X input of the multiplier swings through its maximum voltage range at any frequency up to 100 cps. Adjust the Y feed through potentiometer for minimum output.

3) Adjust the X input to zero with an appropriate input voltage or coefficient potentiometer setting.

4) Apply an input voltage into an appropriate channel such that the Y input of the multiplier swings through its maximum voltage range at any frequency up to 100 cps. Adjust the X feed through potentiometer for minimum multiplier output.

The diode function generators (DFG) consist of fixed break points at 0, +2, +4, +6 and +8 volts. Trim potentiometers are provided to adjust the slope of the function at each of these break points. The DFG is designed for plus inputs and plus outputs only. For negative inputs, the output is zero and the output does not go negative. To adjust a function, the following procedure can be used: An input voltage to the DFG through an appropriate channel can be supplied from a low frequency oscillator. The input to the DFG can be patched to the X axis of an oscilloscope, and the output to the Y axis. The slope of the function can then be adjusted starting with the 0 breakpoint and advancing to the +8 volt breakpoint.

For sake of completeness, a list of drawings of the stall inhibitor and automatic departure prevention device is given in the following:

Dwg. No. S40-E001, Sh. 1 & Sh. 2	Stall Inhibitor Func. Gen. PC board
Dwg. No. S40-E002, Sh. 1 & Sh. 2	15V to + 10V Converter Card
Dwg. No. S40-E003, Sh. 1 & Sh. 2	Computer Interface Card
Dwg. No. S40-E004, Sh. 1 & Sh. 2	Stall Inhibitor and Departure Preventer Actuation Monitor Card
Dwg. No. S40-E005, Sh. 1 & Sh. 2	Stall Inhibitor Elevator Stick Actuation Card
Dwg. No. S40-E006, Sh. 1 & Sh. 2	Departure Preventer Elevator Channel Card
Dwg. No. S40-E007, Sh. 1 & Sh. 2	Departure Preventer Aileron Channel Card

Dwg. No. S40-E008, Sh. 1 & Sh. 2	Departure Preventer Rudder Channel Card B and Integrator Card
Dwg. No. S40-E009, Sh. 1 & Sh. 2	Departure Preventer Rudder Channel Card A
Dwg. No. S40-E010, Sh. 1 & Sh. 2 Sh. 3 & Sh. 4	Stall Inhibitor and Departure Preventer Block Diagram
Dwg. No. S40-E011, Sh. 1 of 1	Chassis Wiring Diagram. Stall Inhibitor & Auto. Departure Preventer
Dwg. No. S40-E012, Sh. 1 of 1	External Cables - Stall Inhibitor & Auto. Departure Preventer Chassis
Dwg. No. S40-EM005	Stall Inhibitor/Auto. Departure Preventer Electronic Assy.

REFERENCES

1. Stall/Post Stall/Spin Symposium, Sponsored by ASD/AFFDL, Wright-Patterson AFB, 15-17 December 1971.

2. W. R. Burris and D.E. Hutchins; Effect of Wing Leading Edge Geometry on Maneuvering Boundaries and Stall Departure. AIAA Paper No. 70-904, AIAA 2nd Aircraft Design and Operations Meeting, July 1970.

3. G. Bull; Investigation of Lateral Stability at Stall. Final Report No. TB-679-F-12, WADC TR 54-498, 18 February 1954.

4. J.M. Schuler; Theoretical Development of an Automatic Control System for Stabilizing the Large Uncontrolled Motions of Airplanes. CAL Report No. TB-1132-F-1, April 1958.

5. J.M. Schuler; Flight Evaluation of an Automatic Control System for Stabilizing the Large Uncontrolled Motions of Airplanes in Stalled Flight. CAL Report No. TB-1132-F-2, October 1959.

6. D.P. Rubertus; TWeaD Control Augmentation System. Paper presented at the National Aerospace Electronics Conference, Dayton, Ohio. 15-17 May 1972.

7. W.A. Seth; A-7D Estimated Flying Qualities. LTV/VAD Report No. 2-53320/8R-8089, May 27, 1968.

8. D.D. Smith, E.R. Curtis, and W.G. McNamara; Model A-7 A/B Airplane Spin Evaluation , Final Report. NATC FT-72R-71, 24 September 1971.

9. D.O. Gobert and L.D. Fortner; Military Evaluation (Flying Qualities) of the A-7D with Expanded Aft c.g. Limits. FTC-SD-71-8, April 1971.

10. D.O. Gobert and W.T. Twinting; A-7D Stability and Control Military Preliminary Evaluations (Phase 1C). FTC-SD-69-22, May 1969.

11. J.R. Milner; A-7D Limited Spin Tests. FTC-TR-70-14, May 1970.

12. A-7 Aerodynamic Data at High Angles of Attack. Furnished by AFFDL, February 1972.

13. R.A. Jeske; Final Engineering Report Automatic Flight Control System for A-7 D/E Aircraft. LTV/DAD Report No. 2-53560/9R-5448.

14. C.L. Mesiah; Digital Simulation of a Variable Stability Total In-Flight Simulator. CAL Flight Research Memorandum No. 434, 19 April 1970.

15. C.L. Mesiah; Digital Computer Simulation of the X-22A Six-Degrees-of-Freedom Equations of Motion and Global Aerodynamics. CAL Flight Research Memorandum No. 412, 25 January 1968.

16. MIL-F-8785-B(ASG), Military Specification -- Flying Qualities of Piloted Airplanes, 7 August 1969.

17. F. D. Newell; Departure Preventer/Stall Inhibitor Simulation Test Plan. CAL Flight Research Memorandum No. 474, July 28, 1972.

UNCLASSIFIED

Security Classification

DOCUMENT CONTROL DATA - R&D

(Security classification of title, body of abstract and indexing annotation must be entered when the overall report is classified)

1. ORIGINATING ACTIVITY (Corporate author) Calspan Corporation P.O. Box 235 Buffalo, New York 14221	2a. REPORT SECURITY CLASSIFICATION 2b. GROUP

3. REPORT TITLE

DEVELOPMENT AND EVALUATION OF AN AUTOMATIC DEPARTURE PREVENTION SYSTEM AND STALL INHIBITOR FOR FIGHTER AIRCRAFT

4. DESCRIPTIVE NOTES (Type of report and inclusive dates)

Final Report

5. AUTHOR(S) (Last name, first name, initial)

Chen, Robert T.N.; Newell, Fred D.; Schelhorn, Arno E.

6. REPORT DATE	7a. TOTAL NO. OF PAGES	7b. NO. OF REFS
April 1973	110	17

8a. CONTRACT OR GRANT NO.	9a. ORIGINATOR'S REPORT NUMBER(S)
F33615-72-C-1162	AK-5112-F-1
b. PROJECT NO. 8225 and 8219	
c.	9b. OTHER REPORT NO(S) (Any other numbers that may be assigned this report) AFFDL-TR-73-29
d.	

10. AVAILABILITY/LIMITATION NOTICES

Approved for public release; distribution unlimited.

11. SUPPLEMENTARY NOTES	12. SPONSORING MILITARY ACTIVITY
	Air Force Flight Dynamics Laboratory Air Force Systems Command Wright-Patterson Air Force Base, Ohio

13. ABSTRACT

This report documents the conceptual design, breadboard development and pilot-in-the-loop evaluation of an automatic departure prevention system and a stall inhibitor for fighter aircraft. Using the A-7D as the study aircraft, a departure boundary characterized by α and β was determined from the available data. This departure boundary was then used to help design an automatic departure preventer and a stall inhibitor. The departure preventer provides automatic control inputs to the pitch and yaw axis. The stall inhibitor increases the longitudinal stick force to provide the pilot with cues of an impending stall; however, the pilot retains override capability. The stall inhibitor, while warning the pilot of the impending stall, tends to produce strong pilot-induced oscillations, and would not be acceptable. An automatic departure prevention device as described in this report works smoothly and will benefit the A-7 aircraft. With just the departure preventer, the pilots could maneuver freely, with great confidence and use the full capability of the airplane, well beyond the present departure boundary.

DD FORM 1 JAN 64 1473

UNCLASSIFIED

Security Classification

UNCLASSIFIED

Security Classification

14. KEY WORDS	LINK A		LINK B		LINK C	
	ROLE	WT	ROLE	WT	ROLE	WT
Automatic Departure Preventer Stall Inhibitor Ground-Based Simulator A-7D Aircraft						

INSTRUCTIONS

1. ORIGINATING ACTIVITY: Enter the name and address of the contractor, subcontractor, grantee, Department of Defense activity or other organization *(corporate author)* issuing the report.

2a. REPORT SECURITY CLASSIFICATION: Enter the overall security classification of the report. Indicate whether "Restricted Data" is included. Marking is to be in accordance with appropriate security regulations.

2b. GROUP: Automatic downgrading is specified in DoD Directive 5200.10 and Armed Forces Industrial Manual. Enter the group number. Also, when applicable, show that optional markings have been used for Group 3 and Group 4 as authorized.

3. REPORT TITLE: Enter the complete report title in all capital letters. Titles in all cases should be unclassified. If a meaningful title cannot be selected without classification, show title classification in all capitals in parenthesis immediately following the title.

4. DESCRIPTIVE NOTES: If appropriate, enter the type of report, e.g., interim, progress, summary, annual, or final. Give the inclusive dates when a specific reporting period is covered.

5. AUTHOR(S): Enter the name(s) of author(s) as shown on or in the report. Enter last name, first name, middle initial. If military, show rank and branch of service. The name of the principal author is an absolute minimum requirement.

6. REPORT DATE: Enter the date of the report as day, month, year, or month, year. If more than one date appears on the report, use date of publication.

7a. TOTAL NUMBER OF PAGES: The total page count should follow normal pagination procedures, i.e., enter the number of pages containing information.

7b. NUMBER OF REFERENCES: Enter the total number of references cited in the report.

8a. CONTRACT OR GRANT NUMBER: If appropriate, enter the applicable number of the contract or grant under which the report was written.

8b, 8c, & 8d. PROJECT NUMBER: Enter the appropriate military department identification, such as project number, subproject number, system numbers, task number, etc.

9a. ORIGINATOR'S REPORT NUMBER(S): Enter the official report number by which the document will be identified and controlled by the originating activity. This number must be unique to this report.

9b. OTHER REPORT NUMBER(S): If the report has been assigned any other report numbers *(either by the originator or by the sponsor)*, also enter this number(s).

10. AVAILABILITY/LIMITATION NOTICES: Enter any limitations on further dissemination of the report, other than those imposed by security classification, using standard statements such as:

(1) "Qualified requesters may obtain copies of this report from DDC."

(2) "Foreign announcement and dissemination of this report by DDC is not authorized."

(3) "U. S. Government agencies may obtain copies of this report directly from DDC. Other qualified DDC users shall request through _____."

(4) "U. S. military agencies may obtain copies of this report directly from DDC. Other qualified users shall request through _____."

(5) "All distribution of this report is controlled. Qualified DDC users shall request through _____."

If the report has been furnished to the Office of Technical Services, Department of Commerce, for sale to the public, indicate this fact and enter the price, if known.

11. SUPPLEMENTARY NOTES: Use for additional explanatory notes.

12. SPONSORING MILITARY ACTIVITY: Enter the name of the departmental project office or laboratory sponsoring *(paying for)* the research and development. Include address.

13. ABSTRACT: Enter an abstract giving a brief and factual summary of the document indicative of the report, even though it may also appear elsewhere in the body of the technical report. If additional space is required, a continuation sheet shall be attached.

It is highly desirable that the abstract of classified reports be unclassified. Each paragraph of the abstract shall end with an indication of the military security classification of the information in the paragraph, represented as *(TS)*, *(S)*, *(C)*, or *(U)*

There is no limitation on the length of the abstract. However, the suggested length is from 150 to 225 words.

14. KEY WORDS: Key words are technically meaningful terms or short phrases that characterize a report and may be used as index entries for cataloging the report. Key words must be selected so that no security classification is required. Identifiers, such as equipment model designation, trade name, military project code name, geographic location, may be used as key words but will be followed by an indication of technical context. The assignment of links, rules, and weights is optional.

☆U.S.Government Printing Office: 1973 — 759-495/612

UNCLASSIFIED

Security Classification